NASA CR-15970
RI/RD81-149

NASA-CR-165379
19820003592

NASA

INTERIM REPORT

ADVANCED SUPERPOSITION METHODS FOR HIGH SPEED TURBOPUMP VIBRATION ANALYSIS

by

C. E. Nielson
and A. D. Campany

Rockwell International
Rocketdyne Division

prepared for
NATIONAL AERONAUTICS AND SPACE ADMINISTRATION

May 1981

NASA-Lewis Research Center
Contract NAS3-22480
R. Connelly, Project Manager
N. Hannum, Project Manager

1. Report No.	2. Government Accession No.	3. Recipient's Catalog No.
NASA CR 165379		

4. Title and Subtitle	5. Report Date
ADVANCED SUPERPOSITION METHODS FOR HIGH SPEED TURBOPUMP VIBRATION ANALYSIS	19 May 1981
	6. Performing Organization Code

7. Author(s)	8. Performing Organization Report No.
C. E. Nielson A. D. Campany	RI/RD81-149
	10. Work Unit No.

9. Performing Organization Name and Address	11. Contract or Grant No.
Rocketdyne Division of Rockwell International 6633 Canoga Avenue Canoga Park, CA 91304	NAS3-22480
	13. Type of Report and Period Covered Interim Report 1 Sept 1980 - 1 May 1981

12. Sponsoring Agency Name and Address	14. Sponsoring Agency Code
National Aeronautics and Space Administration Washington, D.C. 20546	

15. Supplementary Notes

16. Abstract

The small, high pressure Mark 48 Liquid Hydrogen turbopump was analyzed and dynamically tested to determine the cause of high speed vibration at an operating speed of 92,400 rpm. This approaches the design point operating speed of 95,000 rpm. The initial dynamic analysis in the design stage and subsequent further analysis of the rotor only dynamics failed to predict the vibration characteristics found during testing. An advanced procedure for dynamics analysis was used in this investigation. The procedure involves developing accurate dynamic models of the rotor assembly and casing assembly by finite-element analysis. The dynamically instrumented assemblies are independently rap tested to verify the analytical models. The verified models are then combined by modal superposition techniques to develop a completed turbopump model where dynamic characteristics are determined. The results of the dynamic testing and analysis obtained with this program are presented and methods of moving the high speed vibration characteristics to speeds above the operating range are recommended. Recommendations for use of these advanced dynamic analysis procedures during initial design phases are given.

17. Key Words (Suggested by Author(s))	18. Distribution Statement
Hydrogen turbopump Centrifugal pump Axial flow turbine Dynamics analysis High-speed dynamics Modal analysis	

19. Security Classif. (of this report)	20. Security Classif. (of this page)	21. No. of Pages	22. Price*
Unclassified	Unclassified		

* For sale by the National Technical Information Service, Springfield, Virginia 22151

NASA-C-168 (Rev. 6-71)

N82-11465#

FOREWORD

The activity reported herein was conducted by Rotating Machinery, Structural Dynamics and Engineering Development Laboratory personnel of Rocketdyne, a division of Rockwell International, under Contract NAS3-22480 from October 1980 to April 1981. Mr. R. Connelly and Mr. N. Hannum, Lewis Research Center, were NASA Project Managers. At Rocketdyne, Mr. H. Diem as Program Manager and Mr. C. E. Nielson as Project Engineer were responsible for technical direction of the program. Special recognition is given to Mr. A. D. Campany and Mr. B. F. Rowan of the Structural Dynamics Department for dynamic analysis and technical expertise provided during the analysis and testing.

Page Missing in Original Document

CONTENTS

Page Missing in Original Document

ILLUSTRATIONS

TABLES

SUMMARY

This report documents the efforts of Task I "Vibration Analysis" of NASA Contract NAS3-22480. The objective of this program was to develop a method of dynamic analysis which would be able to identify and remedy the vibration problem at 1540 Hz which had been observed during Mark-48F turbopump testing in LIMA test stand of the Advanced Propulsion test facility (APTF). This method could then be used in the dynamic analysis of other high speed turbomachinery as a design tool.

The Mark-48 fuel turbopump shown in Fig. 1 is a small, high-pressure liquid hydrogen turbopump which has been developed to establish the technology for turbopump applications in small, high-performance, reusable, versatile, staged combustion rocket engines. During previous test programs of the turbopump, a vibration problem was encountered near the speed of 92,400 rpm (1540 Hz). The turbopump design operating speed is 95,000 rpm.

Critical speed analysis using the rotating assembly-only model had indicated no rotor resonance condition at or near the design speed operating point. Previous analysis and limited test stand rap testing had indicated the possibility of the resonance being in the test stand structure. As a result of preliminary analysis it was recommended that further modal analysis and impact testing of the rotor and casing be done to clearly define the cause of the resonance condition and to develop a better understanding of high-speed pump dynamics.

As higher turbopump speeds are used with advancing technology and state of the arts, better methods and definition of the dynamic models must be used in place of the generally acceptable practice of using rotor-only dynamic analysis to predict turbopump dynamic behavior. Rigid body assumptions commonly used for the turbopump casings with rotor-only dynamic analysis becomes inadequate for turbopumps operating at speeds in excess of 60,000 rpm (1000 Hz). This condition dictates that for turbopumps designed for speeds above those cited, a more complex analysis is required. This study has been directed at developing the analysis procedure, definition of component models, and superposition analysis to determine the sources of the existing condition experienced on the Mark-48F turbopump.

To complete the requirements of this study, the Mark 48 fuel turbopump casing was assembled without the internal rotating components. Similarly, the rotor components were assembled including the three impeller stages, the inducer, the two turbine stages, and the inner races of the bearings. These assemblies were instrumented with accelerometers in the appropriate places. Free-free simulation modal testing of the rotor and case was performed using an HP5451C Modal Analysis System. Simultaneous with this effort, free-free finite element dynamic models of the rotor and case components were developed and run on the computer for natural frequency and mode shape predictions. The results of the modal testing and the analysis were compared and correlated to refine the dynamic models. The correlated rotor and case models were modally superposed with boundary conditions modeled to those of the LIMA tests at APTF. The results of this combined turbopump model indicate three possible problem modes, the most likely being a backward precessional mode indicated at 95,200 rpm (1587 Hz).

The other next likely candidates include a backward precessional mode indicated at 107,000 rpm (1783 Hz), and a turbine-end bearing support axial mode indicated at 97,260 rpm (1621 Hz). These candidates and others less likely are reported. Recommendations are given for structural modifications of the turbopump to eliminate the problem and requirements for further analytical effort are presented.

INTRODUCTION

HISTORICAL BACKGROUND

The Mark 48F was designed to establish the technology for a fuel turbopump of the Advanced Space Engine (ASE) during 1973. Through October 1979, cold flow pumping tests of a developed prototype were conducted at the Advanced Propulsion Test Facility (APTF) of Rocketdyne's Santa Susana Field Laboratory (SSFL). During these tests, the Mark 48F was driven by pressurized hydrogen gas and pumped liquid hydrogen. As the pump approached the operational speed of 95,000 rpm, it consistently experienced accelerometer redline test cutoffs at approximately 92,400 rpm. (1540 Hz rotor synchronous frequency.) Although critical speed analysis using conventional methods indicated no rotor problem, concern existed that the pump as a whole may have a design related dynamic problem. It has been evident in other turbopump development programs on turbopumps of speeds above 60,000 rpm that conventional rotor-only dynamic analysis was not adequate to define the vibration characteristics of a turbopump. At increased frequency levels developed by the high speed machines the basic assumptions of using solid-body casing and ducting become invalid. Subsequently, impact testing was conducted at APTF to isolate apparatus natural frequencies which might be causing the cutoffs. Based upon functional and impact test data and rotor-dynamic analysis, it was concluded that the resonance which caused cutoff was most probably the test stand structure. As a recommendation of the report, further impact testing of the rotor and casing was advised to verify this conclusion and to obtain a more complete understanding of pump dynamics. In October of 1980, follow-on contract NAS3-22480 was awarded to Rocketdyne. As one of the major objectives of this contract (Task I), development of an advanced more accurate method of dynamic analysis was to be initiated. This method was to use the currently available computer analysis tools and testing was to be conducted on the Mark 48 Liquid Hydrogen turbopump to identify the cause and determine a remedy for the vibration problem observed in previous testing. In this analysis and testing, three potential problem modes were predicted for the Mark 48-F turbopump near the 1540 Hz operating condition. These modes are two backward precessional rotor modes and a turbine-end bearing support mode for the casing which could not be predicted in the original "rotor-only" analysis. It is recommended that these modes be moved above the required operating range by stiffening the casing using stiffening ribs located around the turbine-end bearing and pump-end bearing housing. This report documents the methods, results and conclusions of this analysis.

ANALYSIS SCHEME

An accurate approach to the dynamic analysis was essential to the success of the program. A verifiable approach was required utilizing testing in order to confirm the accuracy of the methods used. The approach also had to utilize currently available methods of dynamic analysis and testing. Using a combination of Rocketdyne's conventional finite element modeling and the newly acquired modal testing technology, the overall scheme was developed. That approach is depicted in the flow chart of Fig. 2.

The basic tenet of this scheme is that of modal superposition. In order to verify the rotor model accuracy, the rotor must be tested independent from the casing such that measurements may be directly related to rotor dynamics. Later in the analysis, verified rotor and case models are superposed to obtain the overall pump dynamics. A theoretical discussion of the modal superposition principle is contained in Appendix A.

The scheme proceeds along two simultaneous paths. The analytical path develops finite element models of the rotor and casing which are processed to obtain natural frequencies and mode shapes for free-free versions of each component. The experimental path tests the rotor and case independently using modal impact testing (see Discussion; Test Description; Procedure). Free-free conditions and component operating fits are simulated. By obtaining transfer functions at selected points on the components, frequencies and mode shapes can be obtained. The analytical results are then compared with the experimental results for correlation. Adjustments are made to the finite element models where required until correlation is very good (within ±10% difference). The correlated models are then translated from their physical coordinates into modal coordinates with the appropriate Advanced Propulsion Test Facility (APTF) boundary conditions added. The models are modally superposed producing a complete turbopump model at test conditions. Where the design has not been developed into testable hardware to verify the analytical models, the analytical finite element models must be used without verification. The accuracy of the model is dependent upon the care and expertise used in the model development. Even so, this method of using combined dynamics of rotor, casing, and boundary conditions will provide improved recognition of possible high speed vibration modes.

Because the modal superposition method combines the effects of each mode to describe the structure dynamics, the results are sensitive to the number of modes included from the component finite element models. Typically, modes from 2 to 5 times the highest mode desired are necessary. Therefore, the performance of a sensitivity study, where the effect of progressive inclusion of higher frequency modes is examined, is desirable. True results are obtained where the inclusion of higher modes yields no change in the turbopump frequencies and mode shapes (the modal solution becomes stable). The frequencies and mode shapes obtained from the modal superposition describe the turbopump dynamically throughout its operating range. Conclusions and recommendations are based, in part, upon those results.

TECHNOLOGY DEVELOPMENT

As a product of the Mark 48F dynamic analysis, a method of problem analysis has been developed which can be of use in future pump development. The requirement for verifiable results imposed by the special problem presented had mandated the development of such a method. The use of the superposition method of casing and rotor models in high speed turbomachines without means of model verification by rap testing is still considered a more reliable method than the conventional "rotor-only" analysis. This method is considered to be useful as a tool in both design and development areas of high speed turbomachinery. Having been successfully demonstrated, its utility in the solution of future structural development problems is apparent. As such, this method of analysis represents a new technology.

The method, as described in the Analysis Scheme (above), employs the already developed engineering tools of finite-element modeling and modal testing in a manner of problem solution which maximizes the advantages of both tools. As stated previously, the method proceeds along the two simultaneous paths of analysis and test. Finite-element analysis has the advantages of providing as much detail as required and the opportunity for the evaluation of structural changes. Modal testing has the advantage of providing real, measured information about a structure's dynamic characteristics. So long as basic assumptions of the testing are preserved, and the test is conducted with integrity, the information obtained is valid. Modal testing may be conducted in such a way as to obtain the predominant, lower frequency modes of a structure. Finite-element modeling may be as detailed as is necessary. Finite-element mode shape predictions are then compared with those of testing to identify key modes to be used for correlation. Adjustments (consistent with engineering theory) are then made to the finite-element model(s) to optimize overall correlation for the key modes. This having been accomplished, the finite-element mode(s) may be used with their full level of detail to predict natural frequencies and mode shapes to be superposed (Appendix A) or for response analysis. Results obtained may be viewed with confidence because finite-element modeling was correlated with actual testing and because the tenets of modal analysis are well developed and verifiable. Further, if problems are indicated, changes to the structure may be modeled to evaluate the effects of such changes. Thus the advantages of the method become apparent.

1. Verification of analysis means structural recommendations may be proposed with confidence

2. Verified models may be able to predict modes undetectable during modal test (due to insufficient input or instrumentation) because of their detail and theory-based modal extraction (number of natural frequencies = number of dynamic degrees of freedom)

3. Changes to structure may be evaluated through modification of verified analytical models

4. Analysis of turbomachinery includes effects of casing dynamics and thus provides a more complete picture of machine dynamics

The accuracy of the modeling can be enhanced by the use of rap test verification of the components. It should be noted however, that in the progress of this study it was found that the analytical rotor and casing model developed without rap test verification did provide a relatively good model. This does indicate that with proper care and attention to detail, a model can be developed for a turbomachine in the initial design stages. The accuracy will be directly related however to the expertise of the analyst and the detail of the model. The approach is most certainly more accurate than the conventional rotor-only analysis. The conventional analysis uses the assumption that the turbopump casing and test stand monitoring are absolute rigid bodies. This is the method originally used for the Mark 48-Fuel turbopump analysis. In the original analysis no high speed vibration characteristics were identified in the turbopump operating range.

The particular analysis scheme employed for the Mark 48F is that of Fig. 2 (less sensitivity study). This is the first time Rocketdyne has used such an approach, but results obtained were very good. Based on these results, it is recommended that the method by employed in future pump design and development studies.

APPROACH

GENERAL DESCRIPTION OF MODAL TEST METHOD

The modal test method employs the theoretical concepts of modal analysis (Appendix A) and recently developed hardware and software to experimentally determine the frequencies and mode shapes of a structure. The hardware generally includes a calibrated excitor (e.g., a vibration shaker or load cell hammer), accelerometers, a Fast-Fourier Analyzer (FFA), and a digital data recording device. The software includes programs for curve fitting raw data, performing various types of spectral analyses (e.g., power spectral density, transfer function gain, phase, coherence), and data reduction routines for the comparison and normalization of like measurements.

A series of measurements is made on the test structure which form a geometric grid capable of defining the structure under motion. The purpose of these measurements is to obtain transfer functions between the excitation and response points. To obtain each measurement, an accelerometer is placed at one of the grid locations to record response while a broadband excitation is applied at another grid point. The broadband excitation may be produced by broadband random signal through a shaker system or by impact from a load cell hammer of sufficiently short period. The input and response motion signals are amplified, passed through an anti-aliasing filter, simultaneously sampled (digitized), and recorded on a digital recording device. At this point, the FFA performs spectral analyses of the time sampled data to produce transfer function gain, phase and coherence between input and response. Gain and phase define the relationship between motion at each grid point while coherence is used by the experimenter to evaluate the validity of the measurement.

When all transfer functions for the grid have been thus obtained, normalized and compared, the motion of the structure at a normal mode of vibration can be described.

In order to assure the validity of results obtained via modal testing, two basic assumptions of modal analysis must be preserved. These are:

1. The test structure is linear. In order to develop true modal parameters during frequency domain curve fitting, the structure must be linear. Discontinuities of structure, nonlinear springs and nonlinear damping may exist in real structures. The extent of their existence should be determined before testing begins. This is accomplished through preliminary reciprocity checks. Stated simply, reciprocity says that a transfer function from point A to point B will be the reciprocal of a transfer function from point B to point A in linear structures.

2. All modes in the frequency range of interest may be identified and curve fit. Sometimes, structural modes are closely spaced so that the existence of several modes appears as a single peak. The experimentor must exercise care in the selection of a sufficient number of test grid points to be able to discern such modes. Having identified these, capability must exist to independently curve fit each mode.

Because a linearly elastic structure will demonstrate reciprocity (i.e., transfer function from point A to point B is reciprocal of transfer function from point B to point A), it makes no difference whether the excitor or accelerometer remains stationary while the other instrument moves to each grid location. In testing the Mark 48F rotor, the accelerometer was moved to grid locations while the impact location remained fixed. In testing of the Mark 48F case, the accelerometer remained fixed while the hammer was moved to the various grid locations. Also, because reciprocity is an assumption of this test technique, pretest reciprocity checks must be performed on the structure to determine the degree of validity of this assumption and to isolate nonlinear areas of the structure.

Both components were tested by the impact method under simulated free-free conditions.

EQUIPMENT

The following equipment was used in the modal testing of the Mark 48F.

Equipment	Figure No.
1. HP5451C Modal Analysis System with Fast-Fourier Analyzer and Tektronix Graphics Plotter (1)	3
2. PCB Load Cell Hammer with 500 pounds force transducer (1)	7
3. Endevco Model 22 lightweight accelerometer (1)	5
4. Endevco Model 2E3 accelerometers (14)	5,7
5. Charge amplifiers (3)	3
6. Elastic Suspension Cords (bungee cords) and Safety Cables (2)	6,7

Photographs of the rotor and case test apparatus and configuration are given in Fig. 3 through 7.

ROTOR ANALYSIS AND TESTING

ROTOR ANALYTICAL MODEL

An analytical, finite element rotor model was developed under previous contract (NAS3-21008/ NASA Report CR-159821, pp. 179, 183-189). This model consists of 59 modes and 67 beam elements. Figure 8 shows the model configuration and the load-line diagram from which rotor stiffness is developed. Because the one objective of the modal testing was to verify the accuracy of the model, the rotor was analyzed in a free-free condition (without bearings or supports) and at zero-spin (no gyroscopic effects) for frequencies and mode shapes. These results were compared to modal test results for correlation. Adjustments can then be performed on the model to make predicted results more accurate, if required.

ROTOR MODAL TESTING

Several basic considerations guided the design of the rotor modal test technique. Foremost in any test is the assurance of test integrity. In modal testing, this means verification of the basic assumptions of the modal analysis method. Important among these assumptions is that of a linearly elastic structure or "reciprocity." Therefore, before the acquisition of measurements, pretest reciprocity checks are required. Another consideration is that of matching analysis and test conditions so that results can be compared. Since free-free conditions were required, and given the very light weight of the rotor, a very flexible suspension would be required. This would ensure that rigid-body modes have frequencies far below that of the first structural mode and thus not affect test data.

Because of rotor axisymmetry, general bending modes could be described by a single-plane survey requiring a relatively few axial measurement stations. Other stations could be assigned to disk locations to monitor their effect on the dynamics of the rotor. With these considerations in mind, the procedure described below was used.

The Mark 48F rotor was assembled as closely as possible to test conditions present during pump tests in which the resonance had been observed. This included matching the rotor assembly load (i.e., axial preload) including ball bearing inner races. Checks were made to assure no loose fits existed which might buzz in test and thus introduce non-linearities in data. The rotor was instrumented with two accelerometers located 90 degrees apart, midway between the first and second stage turbines. This allowed the experimentors the option of moving the hammer along the grid while response position remained fixed. The rotor was then taken to the Analog Room facility and suspended for test. Figures 3 and 4 show the resulting test configuration. The rotor was suspended from the ceiling of the facility by web straps in series with heavy rubber bands to produce a very low frequency suspension. Safety ties with slack were used as shown. Next, a series of reciprocity checks were performed to evaluate elastic linearity of the rotor. These were done by affixing a roving accelerometer a given location A, striking the rotor at another location B and obtaining

a transfer function from B to A. Input and response locations were then switched and the A to B transfer function was obtained. Comparison of gain, phase and coherence for the two measurements quickly evaluated the degree of linearity. By moving measurements axially outboard to inboard, a nonlinear region of the rotor was identified. The region where this occurs is shown in Fig. 5. Examination of a rotor cross-section drawing reveals that there is an axial discontinuity in the structure just below the pump-end bearing inner race at the location where the nonlinearity is noted. As such, this portion of the rotor is somewhat free to pivot. Further along there is a washer which also provides some axial discontinuity between the speed nut and tie-bolt stretch nut. These two features account for the observed behavior. In test, measurements were not taken in this nonlinear region. Several trial runs were then made to obtain measurements and evaluate the best technique and measurement locations. The final test resulting from these evaluations used 14 axial stations and 10 radial stations, two on each disk, for a total of 24 measurement locations. It was decided to take measurements by roving the lightweight Model 22 accelerometer and striking the rotor radially just downstream from the third-stage impeller. Each input and response was digitally sampled in the time domain and stored in computer memory. Because of the short period impulse required for excitation, a rapid sample rate was required. Time history plots for each measurement were evaluated to assure validity. The stored, digitized data were transformed from the time domain to the frequency domain. Five valid measurements thus obtained were averaged and a multidegree of freedom curve fit was performed to describe the average. This curve fit represents the input and output frequency response functions. The transfer function is obtained by dividing the input transform into the response transform to obtain plots of gain and phase. Typical gain and phase plots from the rotor test are given as Fig. 9 and 10. A coherence plot may also be produced and is used to indicate how much the measured response is due to the input. A coherence of 80% or greater indicates a good relationship and a valid measurement.

After valid transfer functions were obtained for each measurement point, the modal analysis system was used to normalize the functions and specify the relative gain and phase at each measurement point on the structure. This information could be graphically displayed and animated at the graphics terminal when the operator assigned definitions for the degree of freedom of the measurement. Thus, an animated mode shape is produced. Estimates of modal damping, mass and stiffness obtained from analysis of transfer function gain and phase are also produced.

RESULTS OF ROTOR ANALYSIS, TESTING AND COMPARISONS

The results of the rotor analysis and testing are given in the following tables and figures:

1. Table 1. Modal Test Results for Free-Free Rotor
2. Figure 11. Mark-48F Rotor, First Bending Mode Shape From Impact Testing
3. Figure 12. Mark-48F Rotor, First Torsional Mode Shape From Impact Testing

4. Figure 13. Mark-48F Rotor, Second Bending Mode Shape From Impact Testing

5. Table 2. Rotor Modal Test Analysis/Frequency Comparison

6. Figure 14. Free-Free, Zero Spin Rotor Rap Test/Analysis Mode Shape Comparison

Table 1 presents the modal test results for a free-free rotor along with the developed modal parameters of mass, stiffness, and damping. The three natural frequencies given correspond with the mode shapes presented in Fig. 11, 12 and 13. It should be noted that a torsional mode was indicated from the test data at 1251 Hz (75,060 rpm) along with the first and second bending modes at 638 Hz (40,980 rpm) and 1721 Hz (103,260 rpm). Table 2. presents the comparison of modal test to analytically predicted natural frequencies for the two bending modes. The results show a very good comparison between the analytical prediction and the test results. The comparison of the first and second bending mode shapes between calculated model prediction and the measured test results also show good agreement in Fig. 14.

DISCUSSION OF ROTOR CORRELATIONS

The percent differences indicated in Table 2 and the mode shape comparison of Fig. 14 indicate excellent correlation of the rotor model with modal test results. As such, the use of the rotor model in the modal superposition process should introduce virtually no error in the final analysis of the turbopump and may be used with confidence.

CASE ANALYSIS AND TESTING

CASE ANALYTICAL MODEL

An analytical, finite element model of the Mark 48F case was developed during this contract as part of Task 1 using the STARDYNE computer code. This Computer Code is an automated finite-element program for dynamic structural analysis. It is capable of natural frequency and response analysis including transient, random and steady state conditions. The program is available for use on the CDC® 6600 Computer Systems. *(See Footnote). The model is very detailed and contains 624 nodes, 592 quadrilateral plate elements, 12 triangular plate elements, 20 elastic beam elements, 45 rigid beam elements, and has 3288 dependent or 168 dynamic degrees of freedom. Figures 15, 16 and 17 give views of this model. Structural features included in the model are the entire external case structure, pump end and turbine end internal case structures, LIMA test facility test configuration turbine inlet duct and midcase beam elements representing third stage impeller/ volute section properties. Internal case weights for pump crossover ducts and turbine end components which contribute no sifnificant stiffness have been distributed around external case nodes. Bearing support structures have been modelled in detail (Fig. 16 and 17) to facilitate later modal superposition of rotor and case. As was done with the rotor, frequencies and mode shapes were produced for free-free conditions for correlation with modal test results. Several iterations were required with the case model incorporating minor structural modelling changes before the final correlated model was achieved.

The three basic changes were:

1. Incorporation of turbine end internal case structure to reflect the available load path through the first-stage stator

2. Adjustment of section properties of mid-case beam elements to correct values

3. A sensitivity study of turbine inlet duct connection features; original features were retained.

Once these changes were incorporated and good correlation with modal testing was obtained, pump tie-down features were modelled per the test configuration. These features consisted of trunnion attachments and inlet and exhaust ducting for the pump and turbine. Load carrying capability for each connection was retained in the model consistent with the actual hardware. Effective masses due to each connection were lumped at appropriate nodes based upon first mode of vibration for pump inlet and exhaust ducting and static analysis for turbine

---

*The computer program STARDYNE was originally developed by Mechanics Research Inc. (MRI) of Los Angeles, California. STARDYNE is now maintained and developed by System Development Corporation of Santa Monica, California. It is available for use to any customer on CDC® 6600 Computer Systems operated by Control Data Corporation (CDC) CYBERNET® Service and Data Services/International.

exhaust ducting. Ducting stiffnesses were generally quite low and thus a duct's main effect was due to its mass. Stiffnesses which were found to be significant were added in the modal superposition stage. Frequencies and mode shapes were then generated for this configuration model for use in the modal superposition program.

The analytical model of the case yields a total of sixteen dominant frequencies and mode shapes up to 3200 Hz. The results of the analysis are given in the following figures:

1. Figure 18. Mark 48F Case, Free-Free Analytical Mode Shape for Structural Mode 1, 247 Hz

2. Figure 19. Mark 48F Case, Free-Free Analytical Mode Shape for Structural Mode 2, 336 Hz

3. Figure 20. Mark 48F Case, Free-Free Analytical Mode Shape for Structural Mode 3, 537 Hz

4 Figure 21. Mark 48F Case, Free-Free Analytical Mode Shape for Structural Mode 4, 798 Hz

5. Figure 22. Mark 48F Case, Free-Free Analytical Mode Shape for Structural Mode 5, 906 Hz

6. Figure 23. Mark 48F Case, Free-Free Analytical Mode Shape for Structural Mode 6, 1010 Hz

7. Figure 24. Mark 48F Case, Free-Free Analytical Mode Shape for Structural Mode 7, 1339 Hz

8. Figure 25. Mark 48F Case, Free-Free Analytical Mode Shape for Structural Mode 8, 1400 Hz

9. Figure 26. Mark 48F Case, Free-Free Analytical Mode Shape for Structural Mode 9, 1418 Hz

10. Figure 27. Mark 48F Case, Free-Free Analytical Mode Shape for Structural Mode 10, 1621 Hz

11. Figure 28. Mark 48F Case, Free-Free Analytical Mode Shape for Structural Mode 11, 1747 Hz

12. Figure 29. Mark 48F Case, Free-Free Analytical Mode Shape for Structural Mode 12, 1769 Hz

13. Figure 30. Mark 48F Case, Free-Free Analytical Mode Shape for Structural Mode 13, 2313 Hz

14. Figure 31. Mark 48F Case, Free-Free Analytical Mode Shape for Structural Mode 14, 2410 Hz

15. Figure 32. Mark 48F Case, Free-Free Analytical Mode Shape for Structural Mode 15, 2521 Hz

16. Figure 33. Mark 48F Case, Free-Free Analytical Mode Shape for Structural Mode 16, 3071 Hz

In the figures given, the free-free structural mode shapes are individually presented for each of the natural frequencies predicted by the analytical model. The mode shapes are shown in the casing meridional view and the deflections are exaggerated to provide perspective. The coordinate X1 represents the axial direction for the turbopump. The X2 and X3 represent the plane normal to the turbopump axis (X1 axis). Note the mode shapes include those of the turbine inlet duct welded onto the casing.

CASE MODAL TESTING

The same considerations regarding test integrity apply for the case modal test as did for the rotor. Several differences may be cited in the testing of the case, however. First, the Mark 48F case is a very complex structure containing many asymmetric features. As structure complexity increases, the certainty of modal test measurements and the results obtained from them decreases. This is because there are likely to be many more nonlinearities associated with a more complex structure. Modal test tools assume linear behavior. Thus, a basic assumption of the method can be violated. The analyst must, therefore, either quantify nonlinearities or associate less certainty with results obtained from testing of complex structures. Another difference is that the case is much heavier than the rotor and requires a stiffer suspension for simulation of free-free conditions with stability.

Mark 48F case components were instrumented with internal casing accelerometers prior to final assembly. The purpose of this was to obtain transfer functions between internal case bearing and seal locations and points radially outward on the exterior of the case. Stiffness and damping additions could be applied to the model using transfer functions if such additions were found to be significant. A triaxial accelerometer block was also affixed to the case exterior at the turbine exit flange. These accelerometer locations are shown in Fig. 34. The case was then assembled ensuring that no loose fits existed. After assembly and inspection were complete, the case was taken to the Analog Room where it was suspended as shown in Fig. 6 and 7. The bungee cords provided a low frequency suspension and were mechanically safety tied with cables as shown.

Testing of the casing was subdivided into three test series. First, checks were performed on axial and radial reciprocity. Results indicated good linearity axially and fair linearity radially. These results imply that gross bending modes of the case obtained from a modal test will be good while the hoop modes (generally referred to as breathing modes) obtained are less certain. This was considered in the analysis of results and during model correlation. The second test series was for obtaining the internal case transfer functions. The final series was to perform the actual modal survey of the case.

A grid of 60 measurement points was selected to describe the modes of the case. A plot of these 60 points is given as Fig. 35. Radial positions are assigned a constant value so that sections of flexure may be easily identified. In this test, it was found to be most convenient to have the response location remain fixed while the hammer impact was roved over the grid. Response was measured radially by a fixed accelerometer at the turbine exit duct. All impacts were applied radially to the grid. A typical transfer function gain for the casing test is given as Fig. 36. Those points where case response amplitude increases represent natural frequencies of the casing. The same test procedure was followed in the acquisition and reduction of data for the case as was followed for the rotor test. Frequencies, mode shapes, and modal parameters were obtained for predominant modes and special modes of interest from 0 to 2500 Hz. Because of its large mass and likely effect on case dynamics, several transfer functions were also obtained from the turbine inlet duct to aid in the correlation phase.

The results of the modal testing were completed and various natural frequencies and mode types have been tabulated in Table 3. The table identifies the mode number and type, natural frequency and modal parameters of mass, stiffness and damping.

RESULTS OF CASE ANALYSIS, TESTING AND COMPARISONS

The results of the case free-free analysis and the free-free modal rap tests on the case were compared in order to determine refinement requirements or to verify the model. The comparison of these results is presented in the following table and figures:

1. Table 4. Case Modal Test/Analysis Frequency Comparison
2. Figure 37. Mark 48F Case, Test/Analysis Mode Shape Comparison, Mode No. 4
3. Figure 38. Mark 48F Case, Test/Analysis Mode Shape Comparison, Mode No. 5
4. Figure 39. Mark 48F Case, Test/Analysis Mode Shape Comparison, Mode No. 6A
5. Figure 40. Mark 48F Case, Test/Analysis Mode Shape Comparison, Mode No. 6B
6. Figure 41. Mark 48F Case, Test/Analysis Mode Shape Comparison, Mode No. 12
7. Figure 42. Mark 48F Case, Test/Analysis Mode Shape Comparison, Mode No. 13
8. Figure 43. Mark 48F Case, Test/Analysis Mode Shape Comparison, Mode No. 15

9. Figure 44. Mark 48F Case, Test/Analysis Mode Shape Comparison, Mode No. 16

10. Figure 45. Mark 48F Case, Test Mode Shape for an Uncorrelated Mode

11. Figure 46. Mark 48F Case, Test Mode Shape for Minor Resonance at 1543 Hz (Special Analysis)

The comparison of the casing modal analysis to test data frequencies are given in Table 4. The difference between analysis and test are made for comparison purposes and indicate variations between predicted and test frequencies of up to 14% in the turbopump operating range. These differences between the analytic model and the test values are relatively good in relation to the complexity of the turbopump casing model. Comparisons of test to calculated values were used to fine tune the analytical model. This improved the accuracy of the component rotor and casing models to the final differences indicated by Table 4. Comparison of the individual finalized mode shapes between the analytical and the test model were developed and are presented in Fig. 37 to 44. In the analysis of the gross bending modes, it is convenient to present a turbopump case cross-section which is a projection of the grid on a meridional view. The measured data points are only assigned radial degrees of freedom. The mode shape comparisons presented in Fig. 37 to 44, therefore, show a section view of modal test results which is the same view as the projection of the analytical models meridional plane (X3-X1 plane). This plane contains and is normal to the turbopump axis (X1 axis). The experimental mode shape of the casing is given for both the upper and lower boundary of the casing.

An experimental mode shape was found at 2454 Hz on the case which did not have a corresponding calculated mode shape from the analytical mode. The mode shape indicates a hoop mode or breathing mode occurs on the pump inlet. This mode is given in Fig. 45. An additional minor resonance condition on the casing was found in testing. This response is located at the 1543 Hz level and is correlated to an analytically predicted mode at 1418 Hz in Fig. 46. It is relatively minor in amplitude as evidenced in the casing response shown in Fig. 36 but is apparent in both model and test results.

DISCUSSION OF CASE CORRELATIONS

The percentage differences indicated in Table 4, and the Test analysis mode shape comparisons of Fig. 37-44, and 46 indicated very good correlation of the free-free case model was obtained for frequencies up to 2200 Hz. The higher percent error for modes 15 and 16 is attributed to the breathing nature of these modes and their localization at the flange areas. These flanges were not modelled in great detail (i.e., with exact geometry and holes) and therefore may predict different frequencies than measured from actual test. However, correlation for these modes is fair and should not affect results in predicting predominant casing modes in the 1500 Hz region of interest. Use of this case model should, therefore, introduce little error in the modal superposition process and may be used with confidence.

MODAL SUPERPOSITION ANALYSIS

TURBOPUMP ANALYTICAL MODEL

One rotor and case free-free condition models were correlated, the generation of the modal superposition model for the entire turbopump at test facility conditions was possible. This was done using the in-house modal superposition computer program. This program is a Rocketdyne developed program called NEWSUP. The program was developed for modal superposition of turbomachinery rotors and casings. It includes capability for varying coupling element (bearings and seals) stiffness and damping as a function of pump speed. Damped critical speeds as a function of pump speed are output as shown in Fig. 47. Rotor stability may also be analysed with this program. Effective weights due to connection ducting were determined and lumped at the appropriate nodes in the STARDYNE casing model. Mode shapes and frequencies were generated for this model. These were then input with free-free rotor mode shapes and frequencies into the superposition program. Rotor and case were connected by stiffness additions of 5.254×10^7 N/m (300,000 lb/in.) at each bearing. This value has been derived by calculations extending the general theory of reference 1 and has been substantiated by Rocketdyne dynamic test and analysis correlations. Seal coupling forces were investigated, but found to be insignificant. Ducting effective stiffnesses and trunnion mount connection stiffnesses (pump to ground) were also added. This model was run to produce turbopump natural frequencies and mode shapes as a function of pump speed (to account for any speed dependent characteristics such as gyroscopic forces, speed dependent spring rates, etc.). The final results are presented on the predicted speed dependent natural frequency and interference plot of Fig. 47. A summary of the Natural Frequencies of the turbopump for the LIMA test facility configuration is given in Table 5. These natural frequencies are identified as they intersect the synchronous frequency line on Fig. 47.

RESULTS OF MODAL SUPERPOSITION ANALYSIS

The results of the modal superposition analysis for three specific modes in the frequency range of 1540 Hz have been summarized in the following figures:

1. Figure 48. Mark 48F Turbopump Model, LIMA Configuration at 95,000 rpm: Predicted Rotor Mode Shape for Mode at 1338 Hz

2. Figure 49. Mark 48F Turbopump Model, LIMA Configuration at 95,000 rpm: Predicted Case Mode Shape for Mode at 1338 Hz

3. Figure 50. Mark 48F Turbopump Model, LIMA Configuration at 95,000 rpm: Predicted Relative Deflection Mode Shape for Mode at 1338 Hz

4. Figure 51. Mark 48F Turbopump Model, LIMA Configuration at 95,000 rpm: Predicted Rotor Mode Shape for Mode at 1587 Hz

5. Figure 52. Mark 48F Turbopump Model, LIMA Configuration at 95,000 rpm: Predicted Case Mode Shape for Mode at 1587 Hz

6. Figure 53. Mark 48F Turbopump Model, LIMA Configuration at 95,000 rpm: Predicted Relative Deflection Mode Shape for Mode at 1587 Hz

7. Figure 54. Mark 48F Turbopump Model, LIMA Configuration at 95,000 rpm: Predicted Rotor Mode Shape for Mode at 1783 Hz

8. Figure 55. Mark 48F Turbopump Model, LIMA Configuration at 95,000 rpm: Predicted Case Mode Shape at 1783 Hz

9. Figure 56. Mark 48F Turbopump Model, LIMA Configuration at 95,000 rpm: Predicted Relative Deflection Mode Shape for Mode at 1783 Hz.

These figures identify the three component shapes for the rotor, the casing, and the relative deflection between rotor and casing for each of the three modes presented. In order to understand the representations of the given mode shapes an explanation follows.

Rotor Group Mode Shape

The rotor group mode shape illustrations of Fig. 48, 51, and 54 show the orbits of the rotor centerline at six axial stations. These orbits are generally elliptical having major and minor axis oriented identically in phase. The line shown connecting the orbits is the rotor centerline at a given instant in time. At a later instant in time, the centerline will move to a new location in each orbit defined by a singular angular change about the pump axis (X1).

Casing Group Mode Shape

The casing group mode shape illustrations of Fig. 49, 52, and 55 may be interpreted the same way as those of the rotor. The line connecting the orbits represents the actual centerline of the casing at any instant of time.

Relative Deflection Mode Shape

The rotor and casing group mode shapes represent normalized, absolute mode shapes with respect to the coordinate system. The relative deflection mode shapes presented in Fig. 50, 53 and 56 are merely the difference between the rotor and casing mode shapes at an instant in time. It may be roughly visualized as relative radial displacement between rotor and case centerlines. The line connecting the patterns at each station is then a plot of relative deflection between rotor and case centerlines as a function of axial station. At a later instant in time, the line has shifted to a new location on each pattern defined by a single angular change about the pump axis (X1). In viewing these figures, it is important to realize that as plots of relative deflection, they do not represent the motion of an individual pump component.

DISCUSSION OF RESULTS

The objective of this analysis effort was to develop an advanced more accurate method of dynamic analysis for high speed turbomachinery. This method was to use currently available computer analysis tools and test procedures. The Mark 48 Fuel turbopump was to be used as a model with the objective of identifying the cause of high-speed vibration characteristics on the turbopump and recommendation of a remedy to correct the problem.

The results of the independent rotor and case analysis have indicated that both analytical models correlated very well with modal test results and could be used with confidence in the formulation of a complete turbopump model via the model superposition method. Since the method has been well established as reliable when basic assumptions are preserved as in this analysis, confidence can be expressed in the validity of the results obtained. The basic assumptions required were defined in the test method description.

Given that a ±15% criterion is reasonable in the prediction of potential problem modes at 95,000 rpm, any modes predicted between 80,750 and 109,250 rpm are suspect as the turbopump vibration problem. Two basic sets of data obtained from the analysis effort may be referred to in the formulation of conclusions. Foremost are those modes predicted by the modal superposition model in the aforementioned speed range. Secondly, are those highly localized case modes which appear in the free-free case analysis and cause little or no boundary condition motion. Using these criteria, the following may be cited as important results in their order of importance:

1. Figures 47, 51-53. Backward Precessional Critical Speed Indicated at 1587 Hz (95,200 rpm)

2. Figures 47, 54-56. Backward Precessional Critical Speed Indicated at 1783 Hz (107,000 rpm)

3. Figures 47, 48-50. Pump-End Case Predominant Mode at 1338 Hz (80,300 rpm)

4. Figure 27. Turbine-End Bearing Support Axial Mode at 1621 Hz (97,260 rpm)

The modal superposition analysis has indicated backward precessional modes present at 95,200 and 107,000 rpm. In this mode the rotor precesses or whirls in a direction opposite of its spin. It may also arise when structural dissymetry exists (thus, could not be predicted by the rotor model). The case of the Mark 48F is highly unsymmetric, especially at the turbine end. This dissymetry creates unsymmetric stiffness and gives rise to both backward precessional modes cited above. The mode at 1587 Hz is, therefore, a very likely candidate for the vibration problem. Next most likely is the mode at 1783 Hz.

It should be noted that generally, backward precessional modes are difficult to excite in practice. However, with the Mark 48F there is an indication that these modes can be excited. Backward precessional modes generally have a steeply decreasing natural frequency with increasing spin speed (e.g., >1000 rpm per 5000 rpm increase in speed). This phenomenon is due to the effect of the gyroscopic forces on the rotor. For the two backward precessional modes cited, however, there is only negligible decrease in frequency as speed increases (<500 rpm per 5000 rpm increase in speed). This observation indicates that the backward precessional component of motion for these modes is not predominant. Observe the flat mode lines for these modes in Fig. 47. This suggests that gyroscopic forces are not significant for the rotor. Indeed, examination of the geometry of the Mark 48F rotor intuitively bears out this conclusion. Impellers and turbine wheels are stoutly proportioned, lightweight and integral to the shaft. As such, the modes may be thought of more as a general structural vibration than as a backward precessional rotor mode and will be far easier to excite than the backward precessional modes generally predicted.

The pump-end case predominant mode at 1338 Hz is a possibility, but unlikely because of its highly localized nature. LIMA test data indicated a rise in pump-end accelerometers prior to cutoff but with the cutoff due to turbine-end levels.

The mode of the turbine end bearing support structure predicted from the free-free case model is a good possibility for the problem. Although the model is free-free, this mode occurs locally in the region where the turbine-end accelerometer was mounted and leaves boundary connections virtually motionless. The predicted frequency is probably valid for LIMA test conditions. The location of this case motion also coincides with the location of the turbine-end accelerometers in LIMA testing. Because it is the bearing support structure, rotor unbalance forces would be transmitted through this region.

The backward precession modes and the bearing support mode are all potentially damaging to the pump.

Because the precessional modes arise due to case dissymmetry and flexibility it is recommended that stiffening ribs could be incorporated on the exterior case structure between both pump inlet and impeller housing and turbine and impeller housing at stations around the circumference 120 degrees apart. This would move these modes up away from the operational speed and decrease the effect of dissymmetry upon case flexibility.

For the turbine bearing support mode, additional stiffening for the support structure is also advised to increase frequency.

Incorporation of these design recommendations should eliminate the vibration problem at 1540 Hz for the Mark 48F.

CONCLUSIONS

1. It has been shown that the conventional rotor-only dynamic analysis failed to predict all the possible vibration modes of the Mark 48F Fuel Turbopump at the high operating speeds required. This is caused in part by the influence the casing and supporting structure stiffness parameters have on the rotor-dynamics at the higher speeds and frequencies encountered. The assumption of treating the casing and support structure as rigid bodies in a rotor-only analysis at high speeds has been shown to be invalid. This does require an increased complexity in the analytical design of a high speed turbopump in order to define more accurately its dynamic characteristics.

2. The risk to future turbopump designs could be reduced if modal superposition methods were to be used in the design stages. On first build the dynamic models could be verified through modal test and analysis.

3. Very good correlation was obtained between analytical and test results of the Mark 48F rotor and case enabling the results of the modal superposition analysis to be viewed with confidence.

4. The confidence in the superposition methods validates its use to correct an existing design problem.

5. Three potential problem modes are predicted for the Mark 48F. These are rated in their order of probability in causing the 1540 Hz problem during LIMA testing as follows:

   a. A backward precessional mode at 95,200 rpm (1587 Hz)

   b. A backward precessional mode at 107,000 rpm (1783 Hz)

   c. A turbine-end bearing support mode for the case at 1621 Hz.

6. Structural modifications to the Mark 48F case can eliminate the 1540 Hz problem (see recommendations).

RECOMMENDATIONS

1. Because of complex dynamic problems encountered with high speed turbomachinery, it is recommended that casing models be incorporated with rotor models using the modal superposition method during final design stage of turbomachinery intended to operate at speeds generally above 60,000 rpm. In all designs, care should be exercised to determine if the operating conditions and turbopump design structure warrant the assumptions of the case and support structure acting as rigid bodies. In cases where the assumption is unwarranted, the modal superposition method is recommended.

2. The following recommendations are given from the analysis of the Mark 48F Turbopump in order to remedy the vibration characteristics found near the design speed:

a. In order to move backward precessional modes above the operational speed, it is recommended that stiffening ribs be applied to the exterior case of the Mark 48F between pump inlet and impeller housings and between turbine and impeller housings at circumferential stations 120 degrees apart.

b. In order to move the turbine-end bearing support structure axial mode above the operational speed, it is recommended that additional stiffening be devised for this structure.

c. To ensure that design modifications proposed will work as intended and not introduce other dynamic problems, it is recommended that analysis of the modifications be performed prior to hardware modifications.

d. Because time, budget and program capabilities did not allow, it is recommended that the modal analysis undergo the sensitivity study for inclusion of higher order modes.

REFERENCES

1. Jones, A. B., "A General Theory for Elastically Constrained Ball and Radial Roller Bearings under Arbitrary Load and Speed Conditions," ASME Journal of Basic Engineering, pp. 309-320 (June 1960).

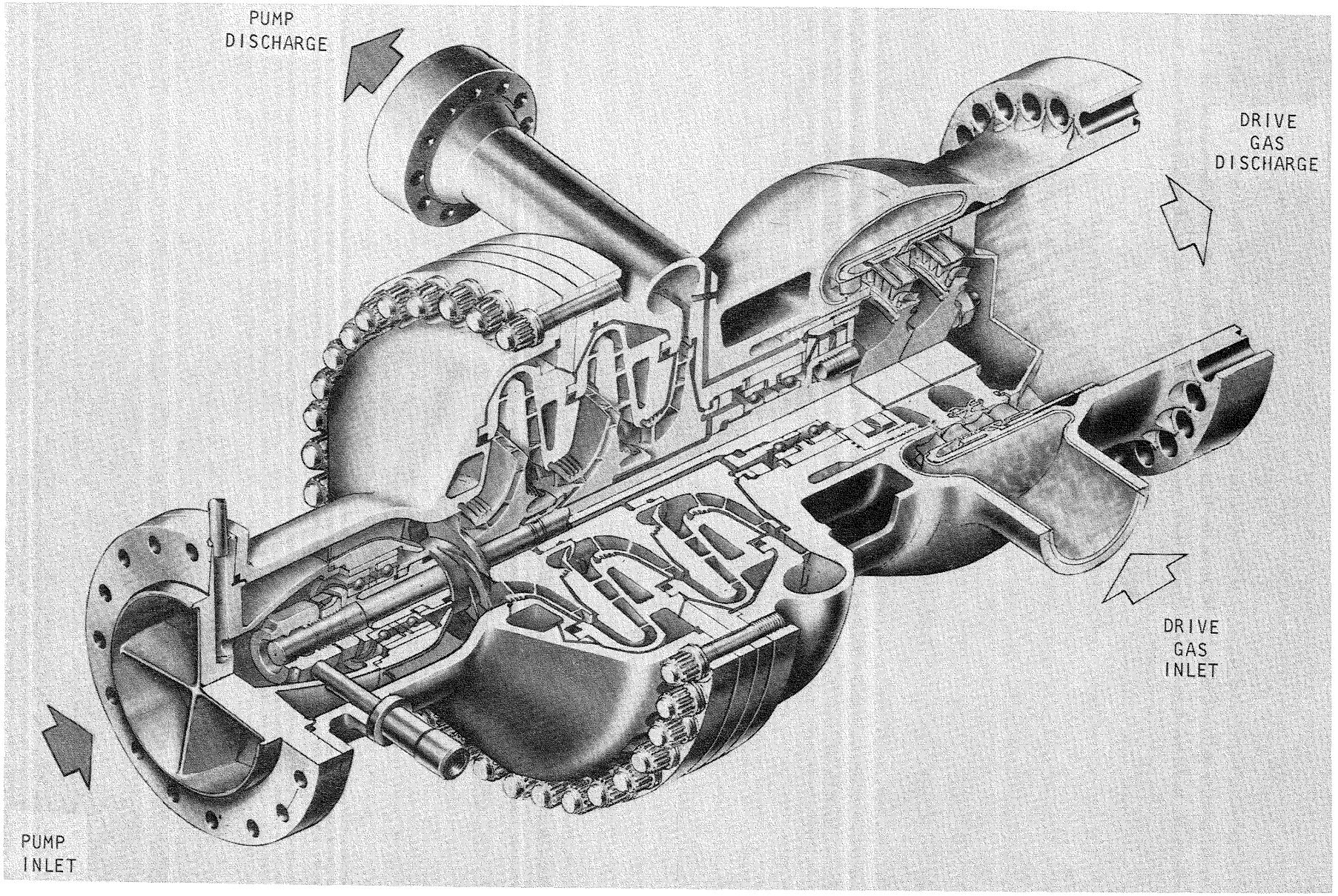

Figure 1. Mark-48 LH_2 Turbopump

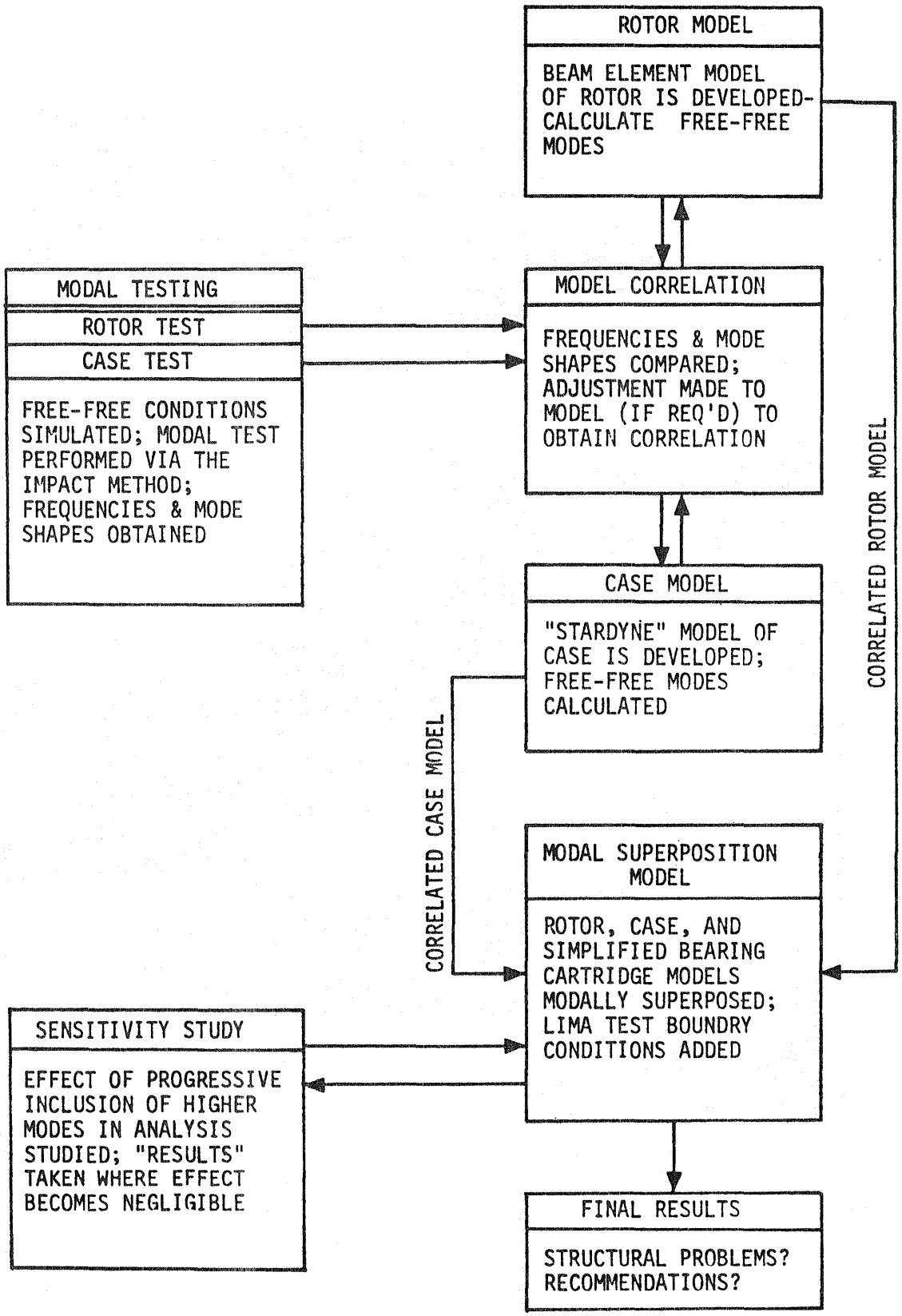

Figure 2. Mark-48F Structural Dynamic Analysis Flowchart of Overall Analysis Scheme

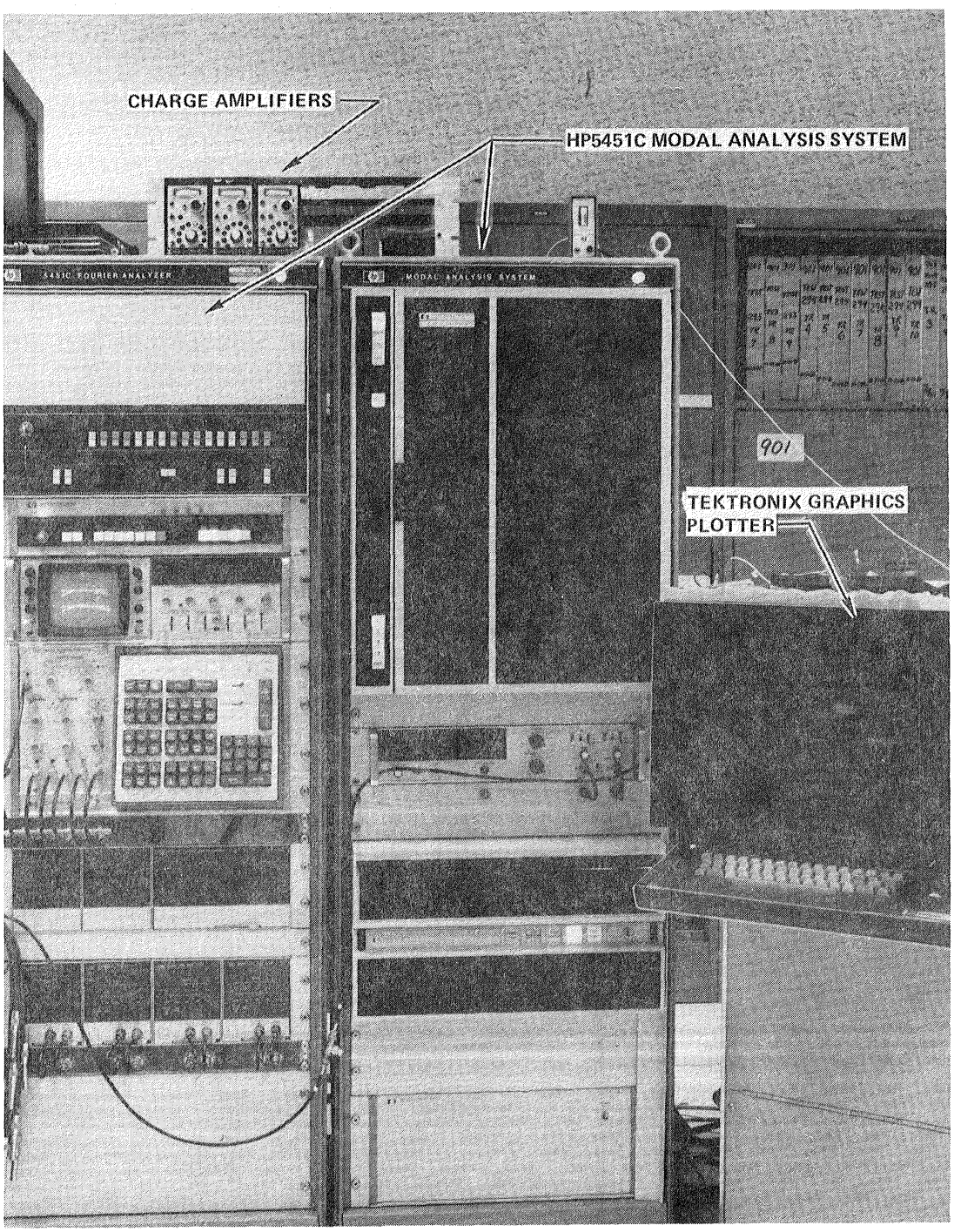

4LS31-11/24/80-C1D*

Figure 3. Mark-48F Modal Test Equipment

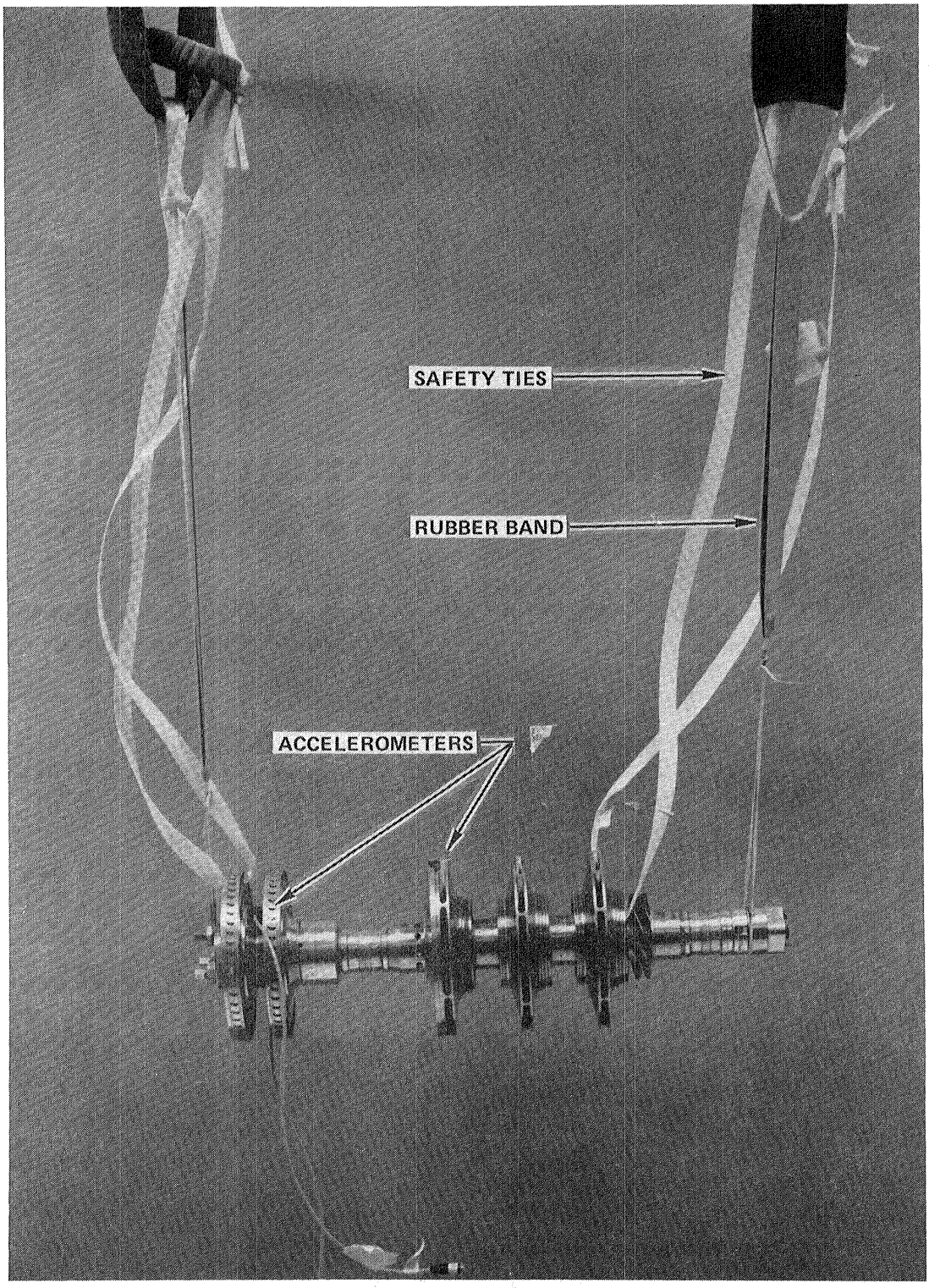

4LS31-11/24/80-C1E*

Figure 4. Mark-48F Rotor on Elastic Suspension

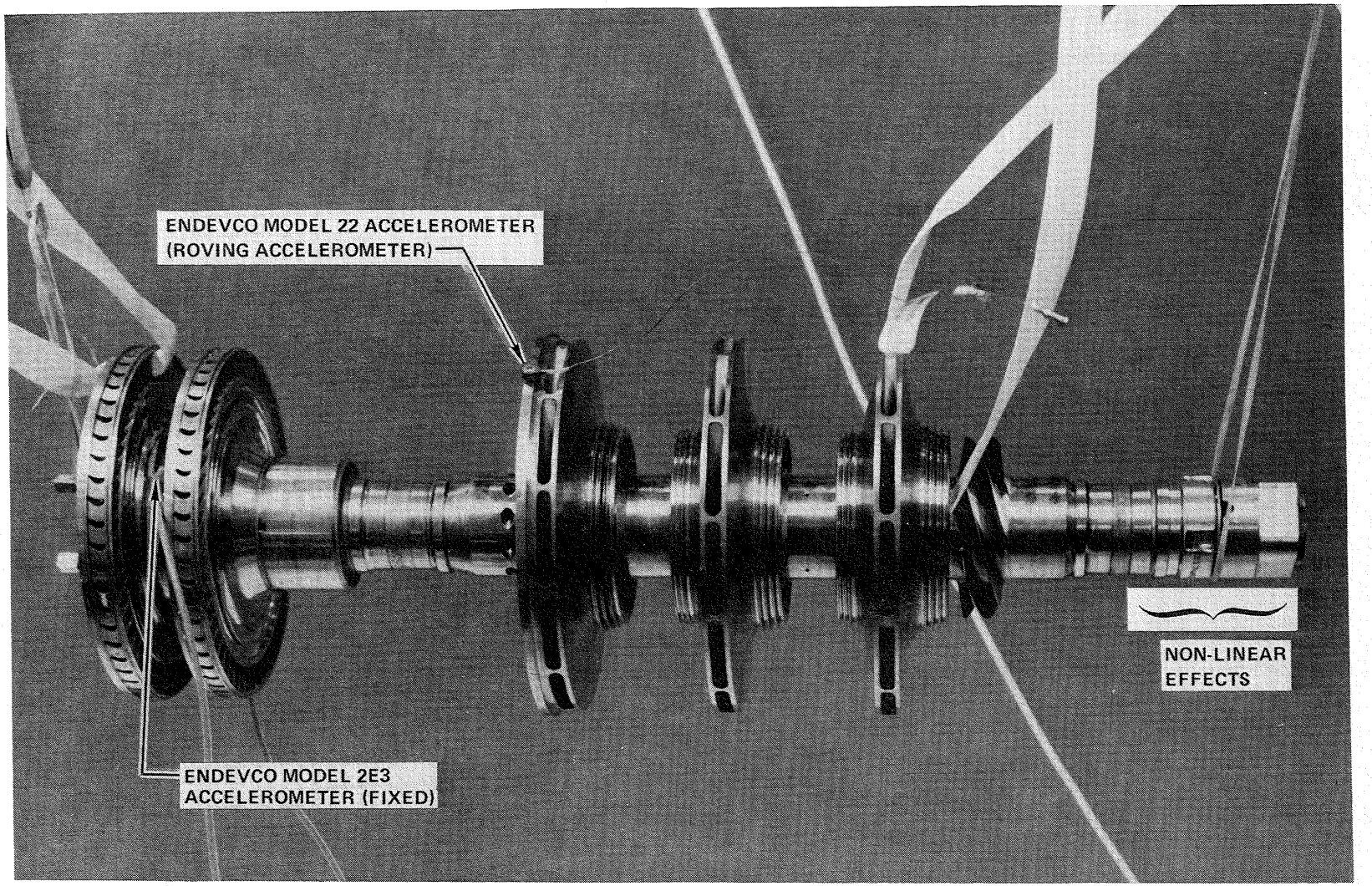

4LS31-11/24/80-C1A*

Figure 5. Close-Up View of Mark-48F Rotor in Test

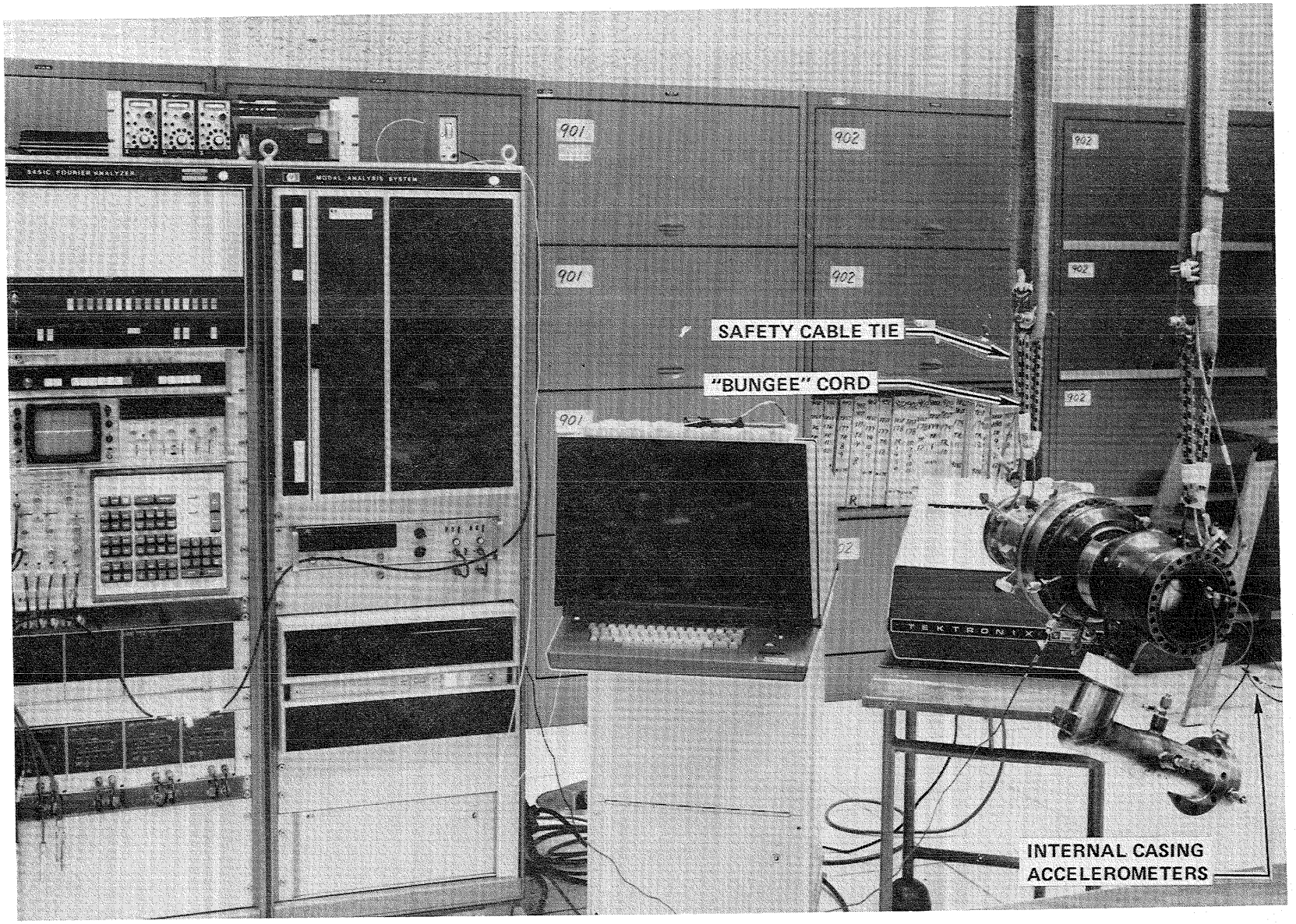

1HS56-11/5/80-C1B*

Figure 6. Mark-48F Case in Test

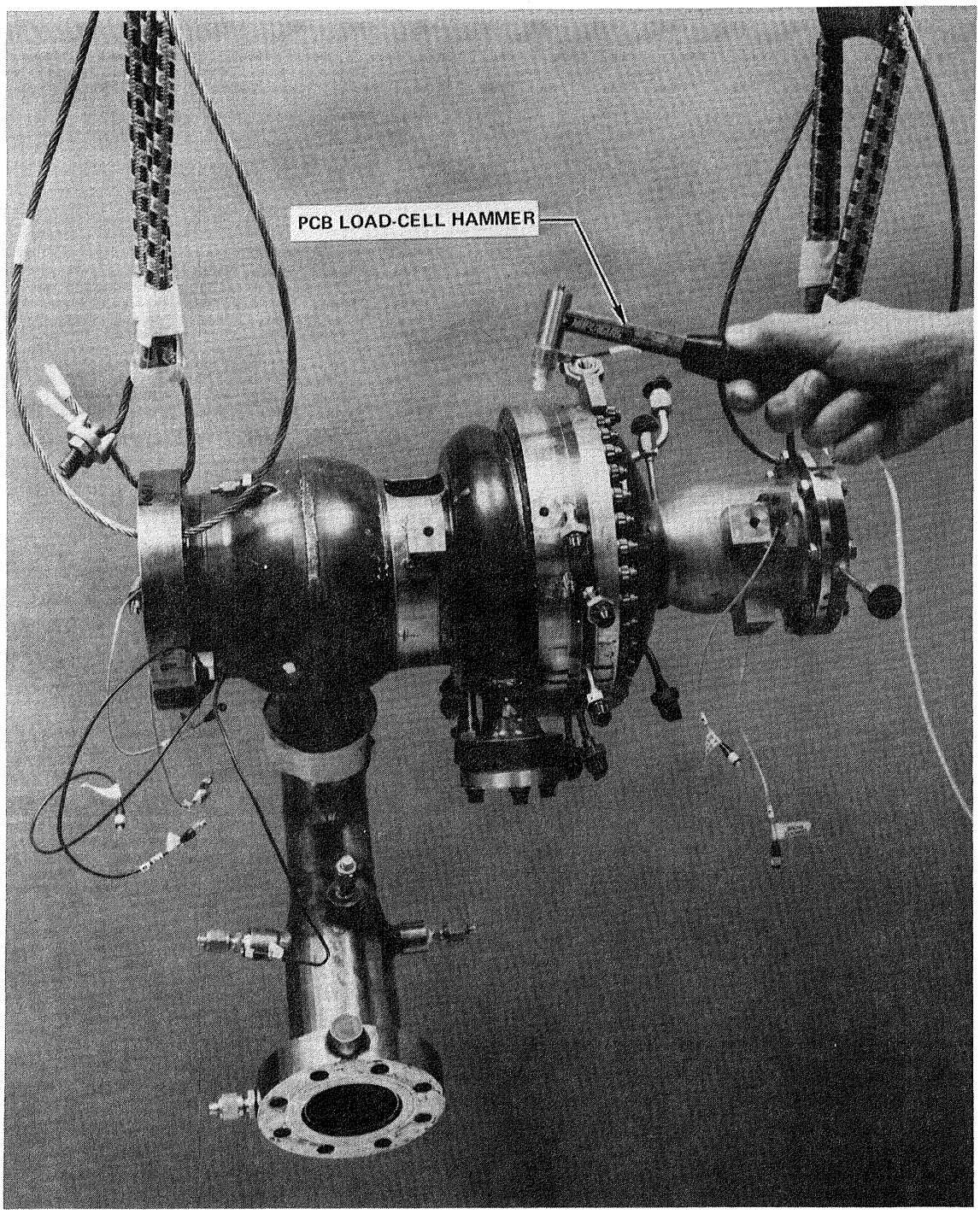

1HS56-11/5/80-C1F*

Figure 7. Close-Up View of Mark-48F Case in Test

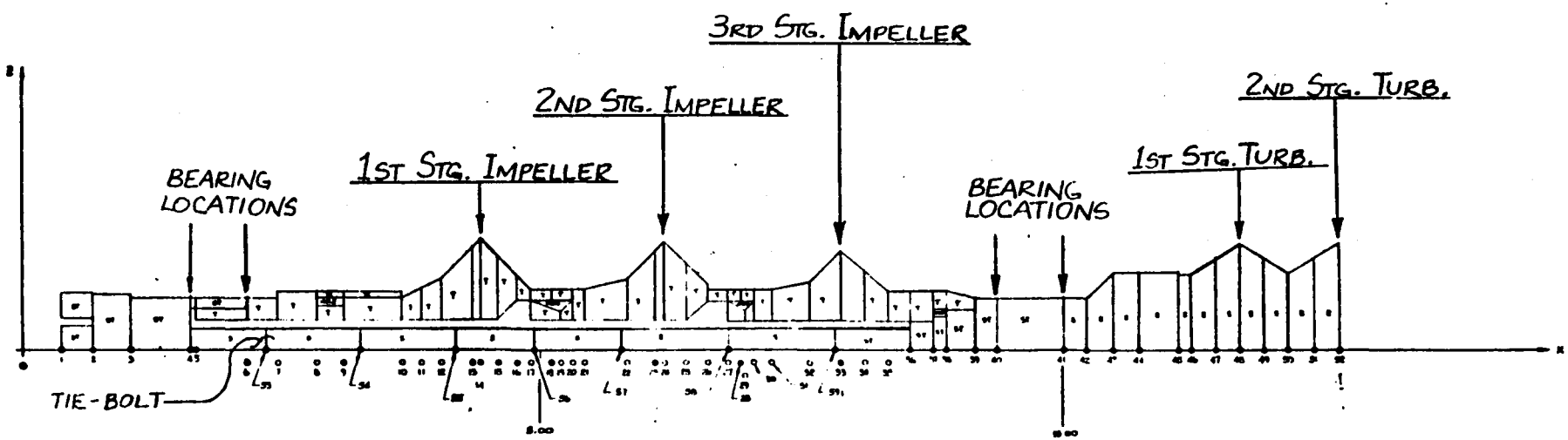

Figure 8. Mark-48F Rotor Model (Load-Line Diagram) Showing Stiffness Contribution of Rotor Components

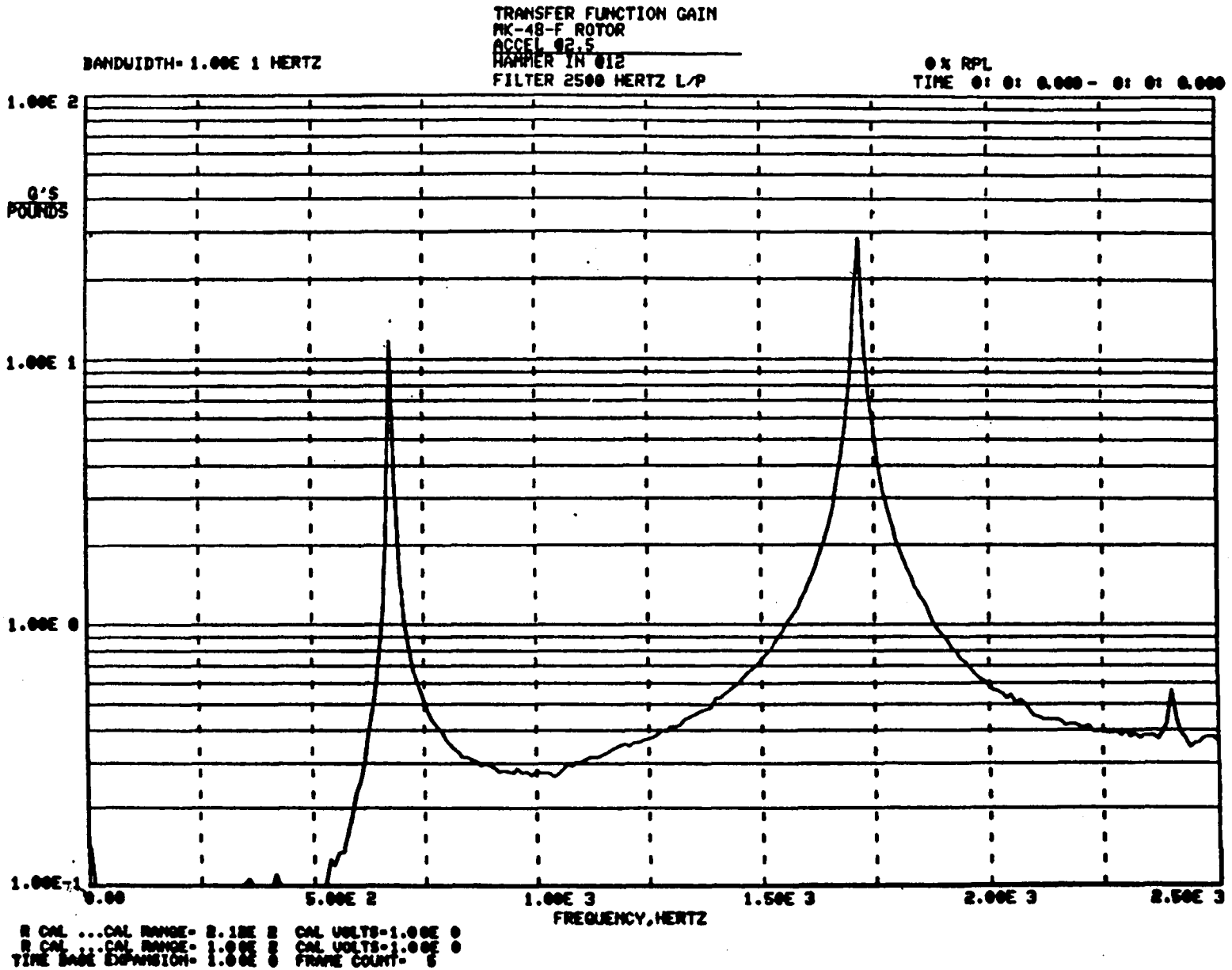

Figure 9. Typical Rotor Transfer Function Gain Plot

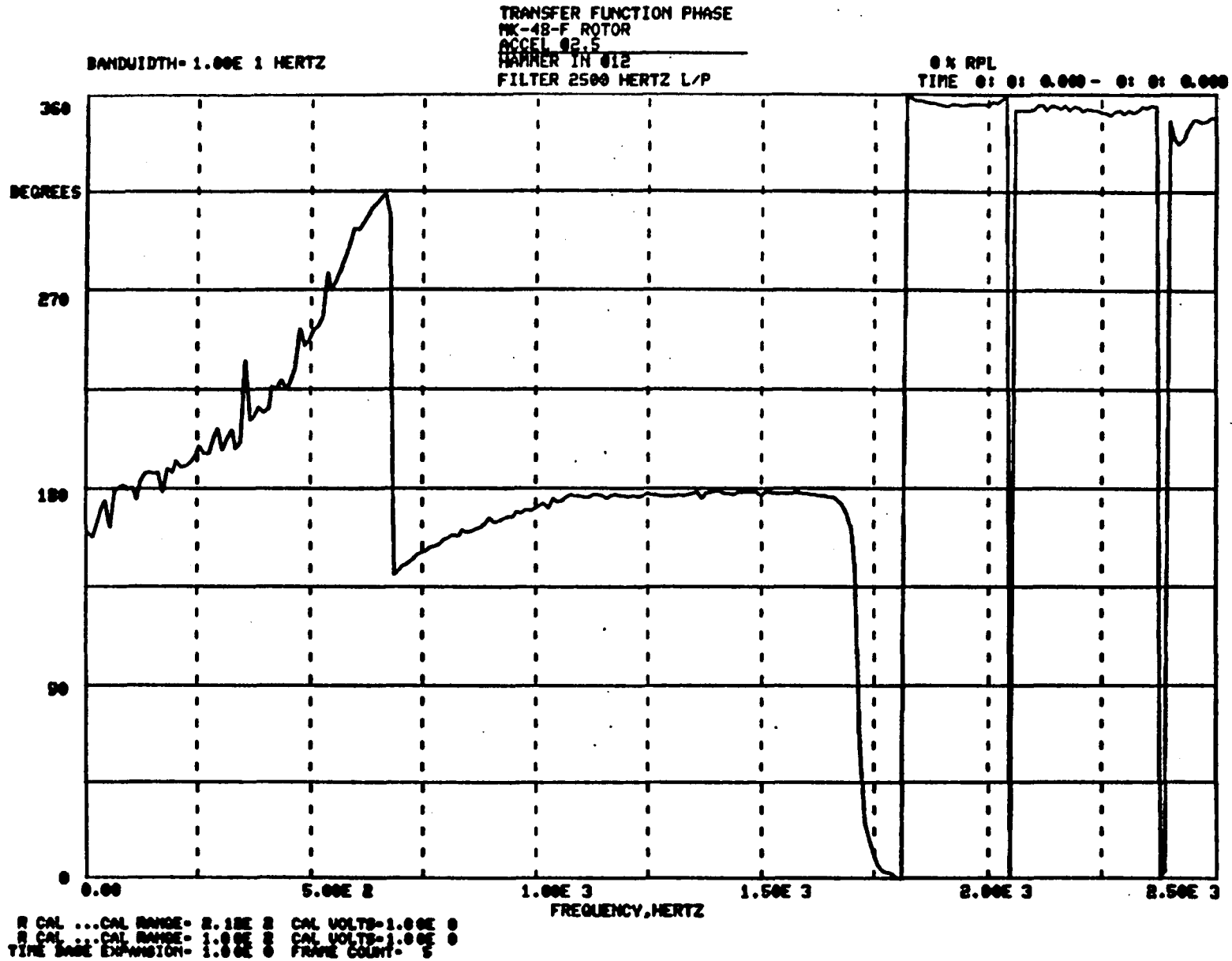

Figure 10. Typical Rotor Transfer Function Phase Plot

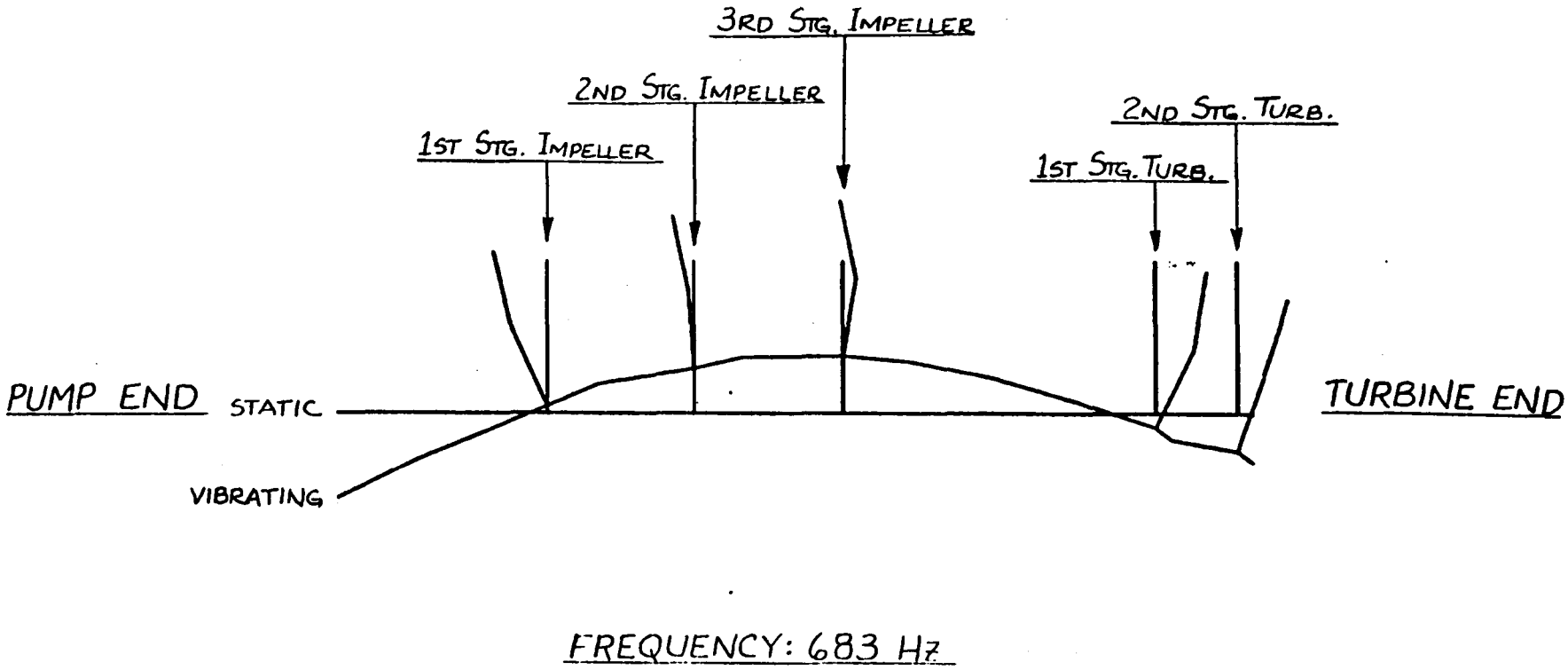

Figure 11. Mark-48F Rotor, First Bending Mode Shape From Impact Testing

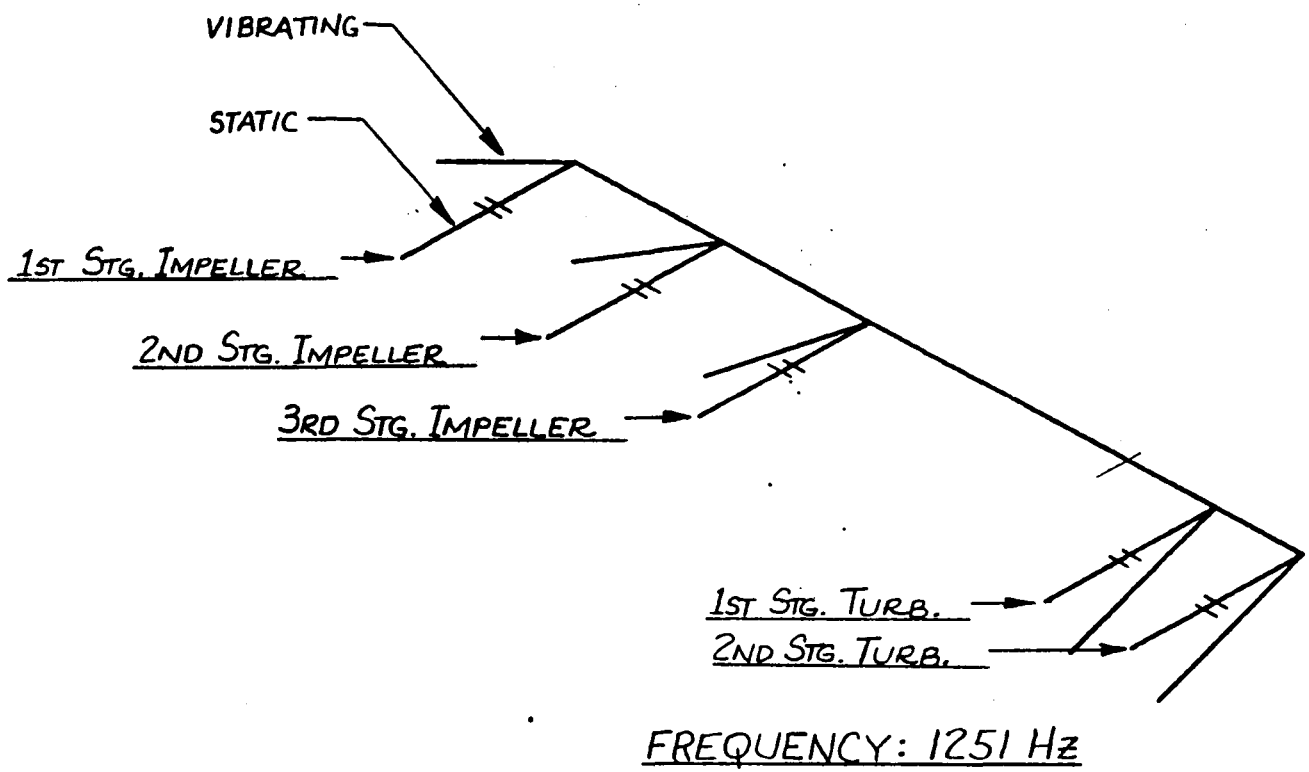

Figure 12. Mark-48F Rotor, First Torsional Mode Shape From Impact Testing

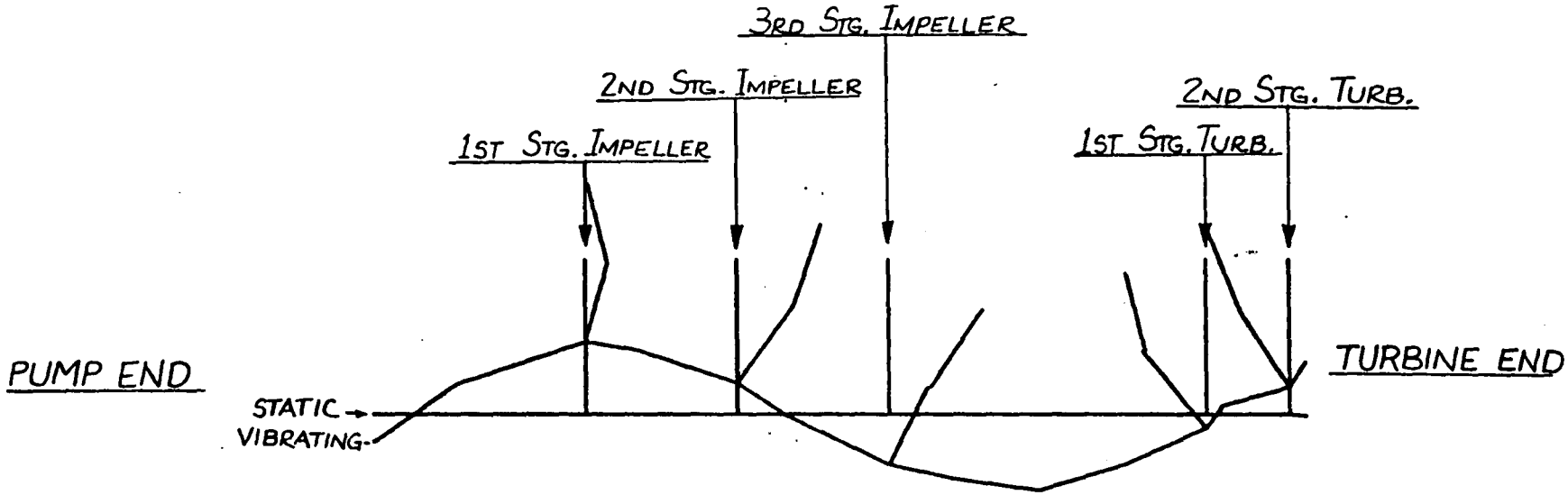

Frequency 1721 Hz

Figure 13. Mark-48F Rotor, Second Bending Mode Shape From Impact Testing

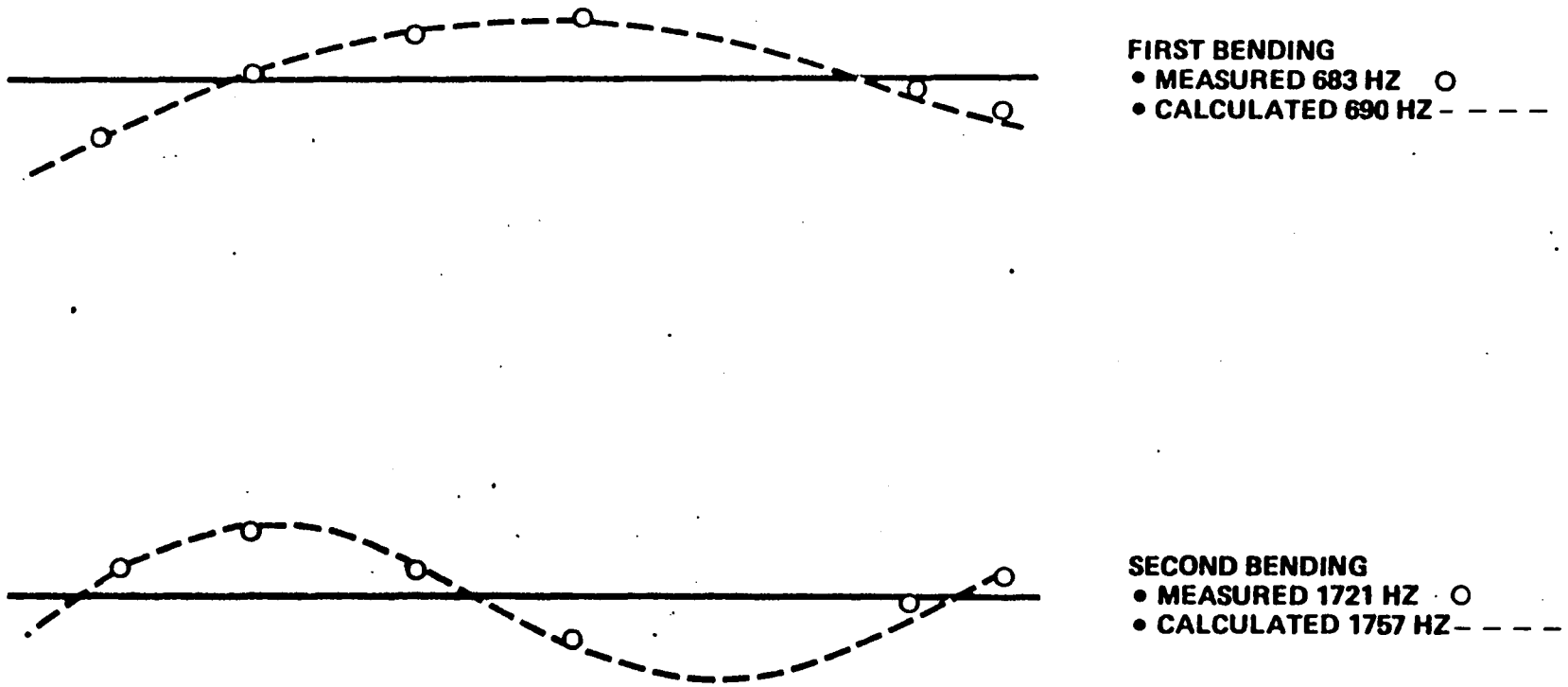

Figure 14. Free-Free Zero Spin Rotor Rap Test/Analysis Comparison

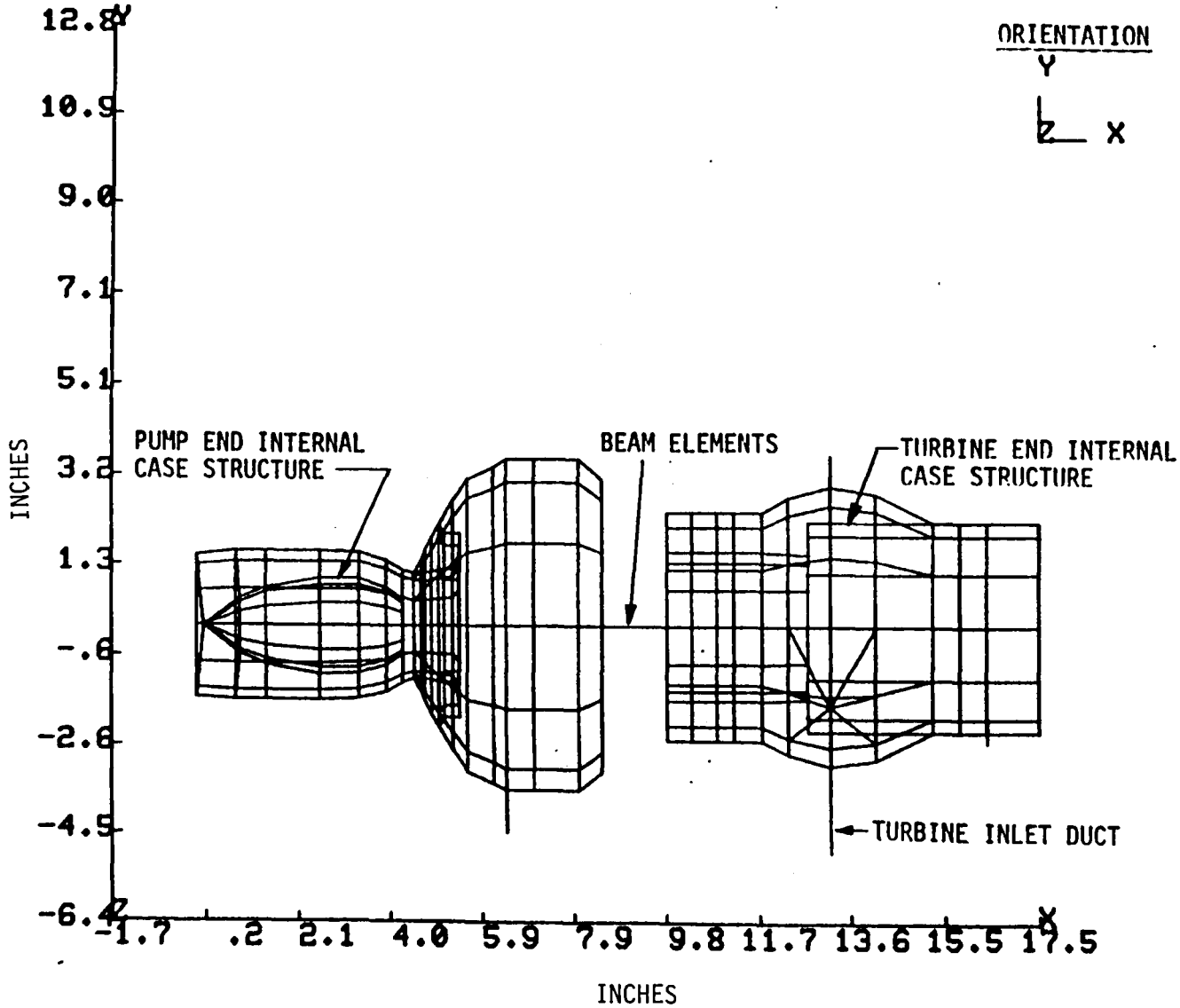

Figure 15. Mark-48F Stardyne Casing Model, View 1

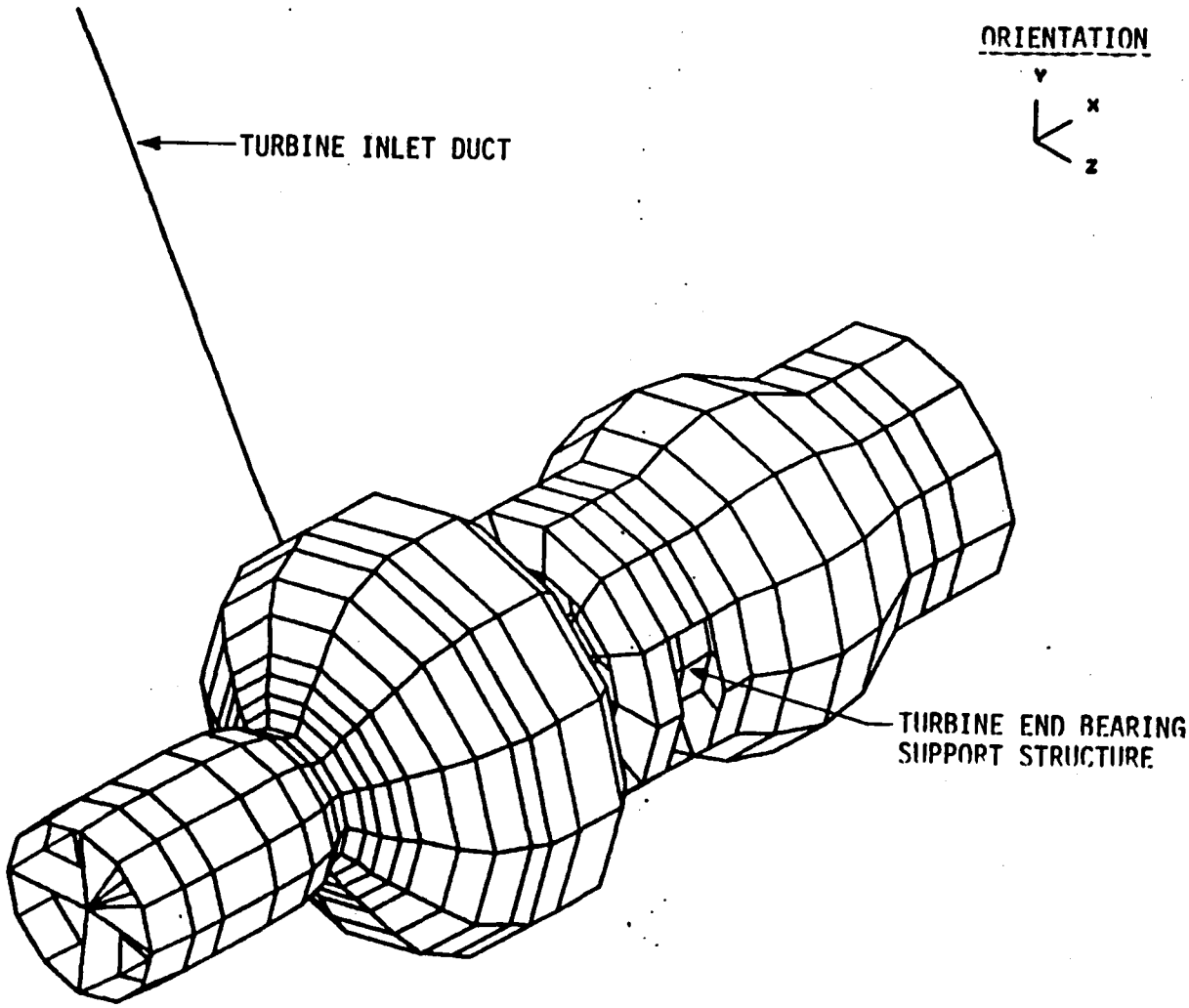

Figure 16. Mark-48F Stardyne Casing Model, View 2

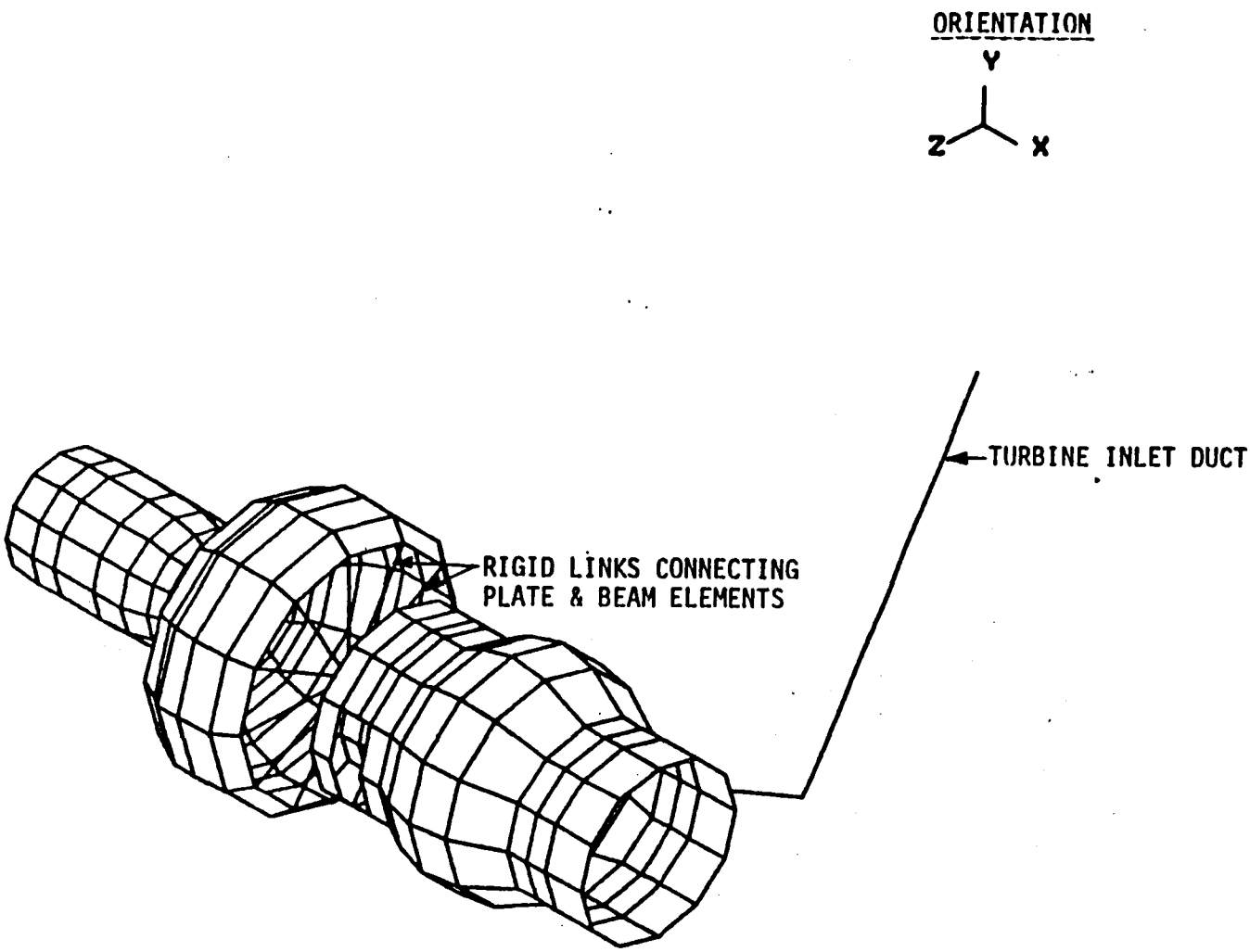

Figure 17. Mark-48F Stardyne Casing Model, View 3

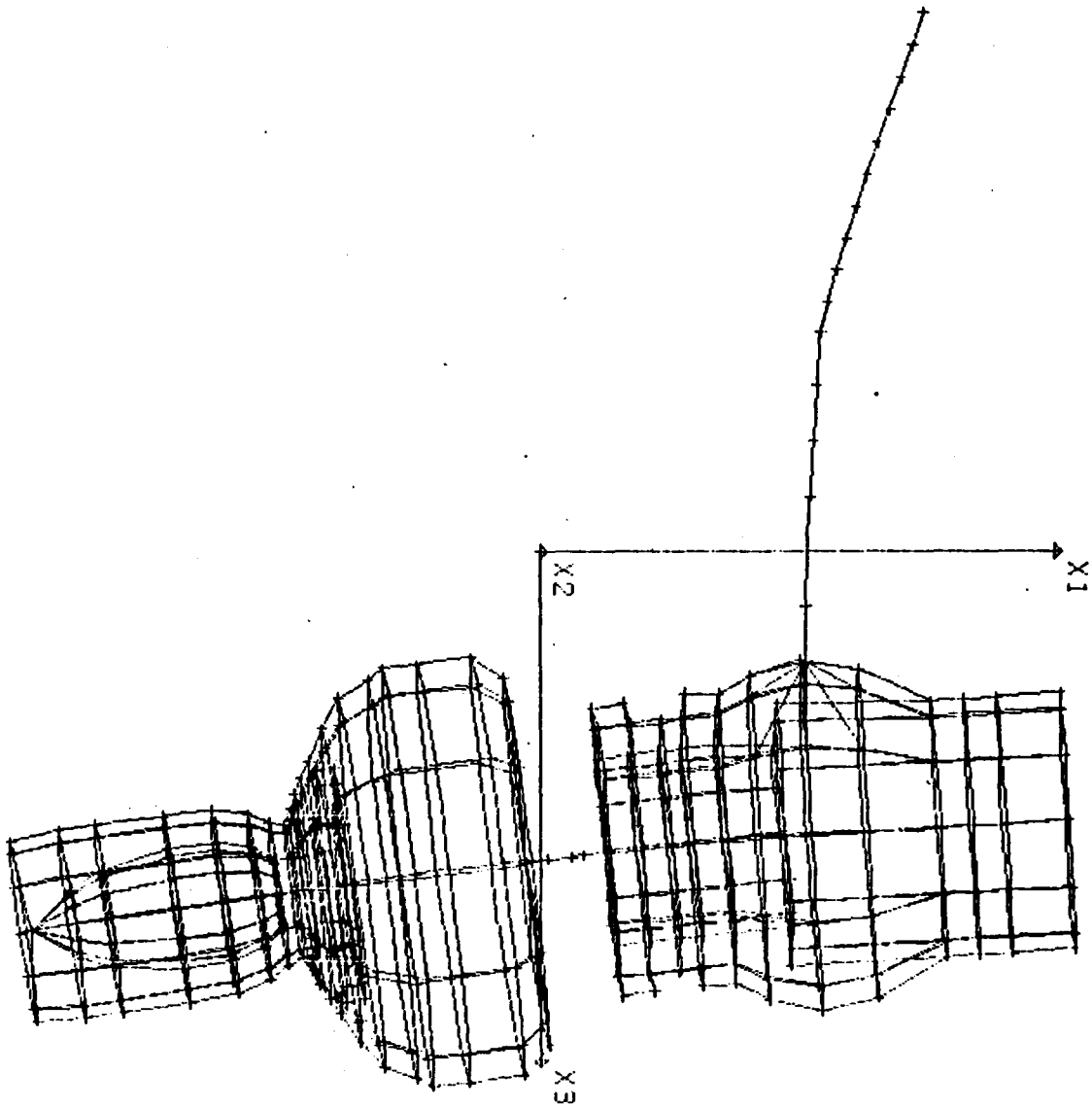

Figure 18. Mark-48F Case, Free-Free Analytical Mode Shape for Structural Mode 1, 247 Hz

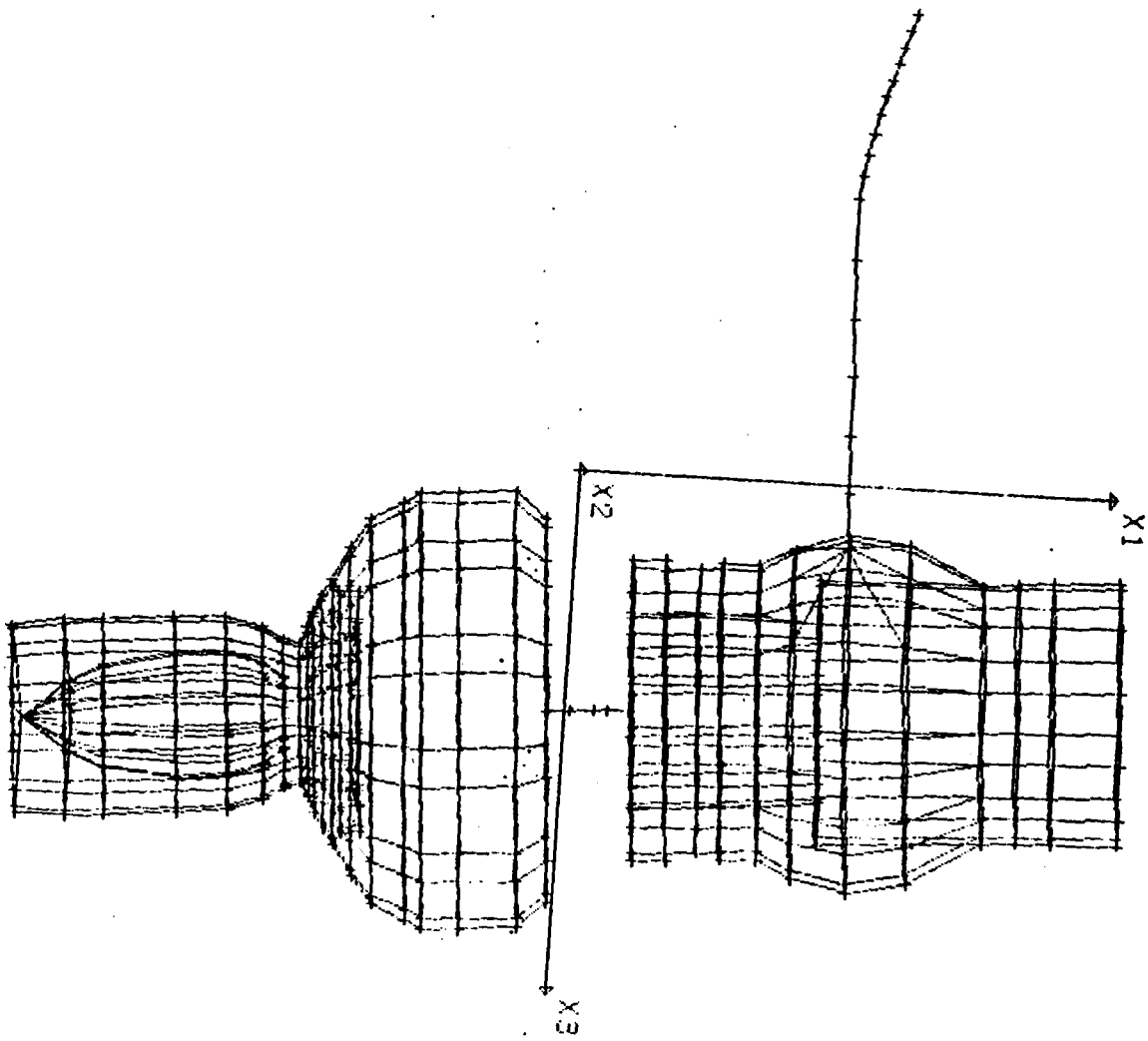

Figure 19. Mark 48F Case, Free-Free Analytical Mode Shape for Structural Mode 2, 336 Hz

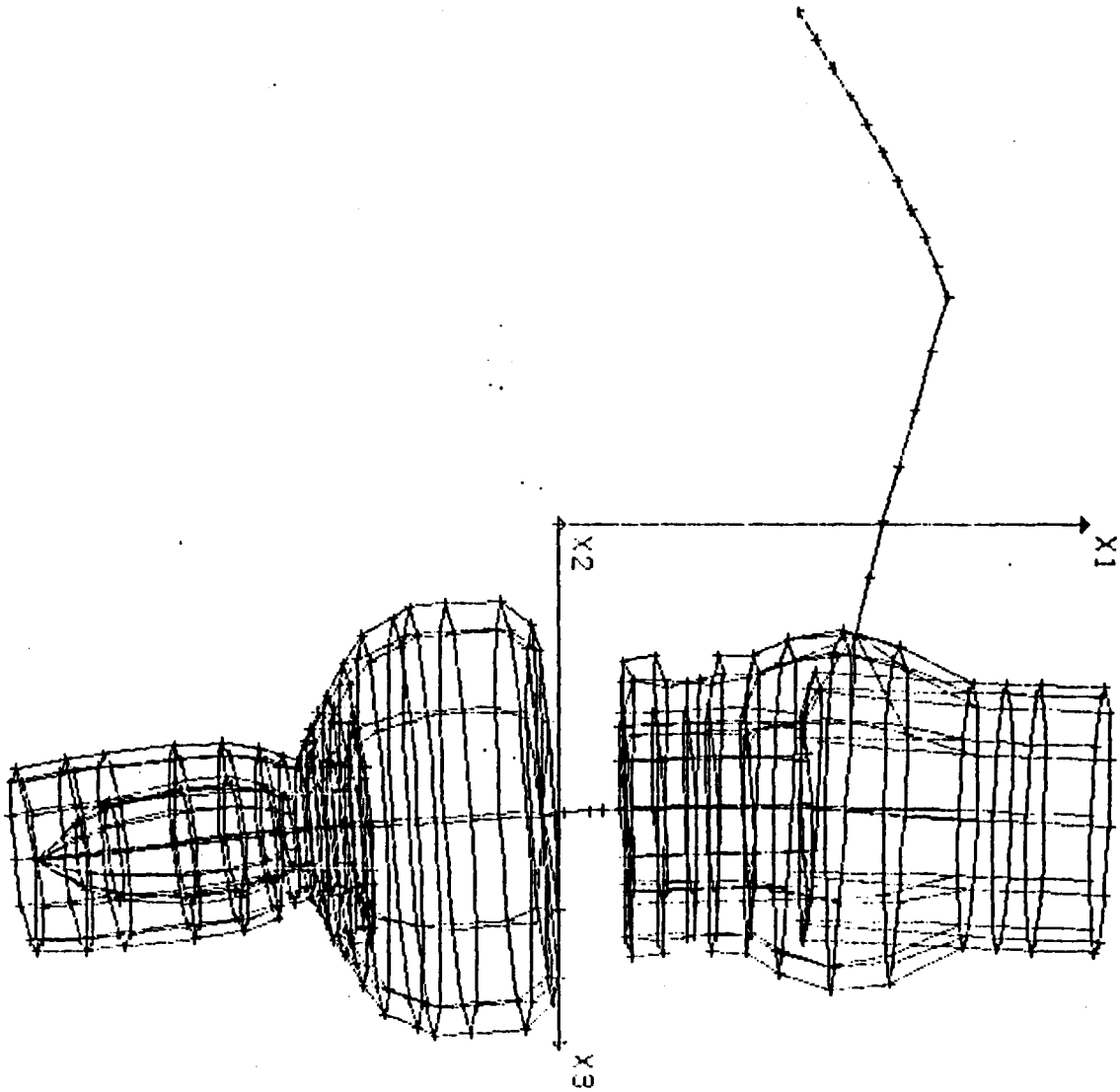

Figure 20. Mark-48F Case, Free-Free Analytical Mode Shape for Structural Mode 3, 537 Hz

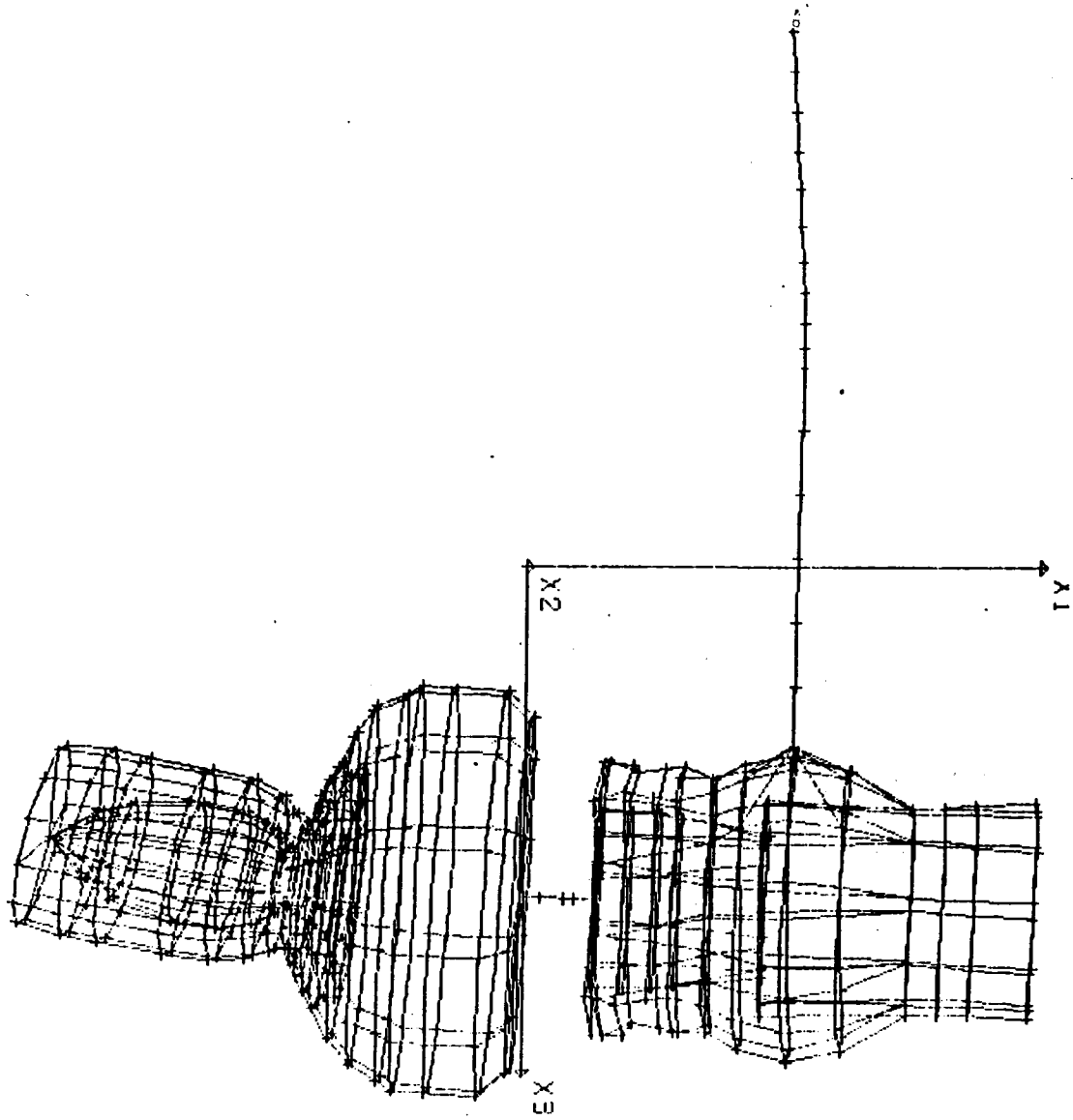

Figure 21. Mark-48F Case, Free-Free Analytical Mode Shape for Structural Mode 4, 798 Hz

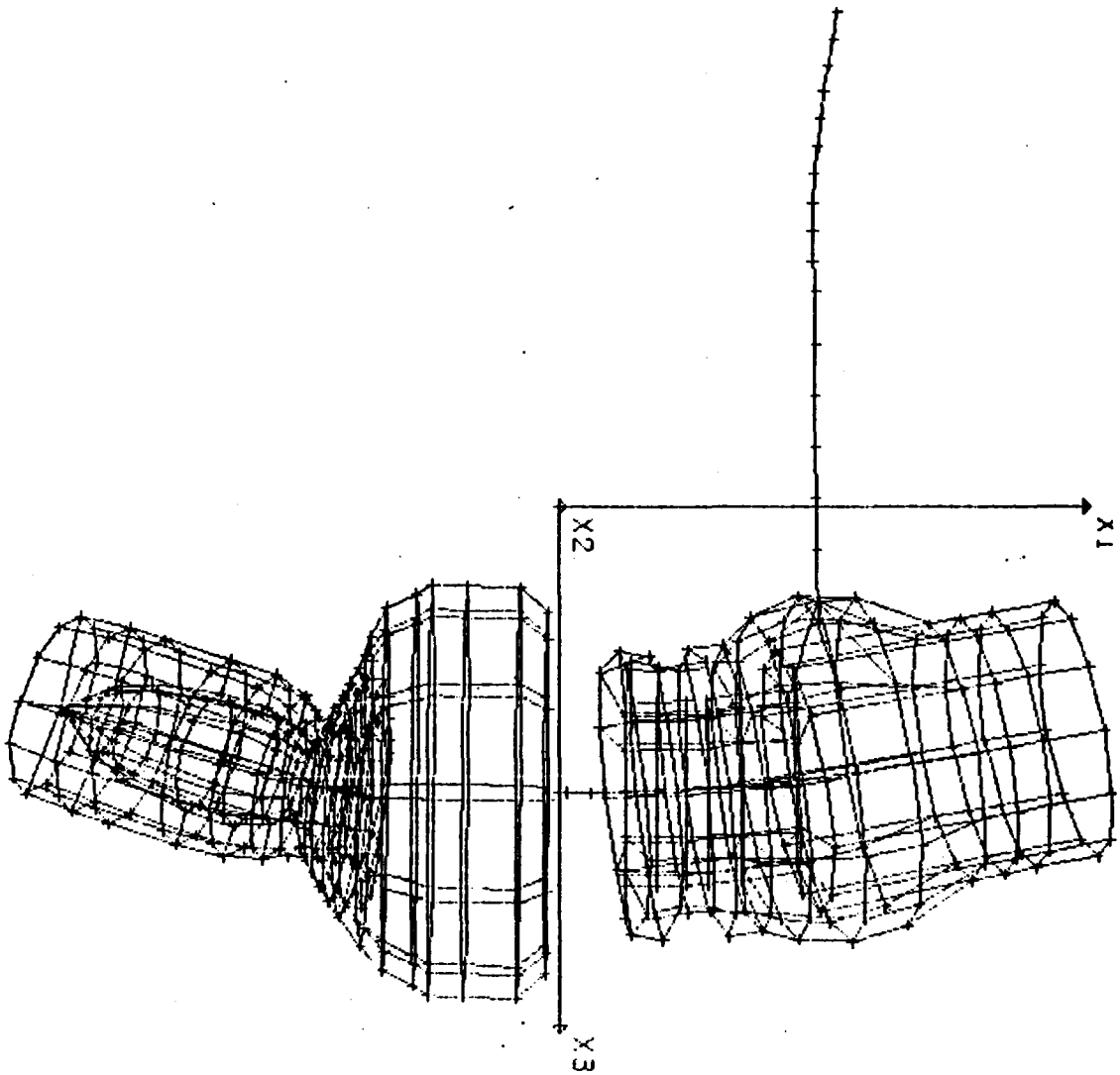

Figure 22. Mark-48F Case, Free-Free Analytical Mode Shape for Structural Mode 5, 906 Hz

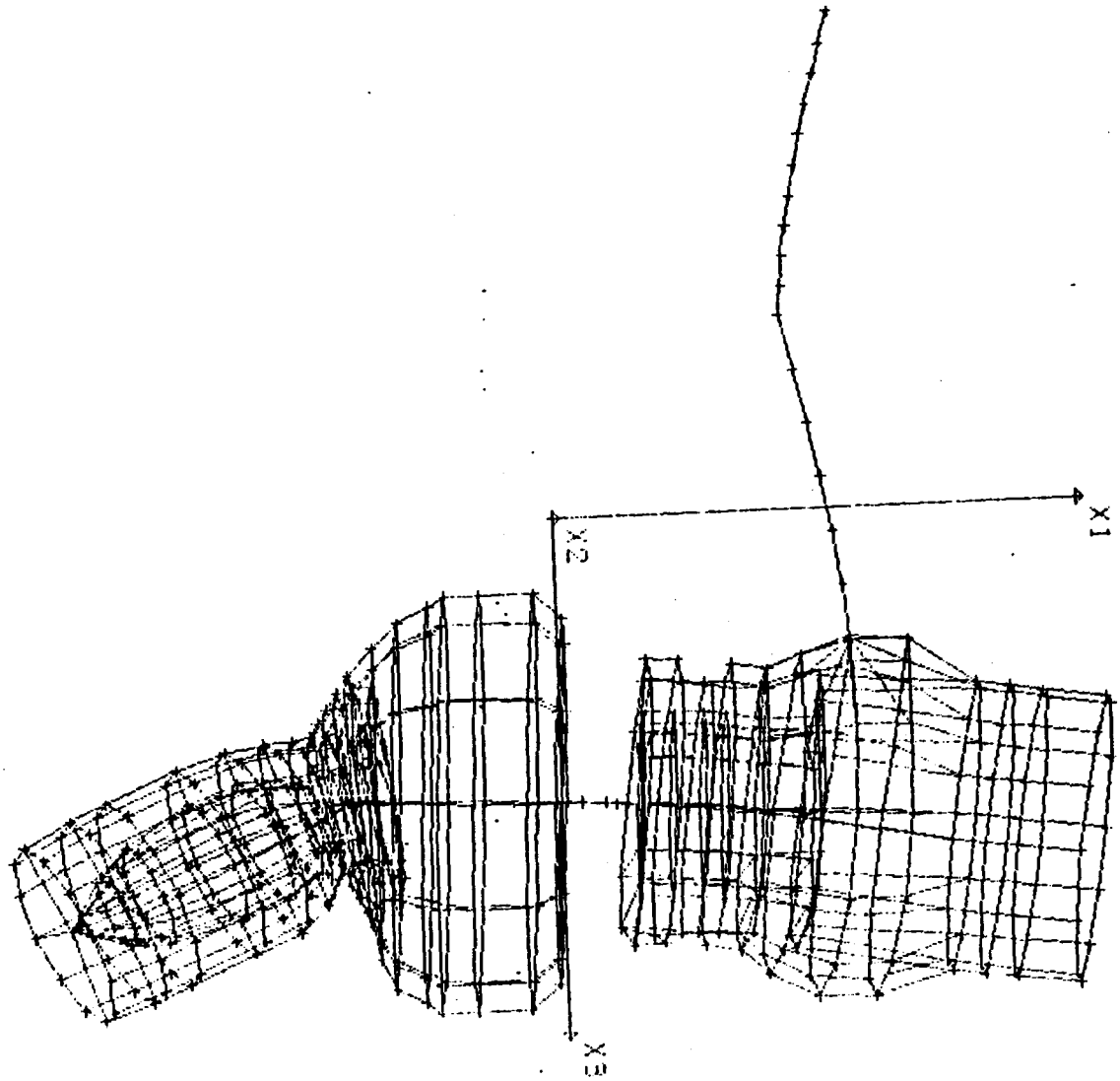

Figure 23. Mark-48F Case, Free-Free Analytical Mode Shape for Structural Mode 6, 1010 Hz

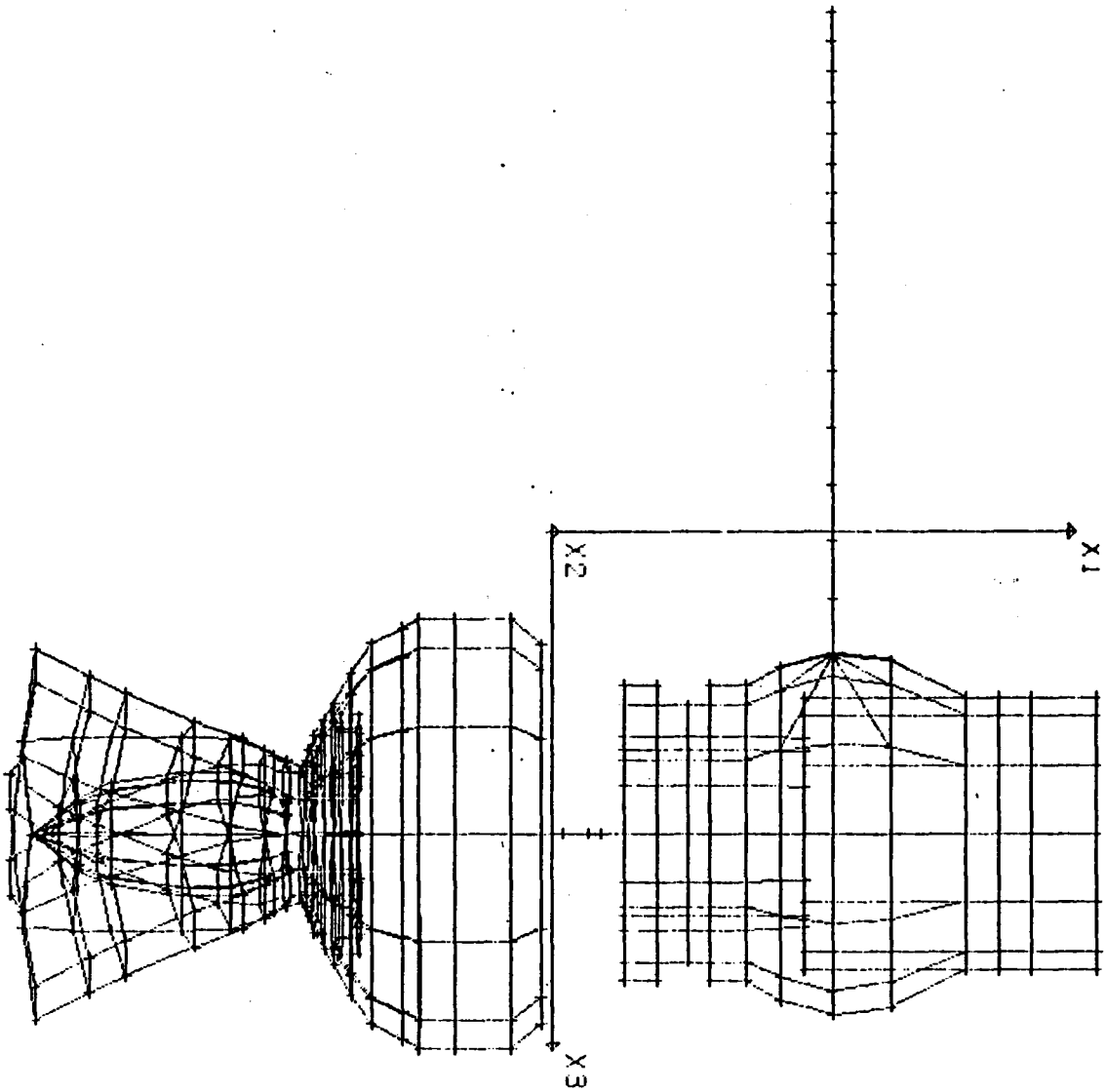

Figure 24. Mark-48F Case, Free-Free Analytical Mode Shape for Structural Mode 7, 1339 Hz

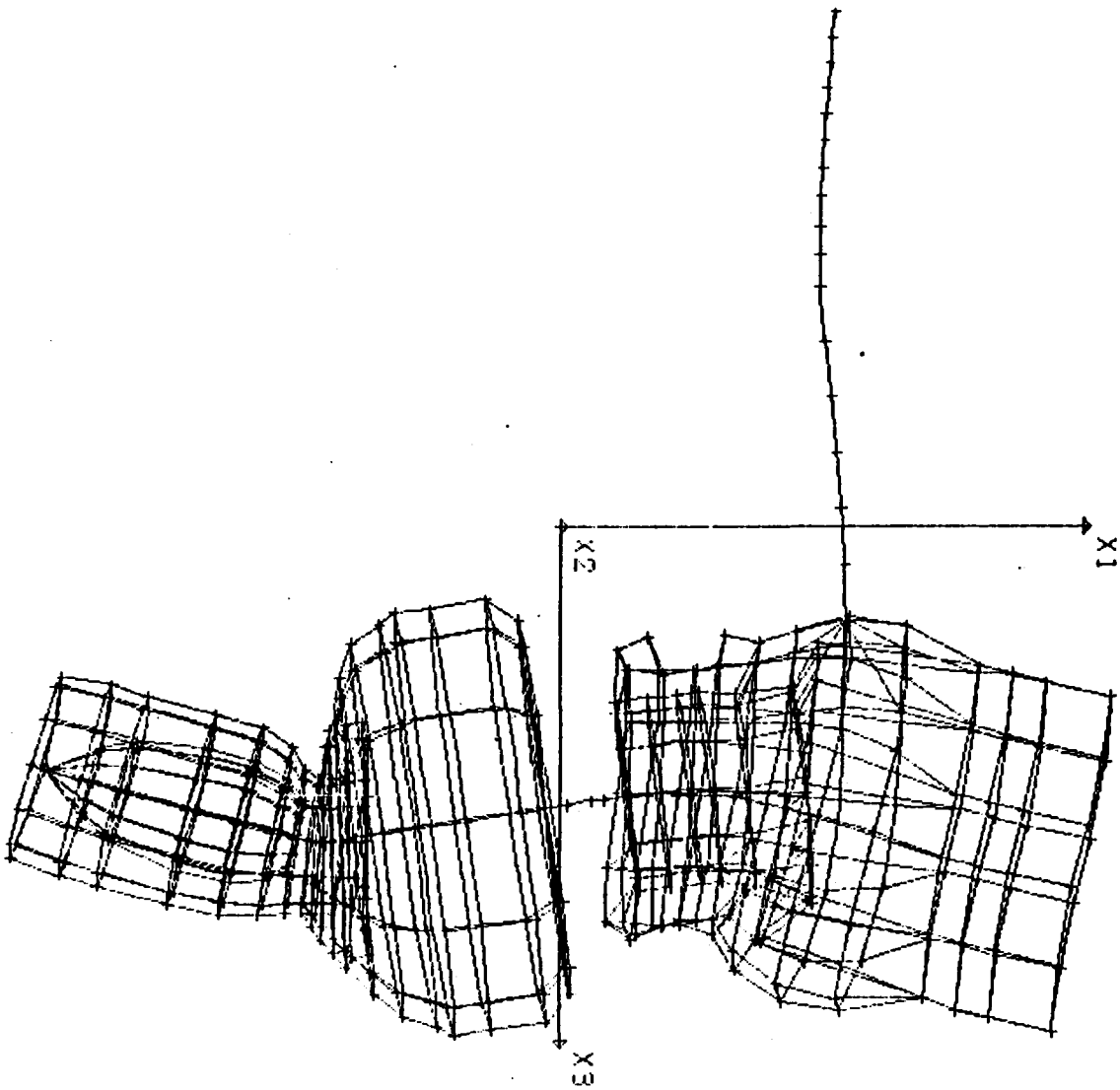

Figure 25. Mark-48F Case, Free-Free Analytical Mode Shape for Structural Mode 8, 1400 Hz

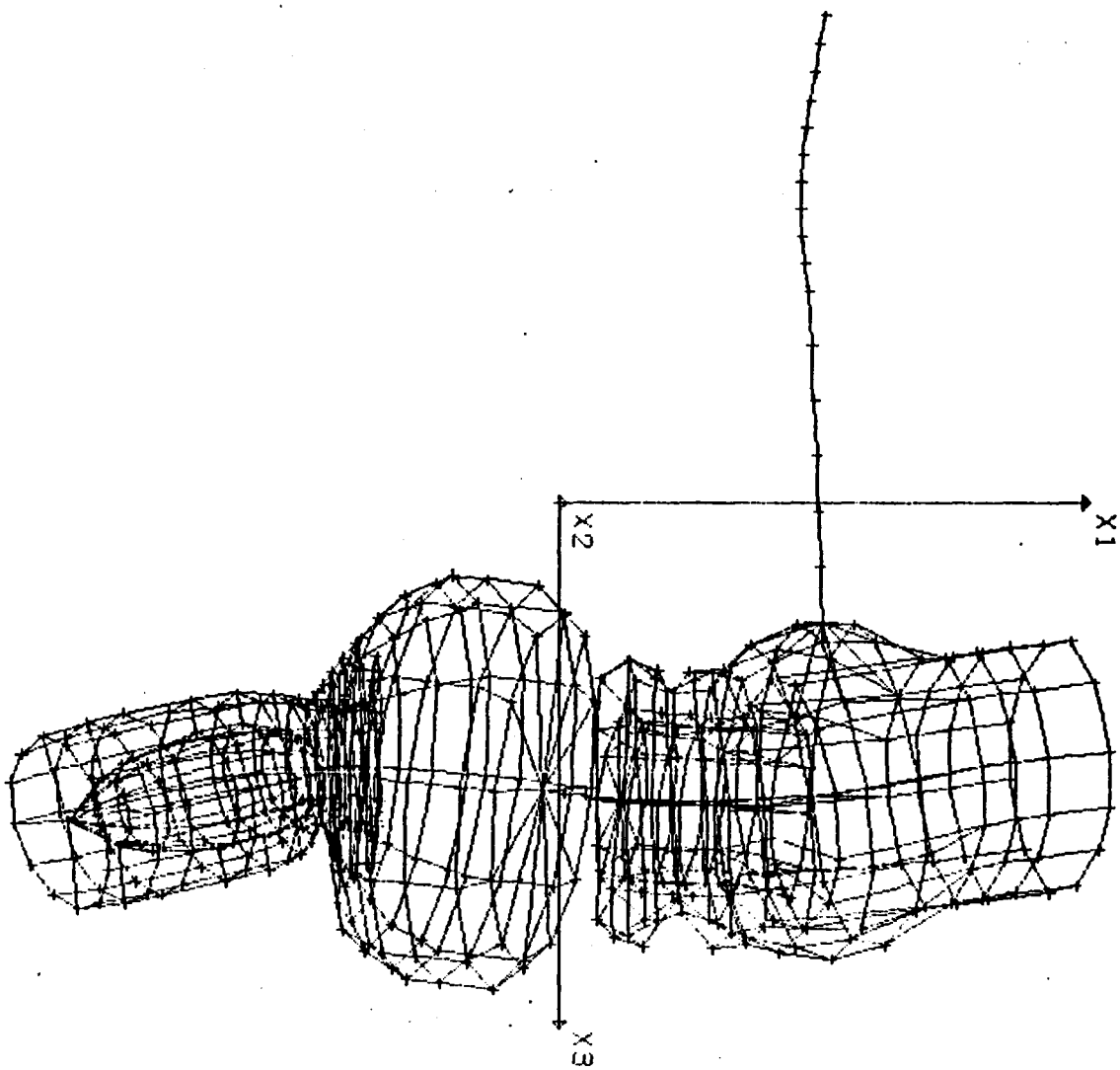

Figure 26. Mark-48F Case, Free-Free Analytical Mode Shape for Structural Mode 9, 1418 Hz

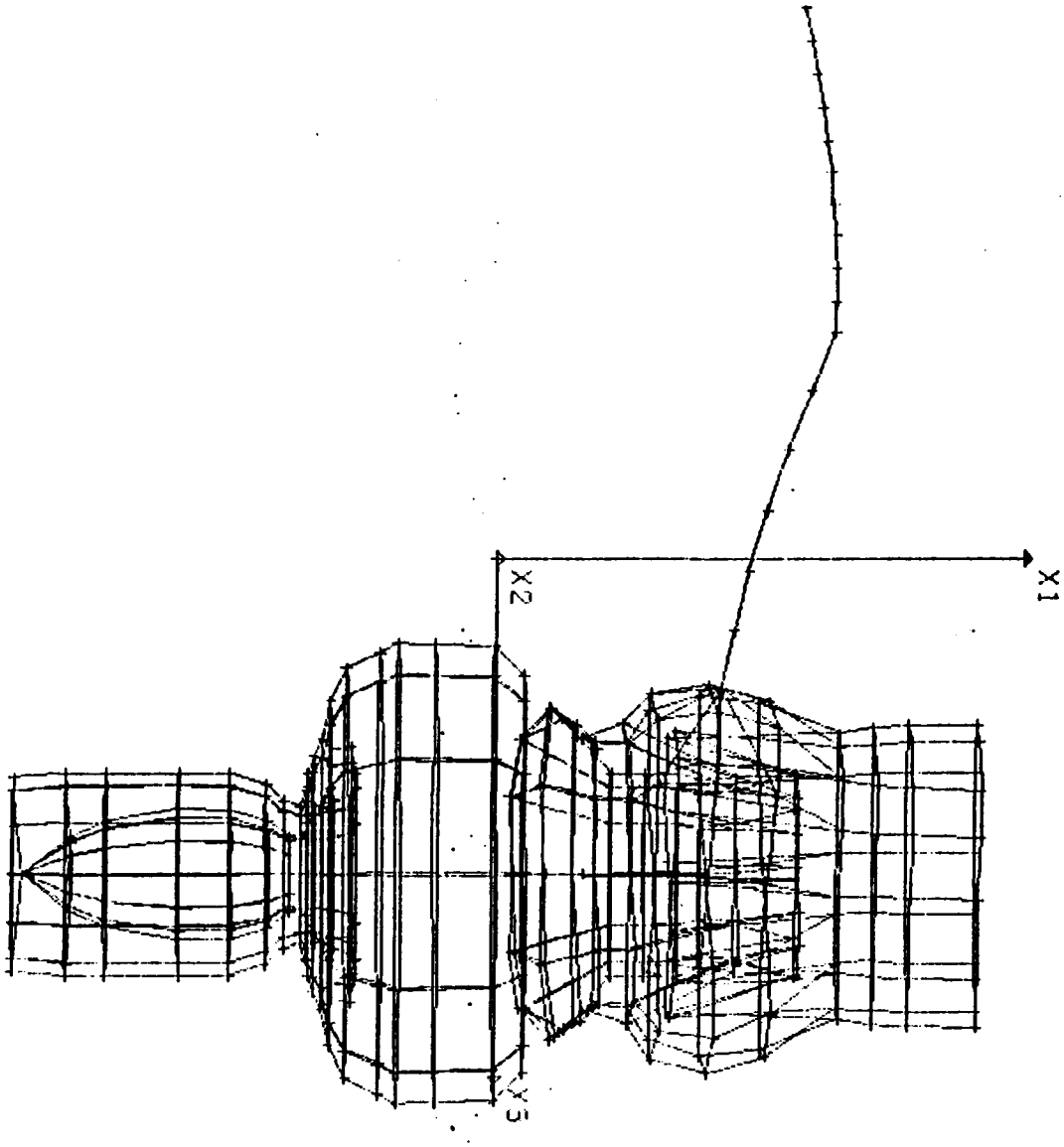

Figure 27. Mark-48F Case, Free-Free Analytical Mode Shape for Structural Mode 10, 1621 Hz

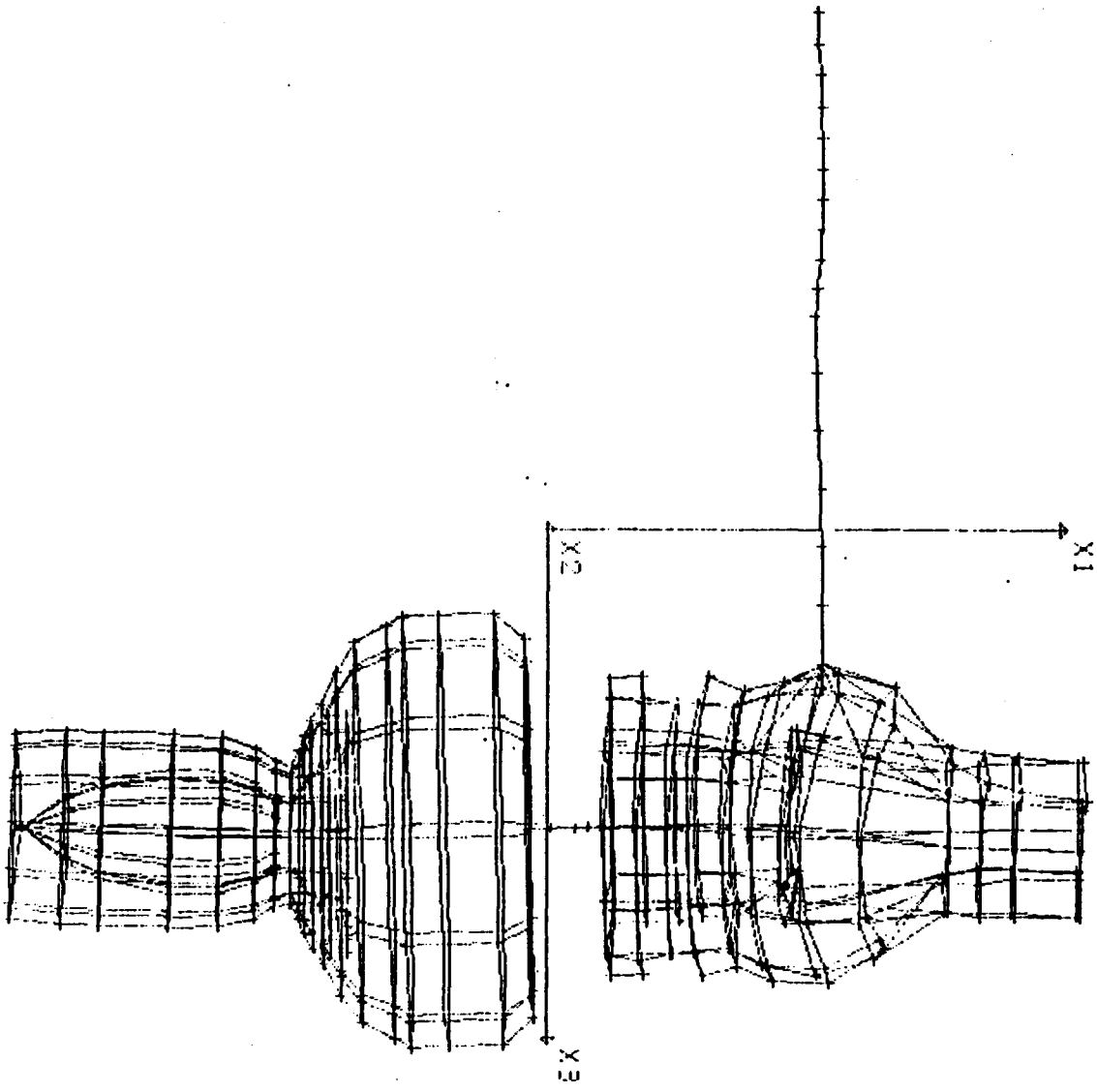

Figure 28. Mark-48F Case, Free-Free Analytical Mode Shape for Structural Mode 11, 1747 Hz

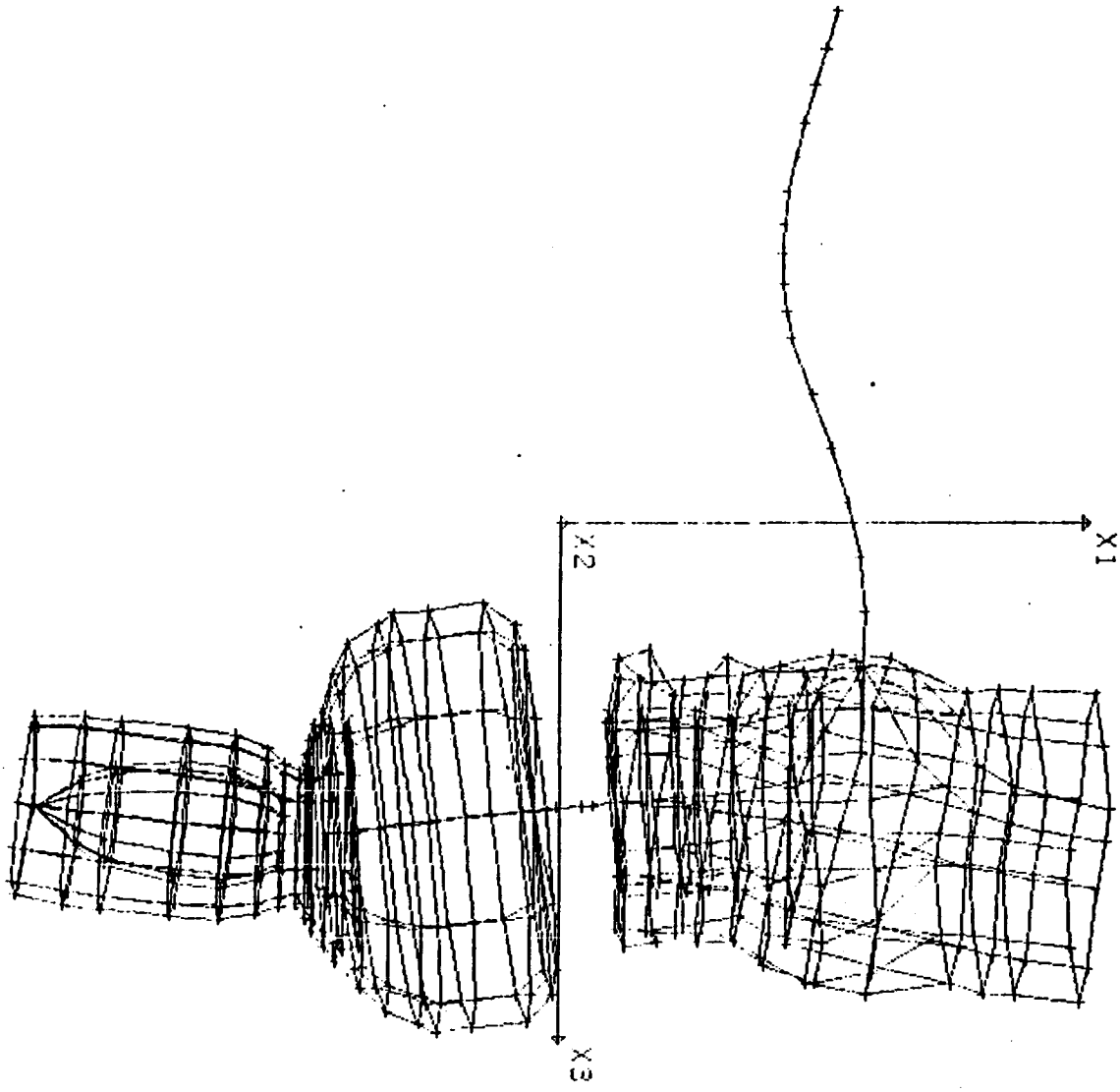

Figure 29. Mark-48F Case, Free-Free Analytical Mode Shape for Structural Mode 12, 1769 Hz

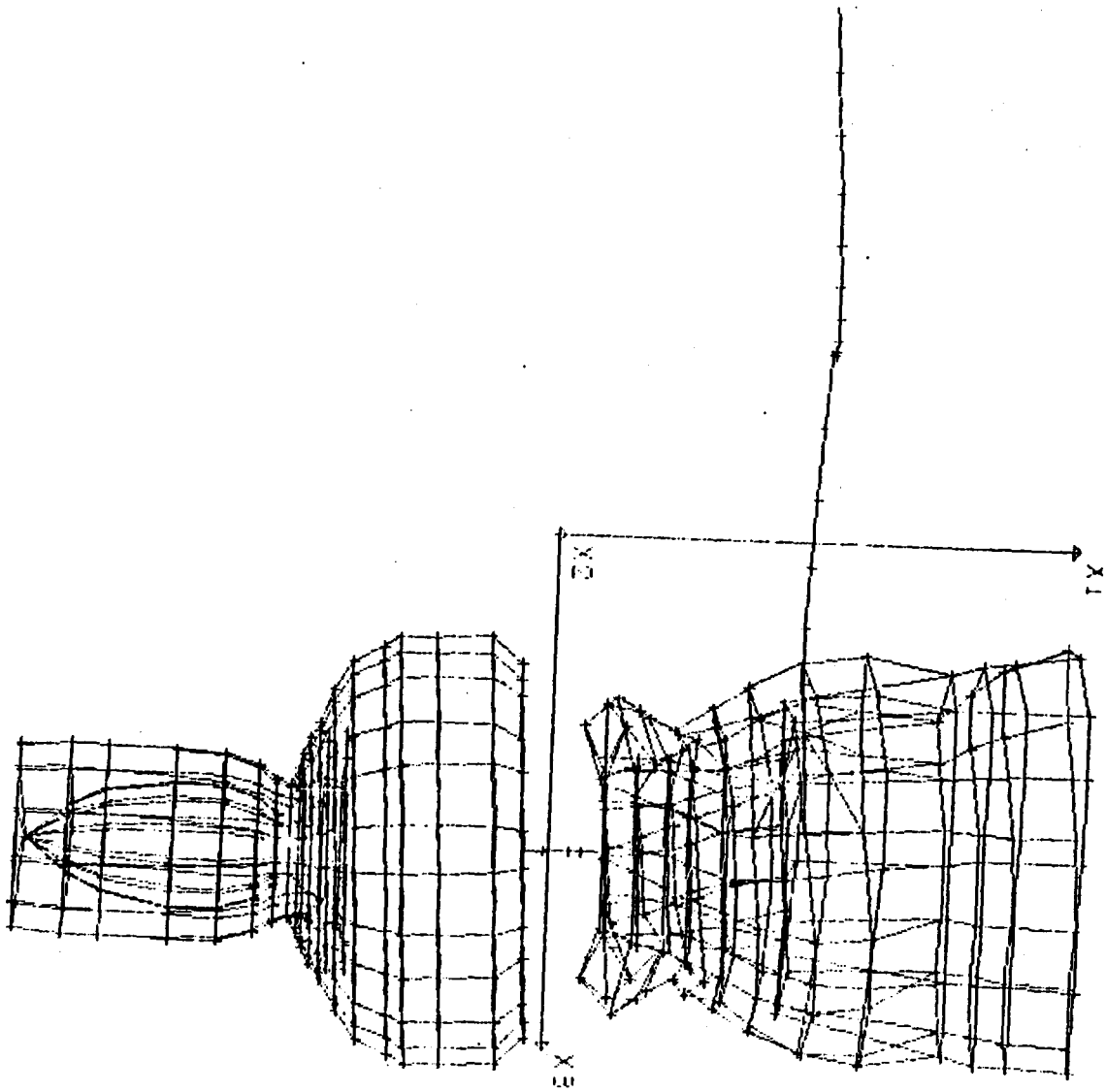

Figure 30. Mark-48F Case, Free-Free Analytical Mode Shape for Structural Mode 13, 2313 Hz

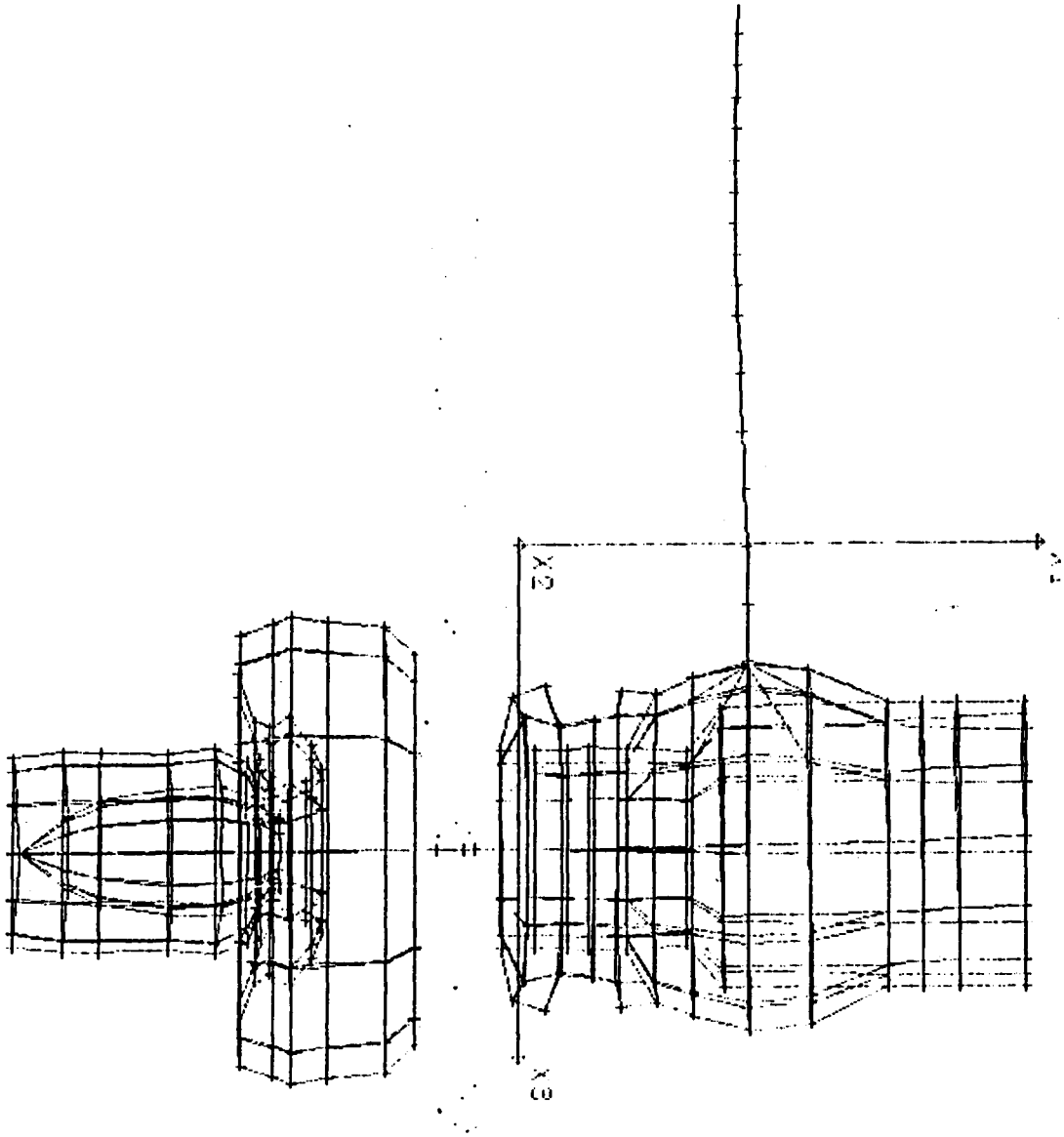

Figure 31. Mark-48F Case, Free-Free Analytical Mode Shape for Structural Mode 14, 2410 Hz

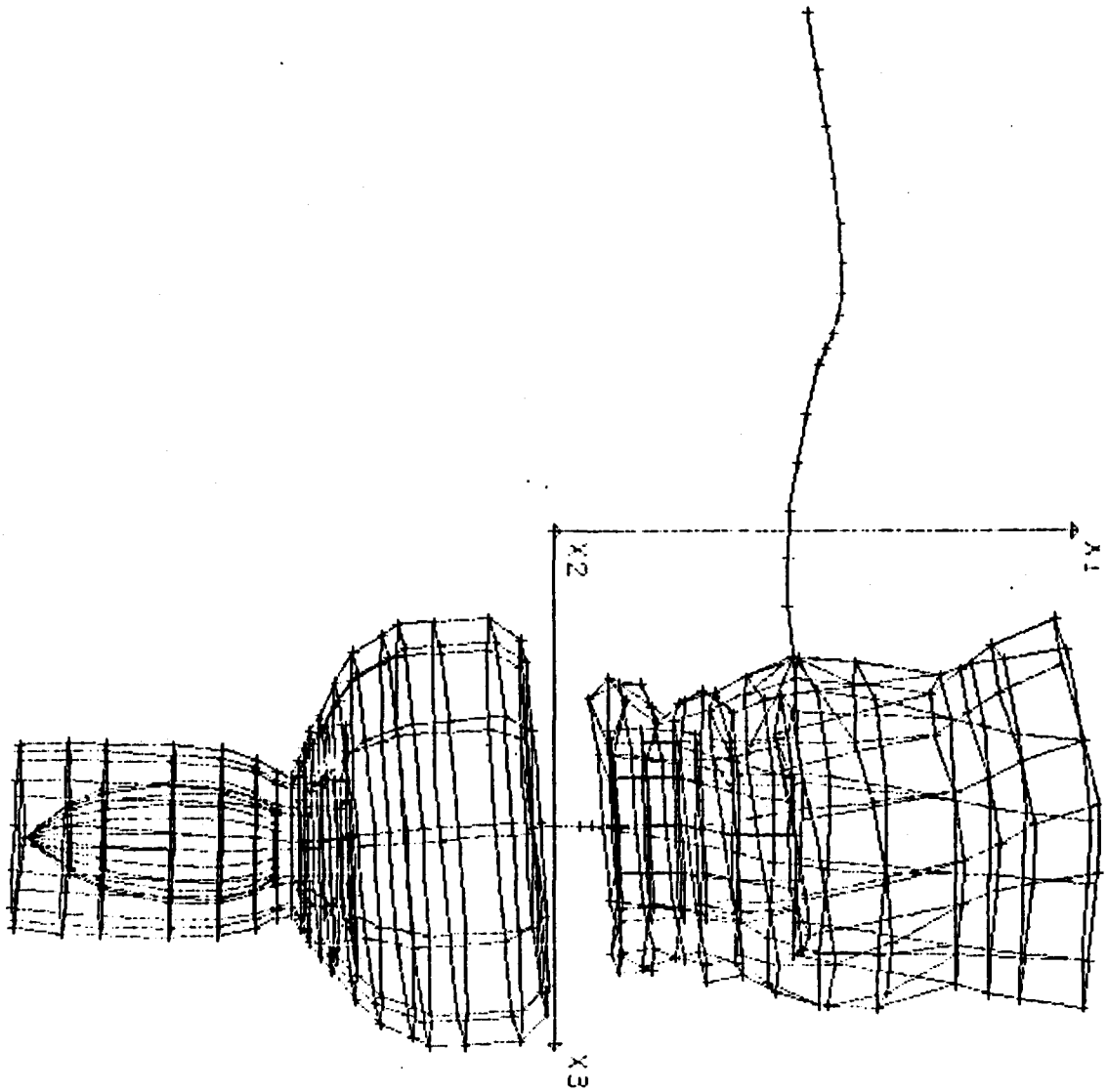

Figure 32. Mark-48F Case, Free-Free Analytical Mode Shape for Structural Mode 15, 2521 Hz

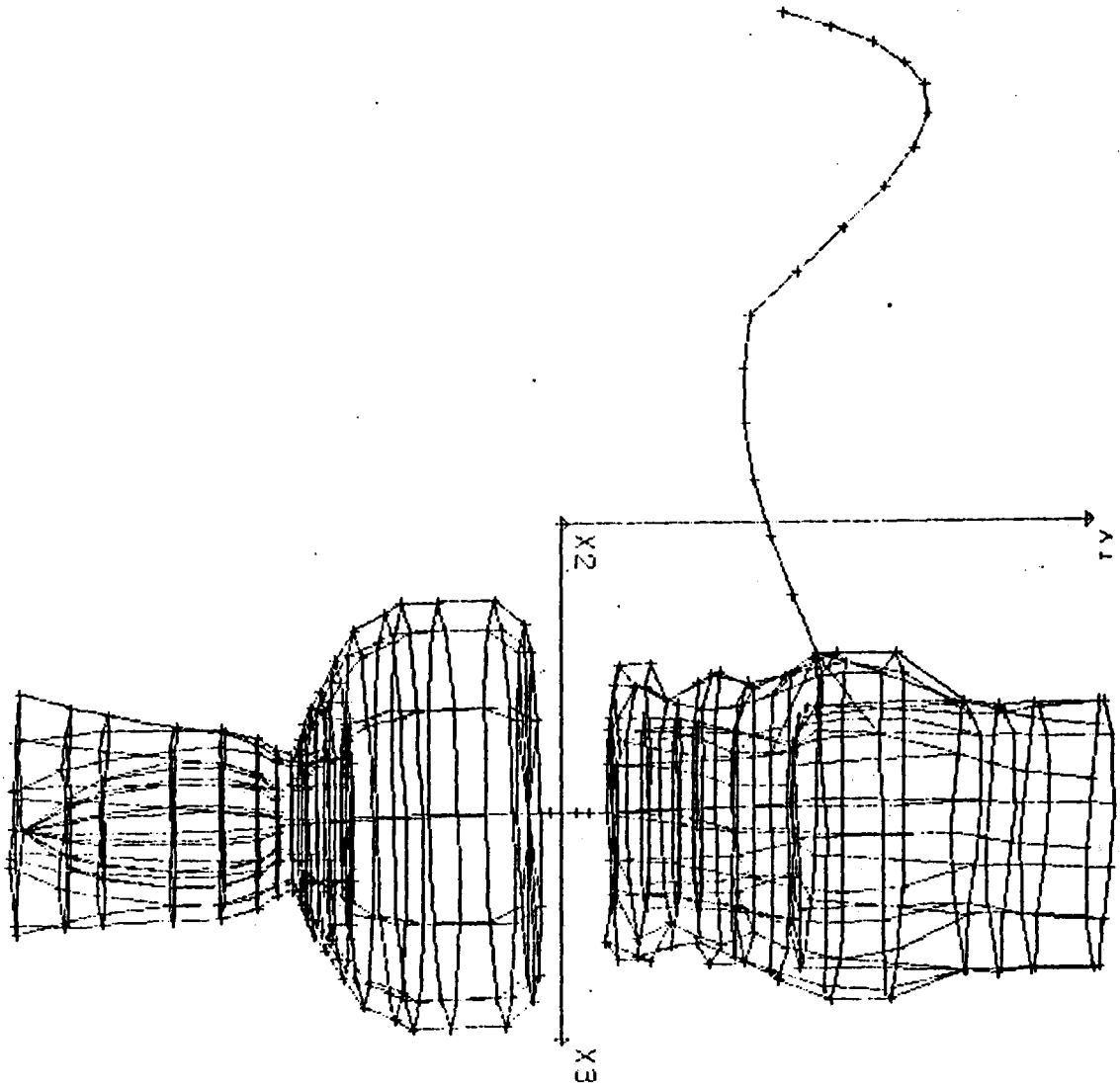

Figure 33. Mark-48F Case, Free-Free Analytical Mode Shape for Structural Mode 16, 3071 Hz

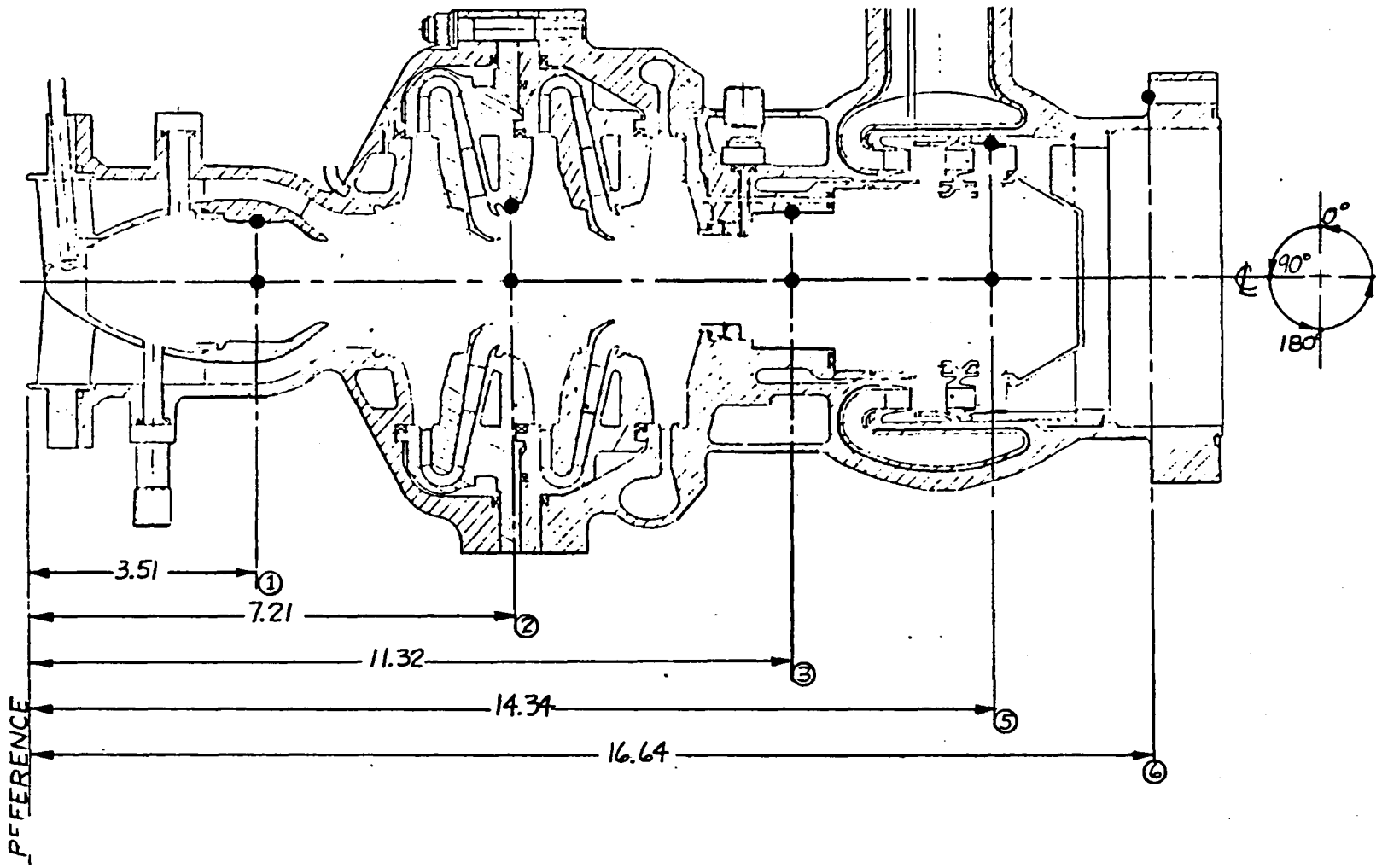

Figure 34. Mark-48F Turbopump With Axial Inlet Showing Accelerometer Locations

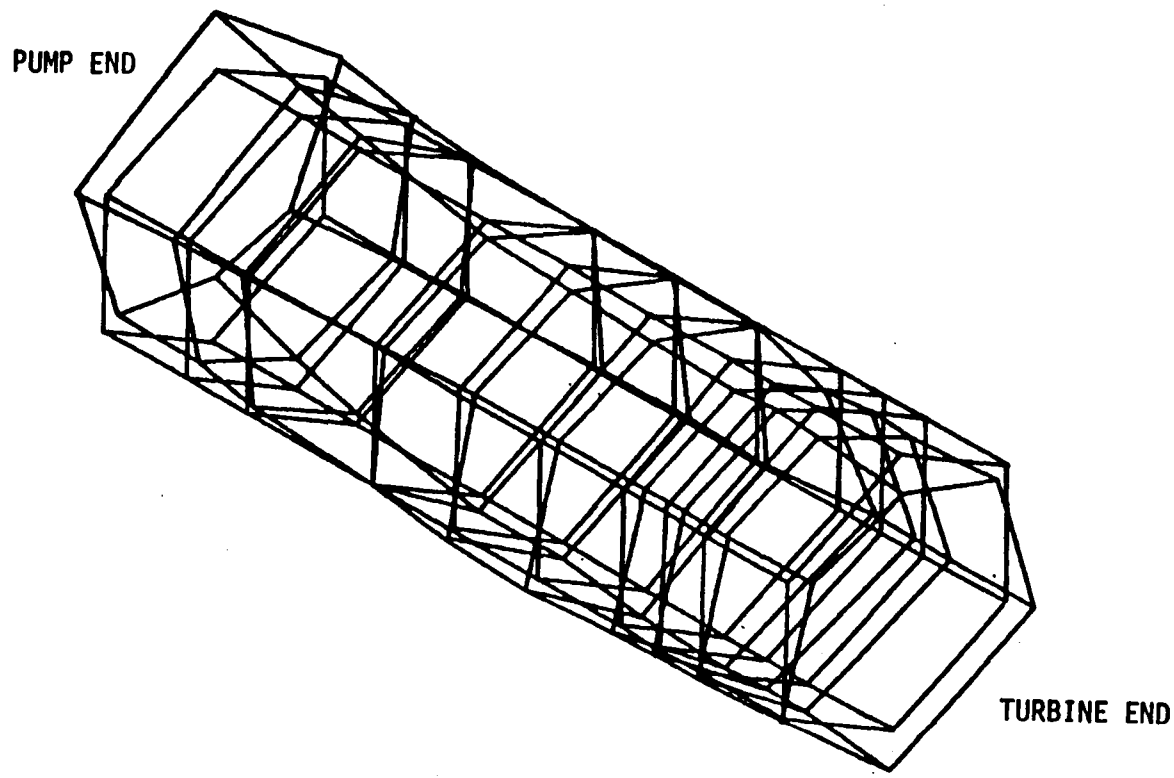

Figure 35. Mark-48F Case, 60 Point Grid Locations Used in Modal Test

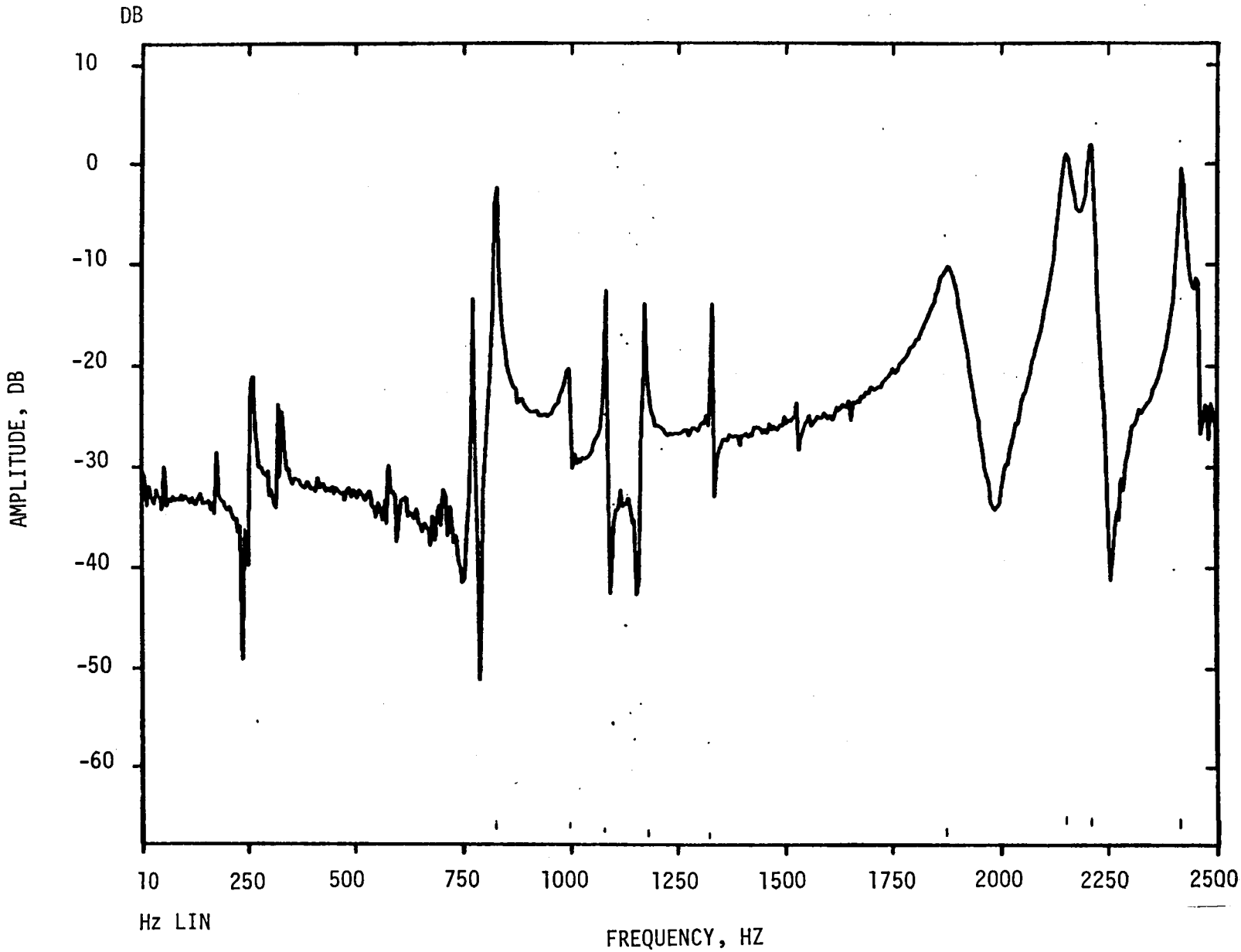

Figure 36. Typical Case Response From Rap Test

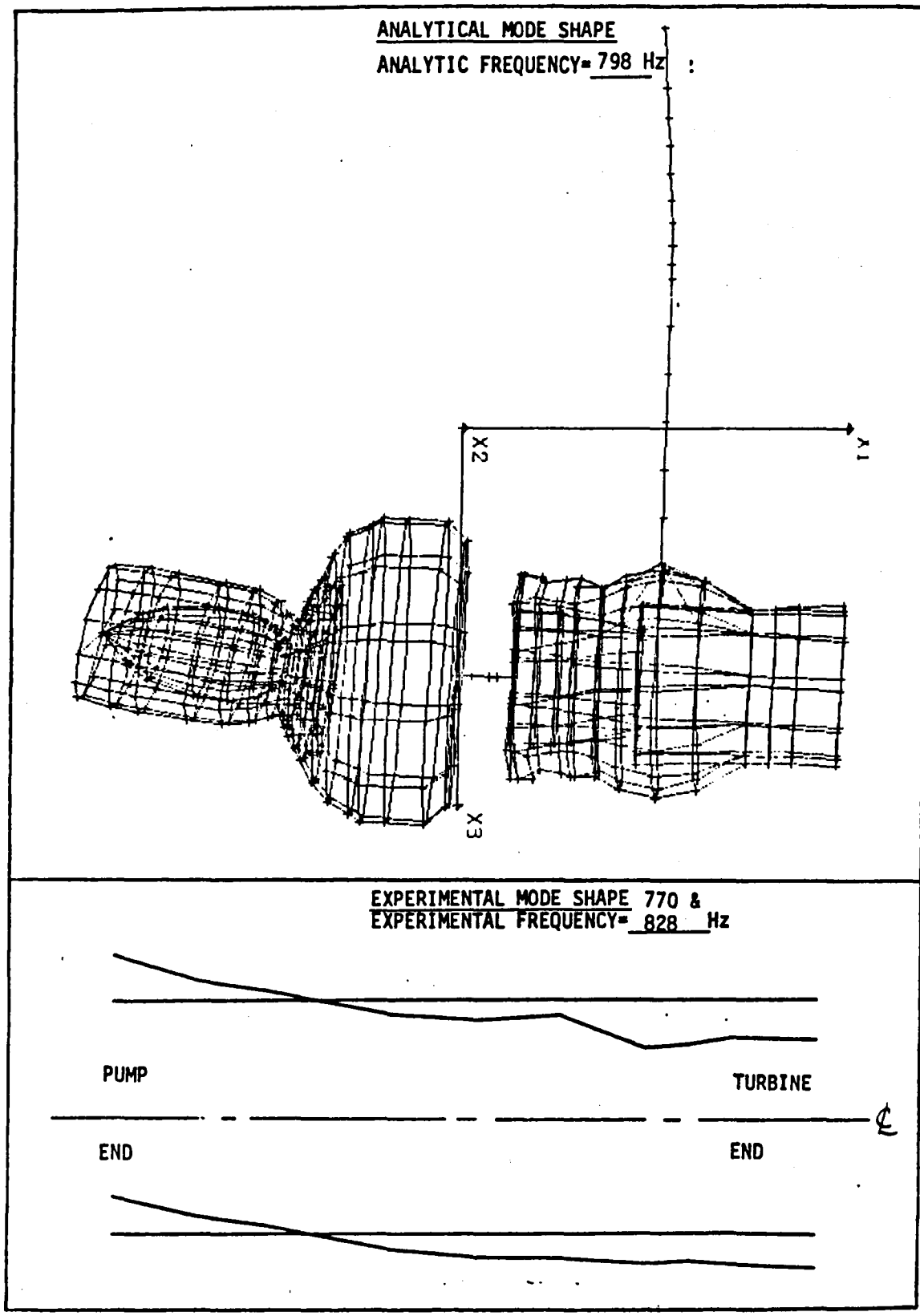

Figure 37. Mark-48F Case, Test/Analysis Mode Shape Comparison, Mode No. 4

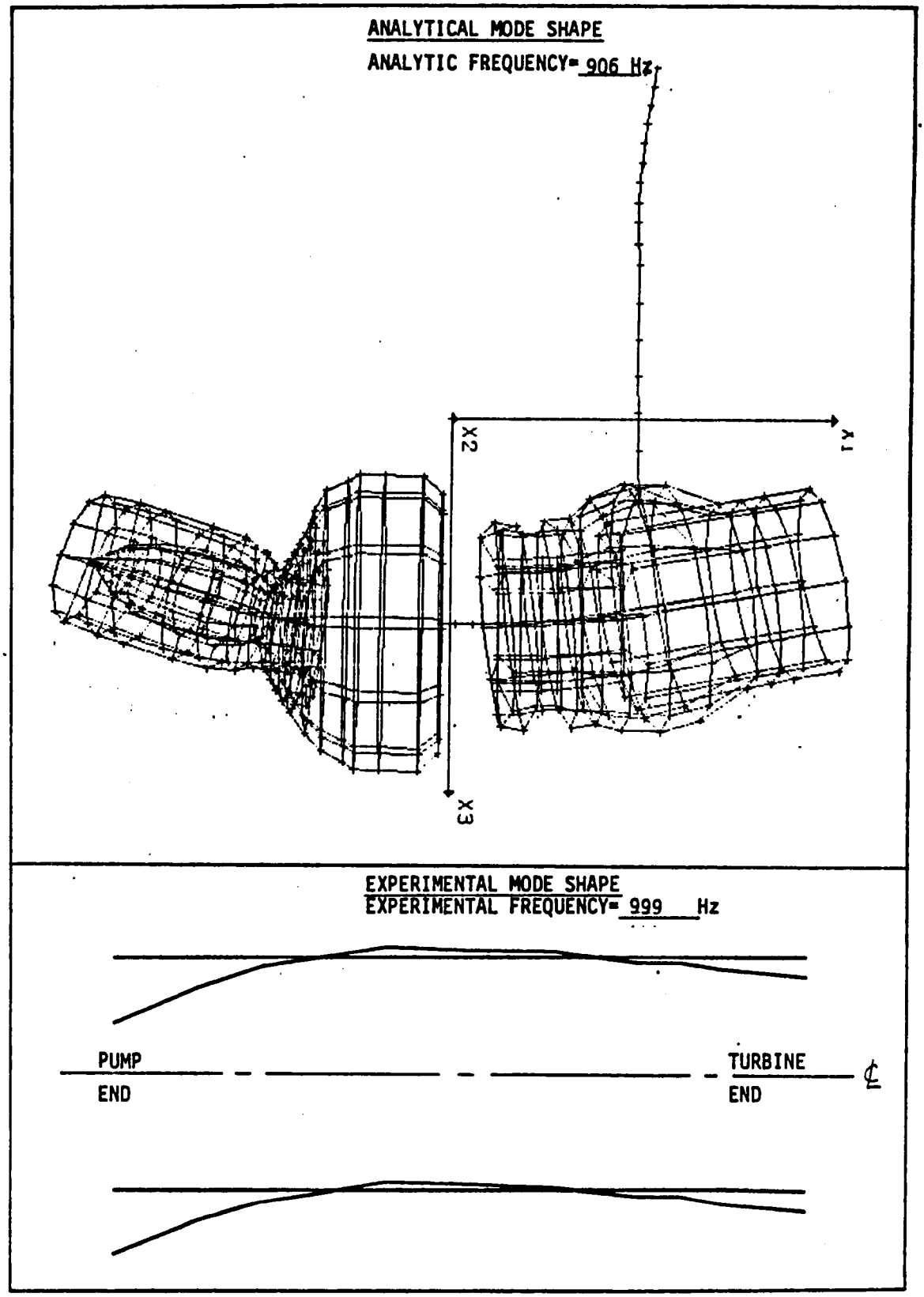

Figure 38. Mark-48F Case, Test/Analysis Mode Shape Comparison, Mode No. 5

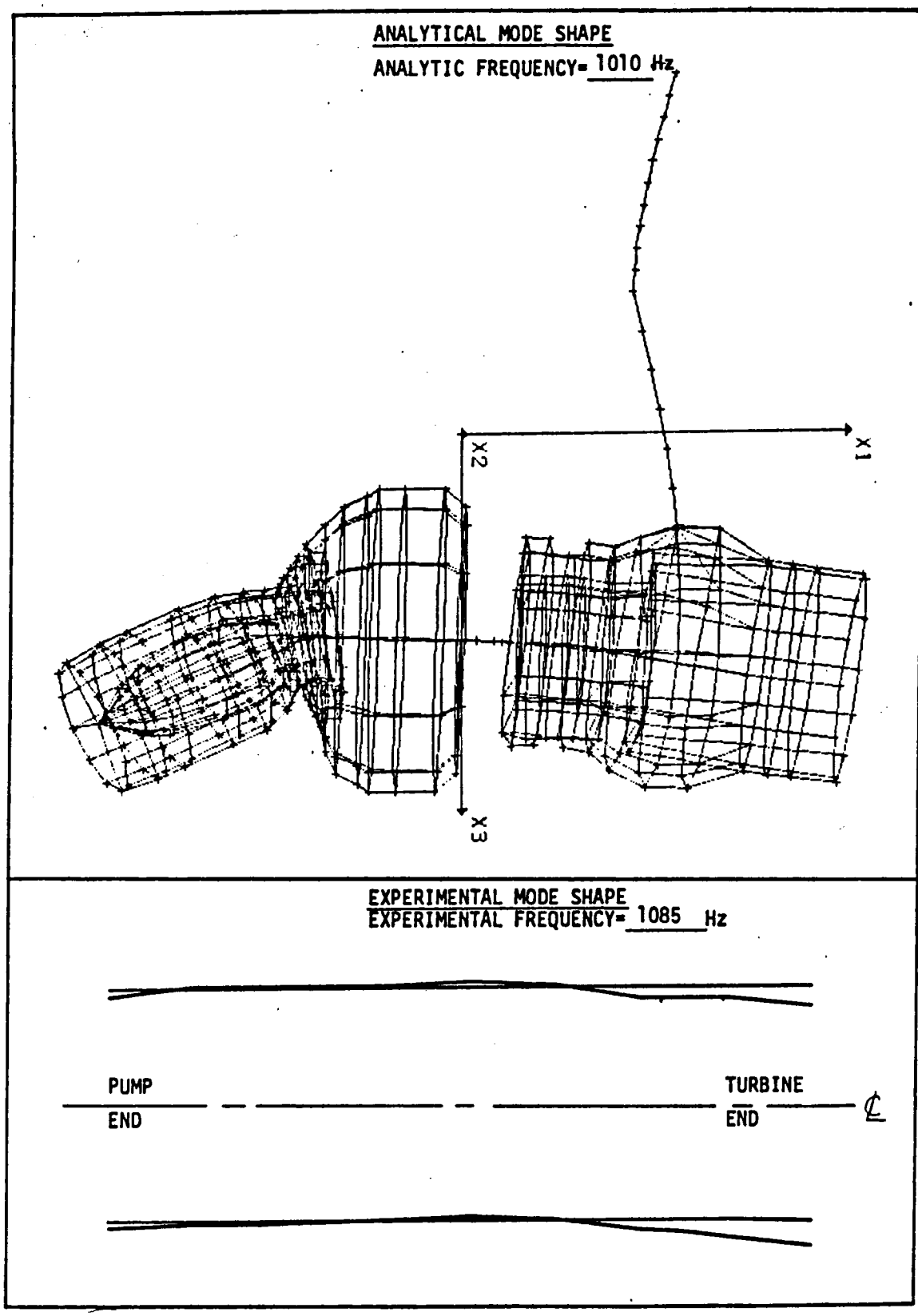

Figure 39. Mark-48F Case, Test/Analysis Mode Shape Comparison, Mode No. 6A

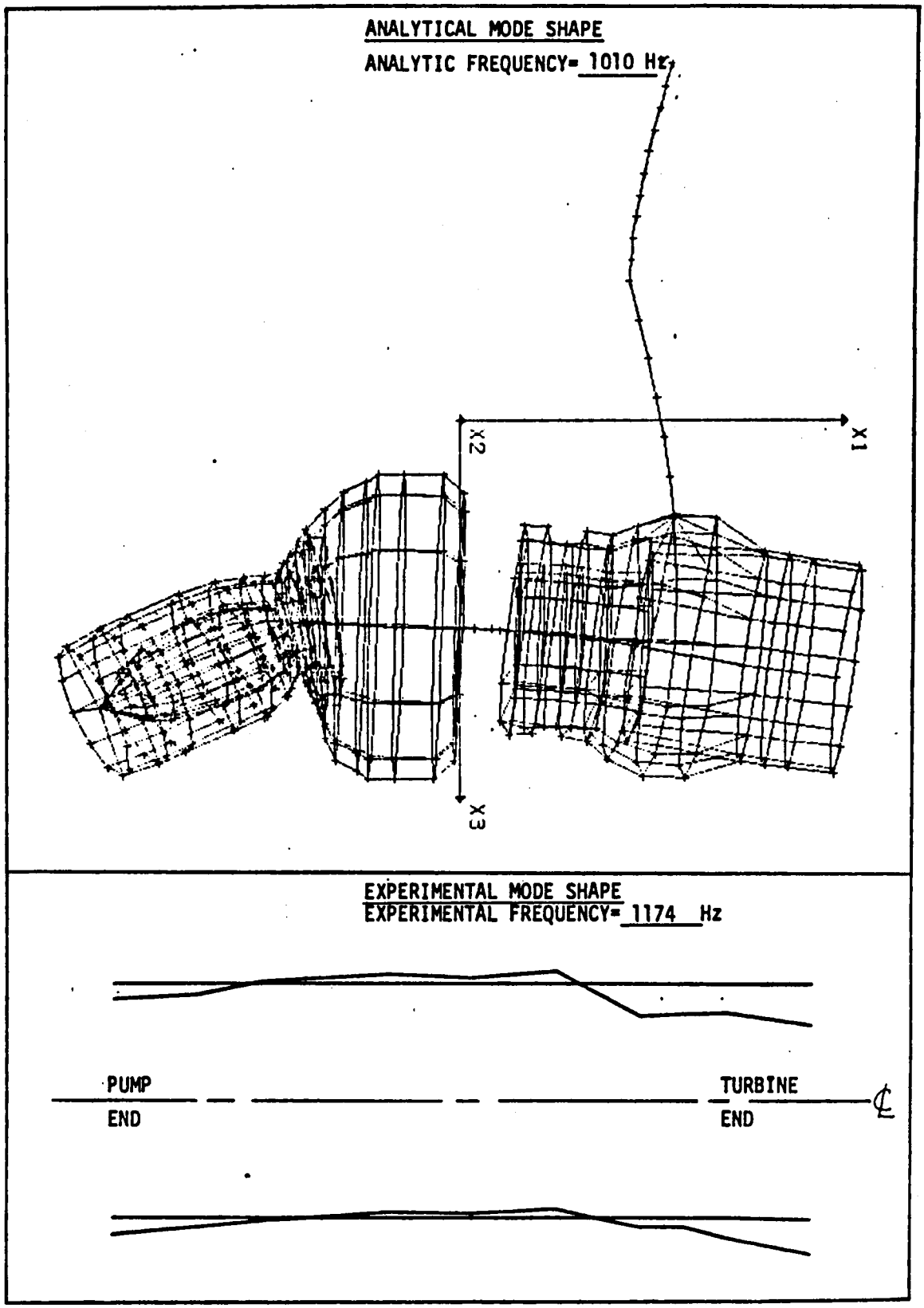

Figure 40. Mark-48F Case, Test/Analysis Mode Shape Comparison, Mode No. 6B

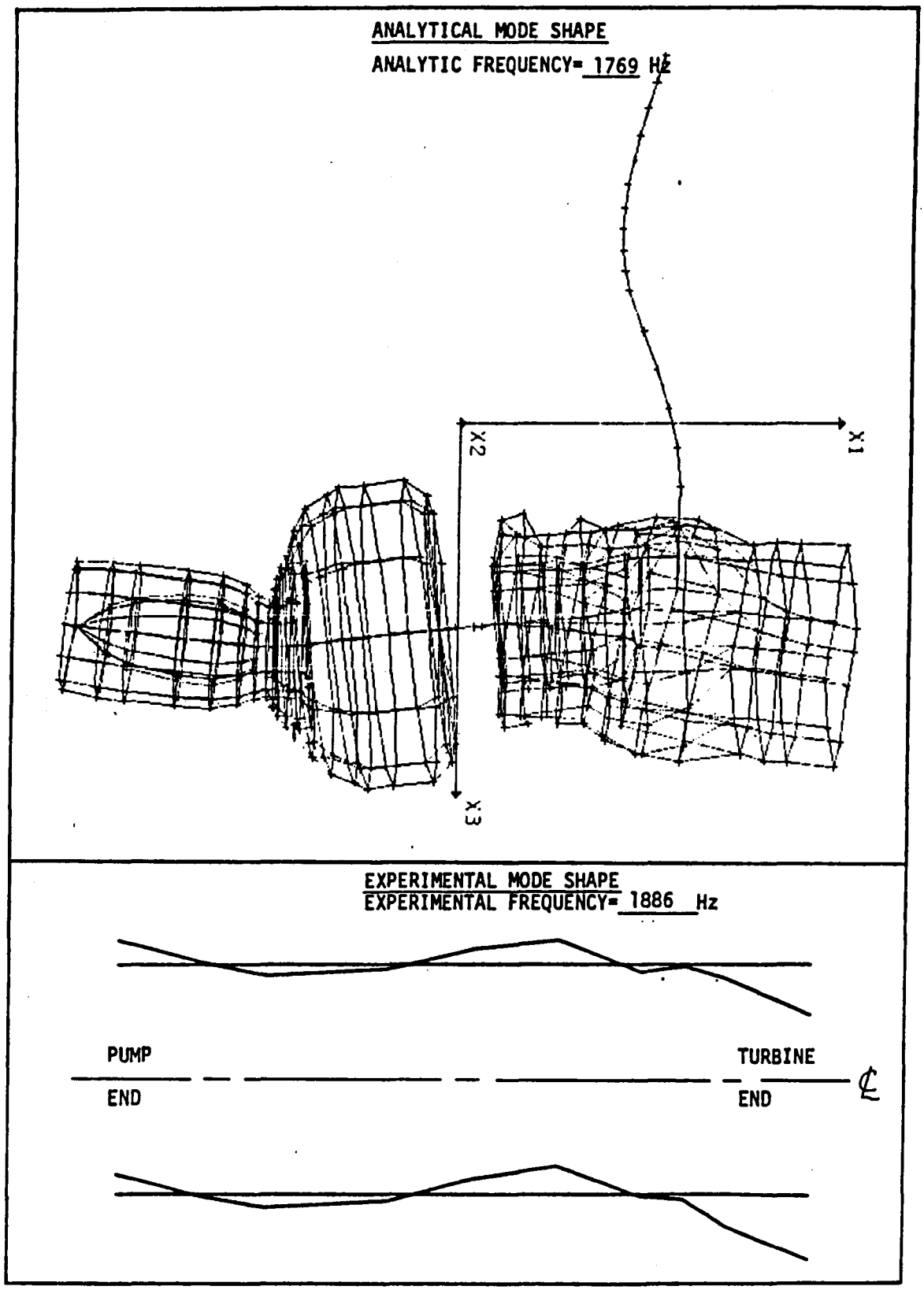

Figure 41. Mark-48F Case, Test/Analysis Mode Shape Comparison, Mode No. 12

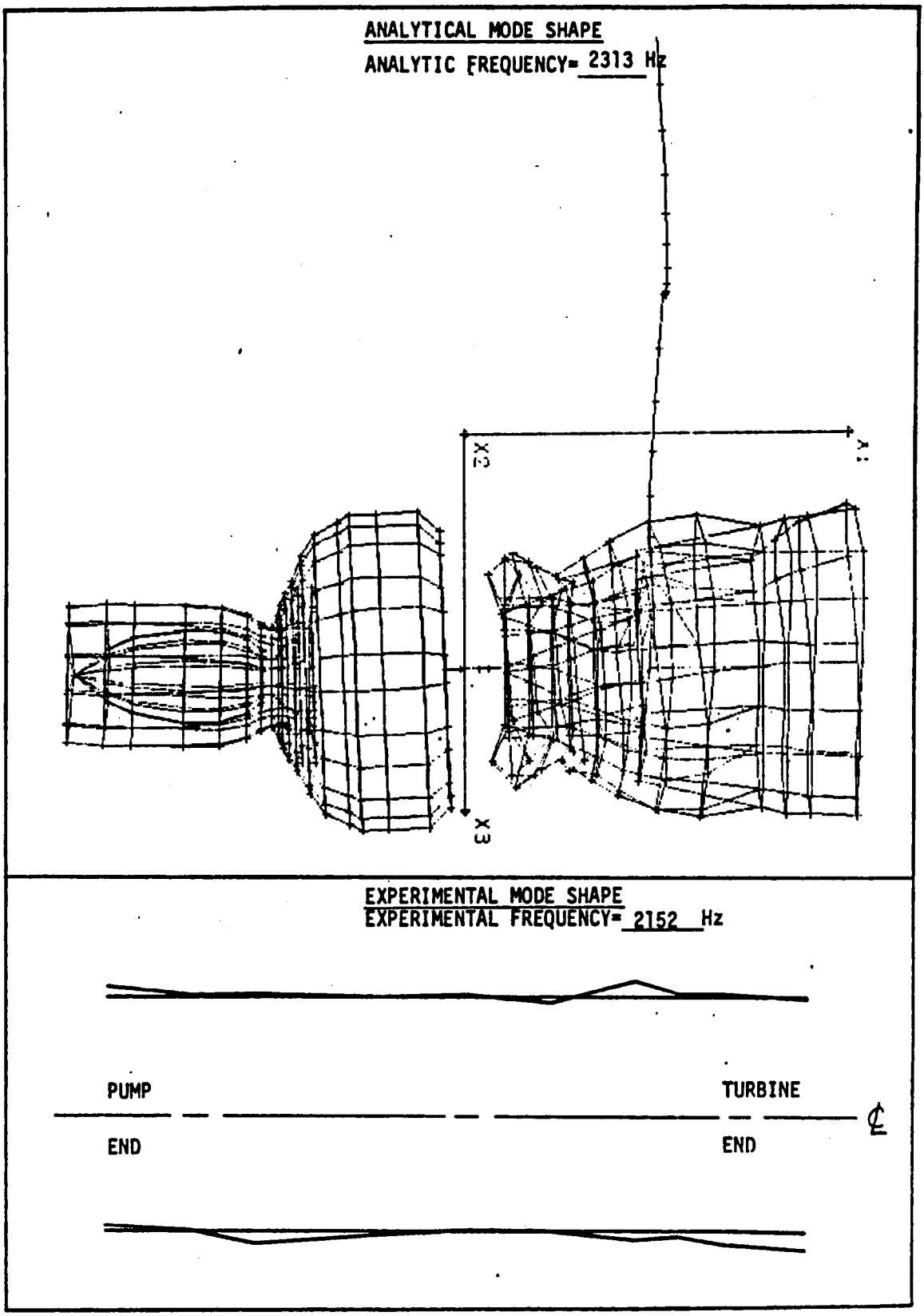

Figure 42. Mark-48F Case, Test/Analysis Mode Shape Comparison, Mode No. 13

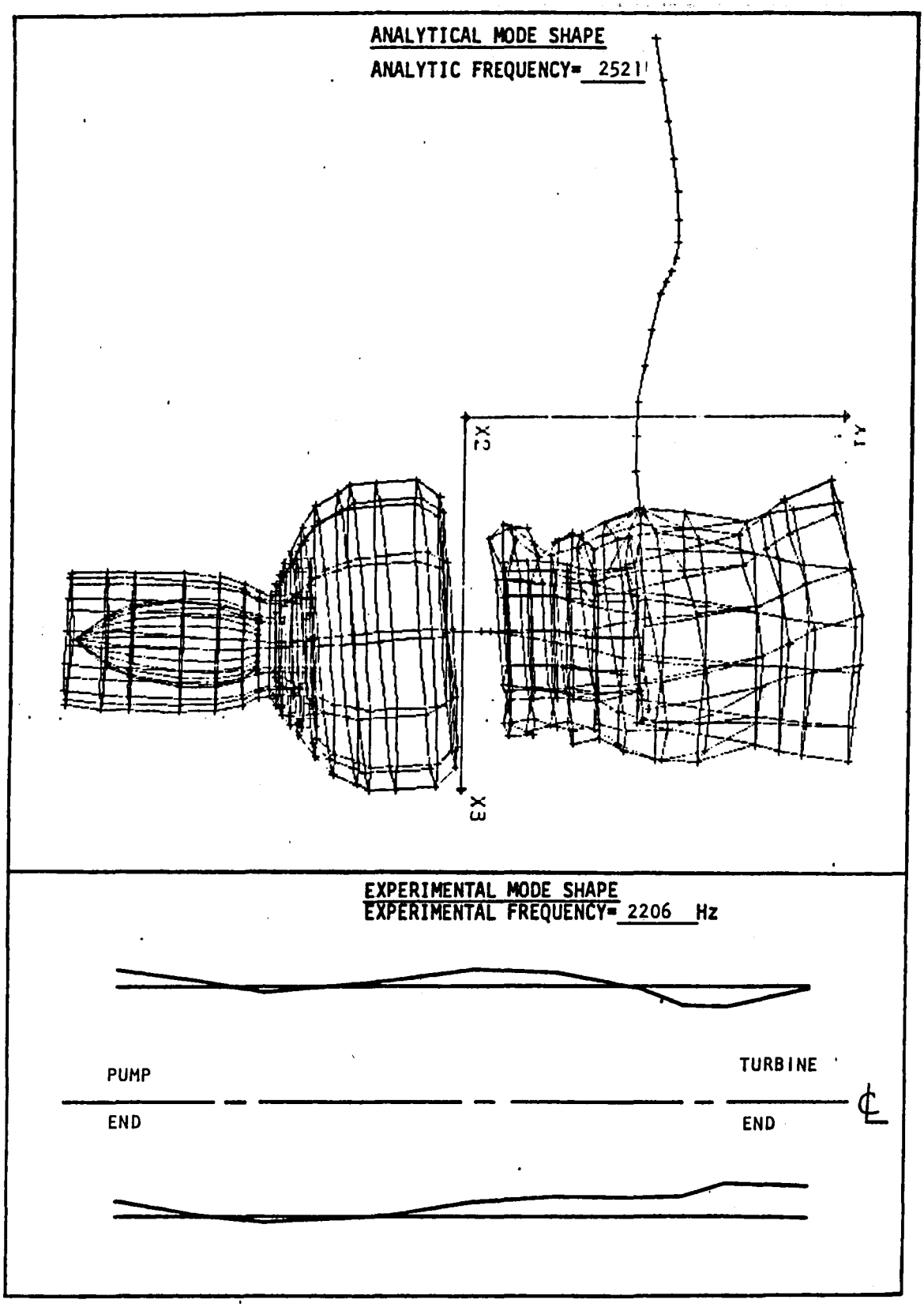

Figure 43. Mark-48F Case, Test/Analysis Mode Shape Comparison, Mode No. 15

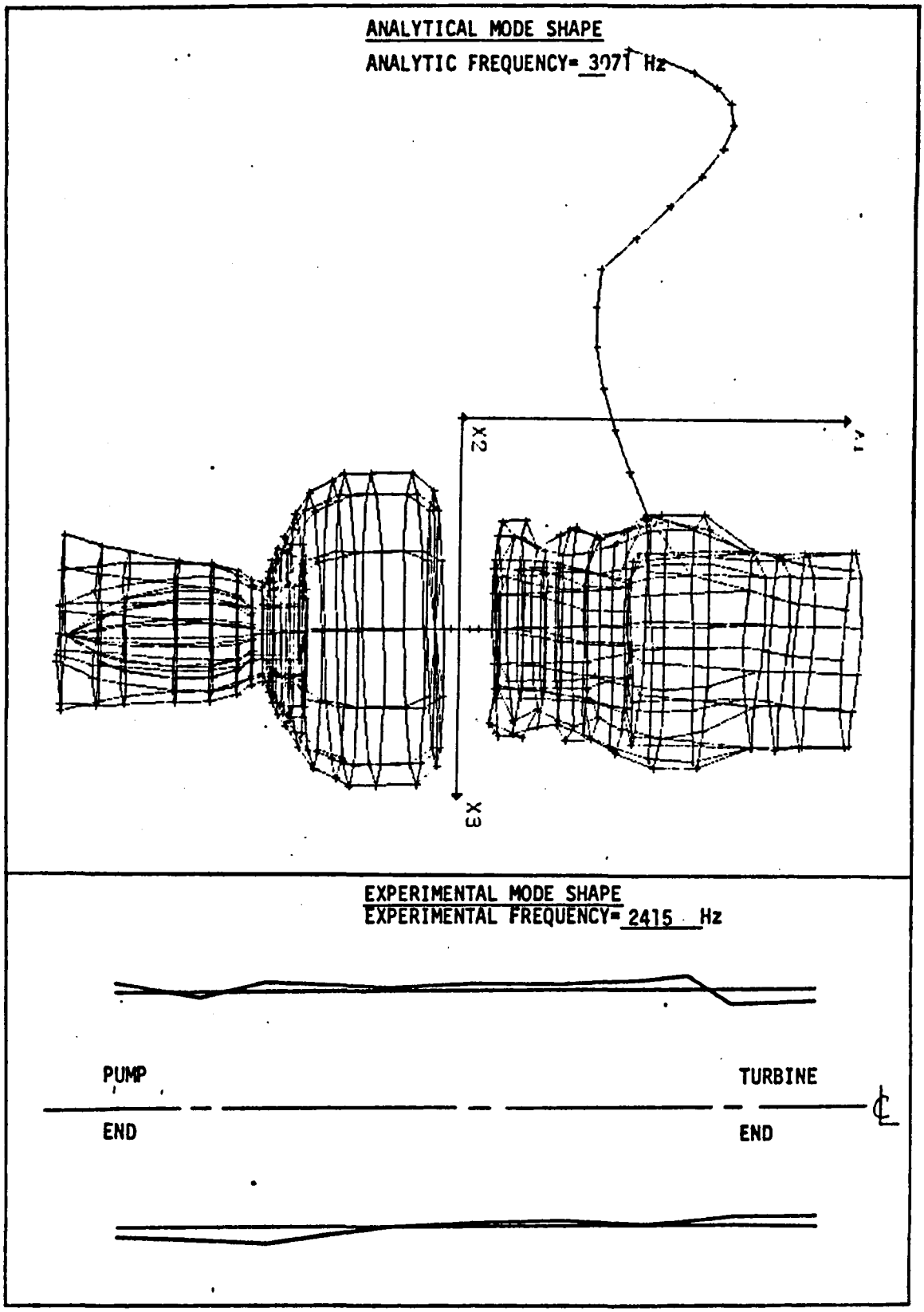

Figure 44. Mark-48F Case, Test/Analysis Mode Shape Comparison, Mode No. 16

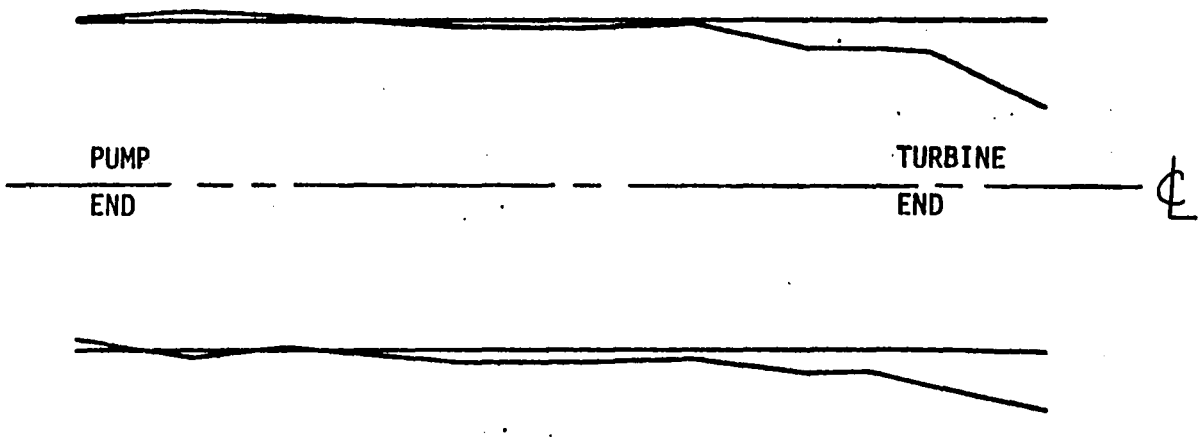

Figure 45. Mark-48F Case, Turbine End Bending/Pump Inlet Breathing Mode From Test, 2454 Hz (Uncorrelated)

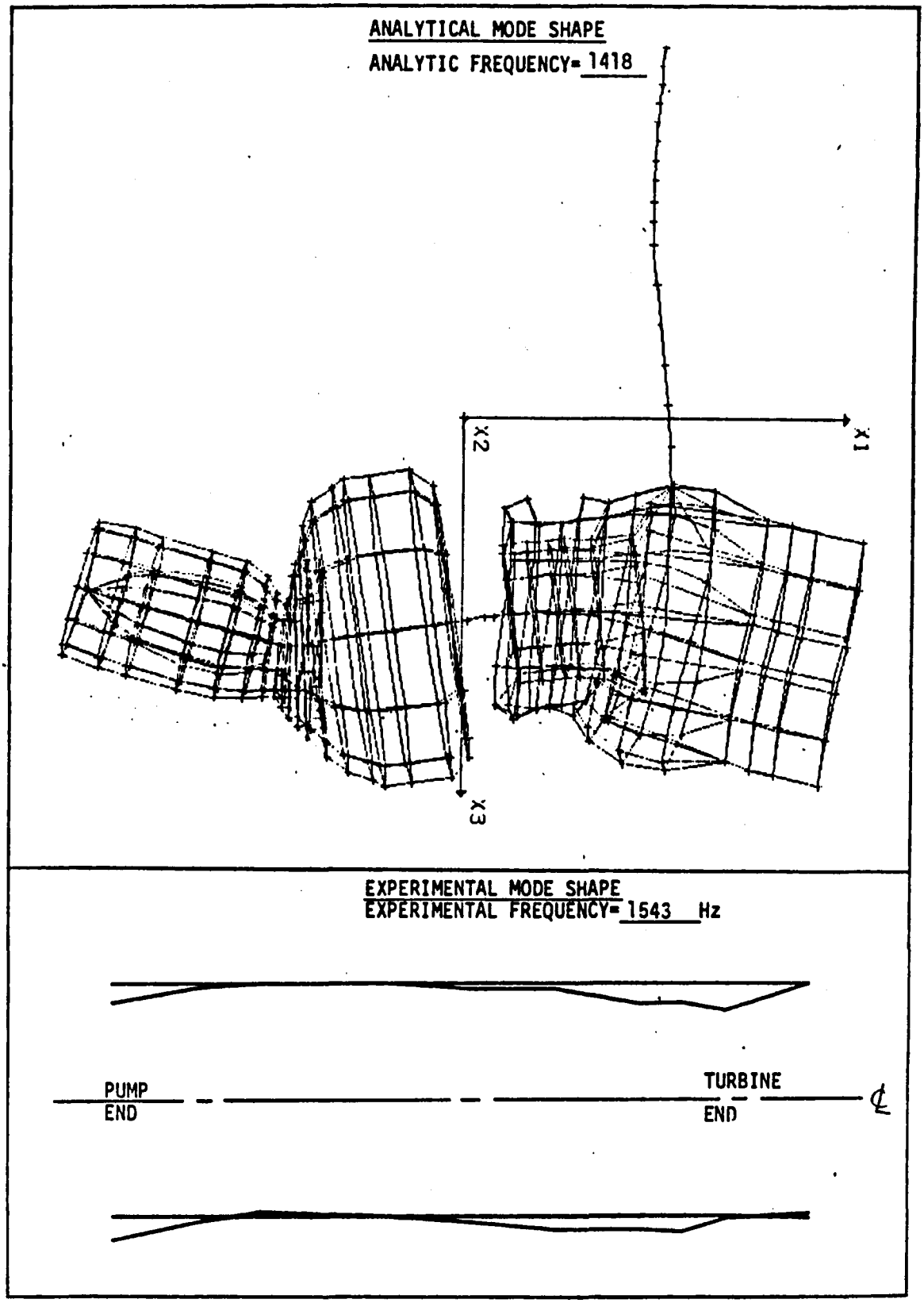

Figure 46. Mark-48F Case, Test/Analysis Mode Shape Comparison, Mode No. 9

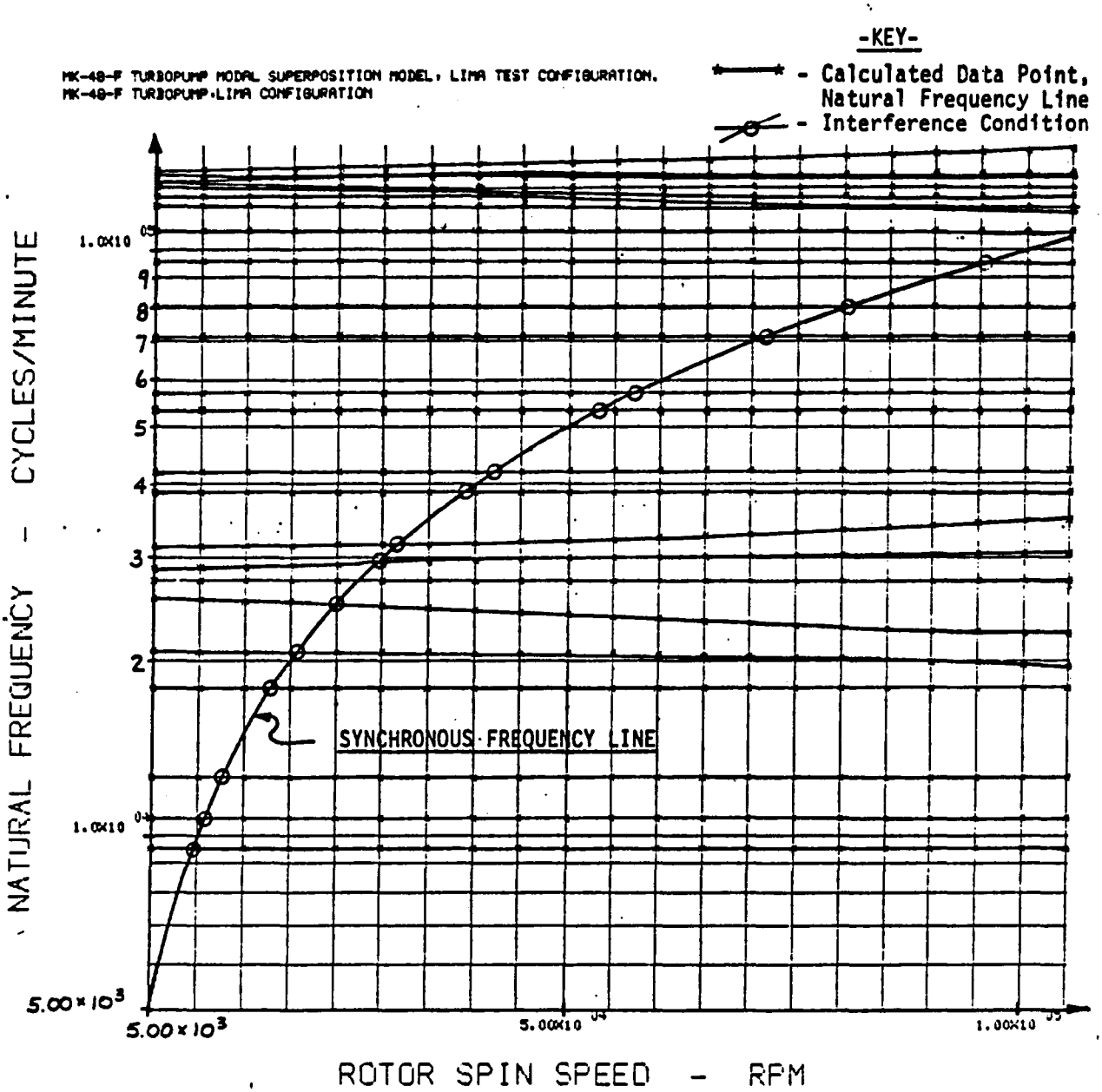

Figure 47. Mark-48F Turbopump, LIMA Configuration, Predicted Speed Dependent Natural Frequencies and Interference Plot

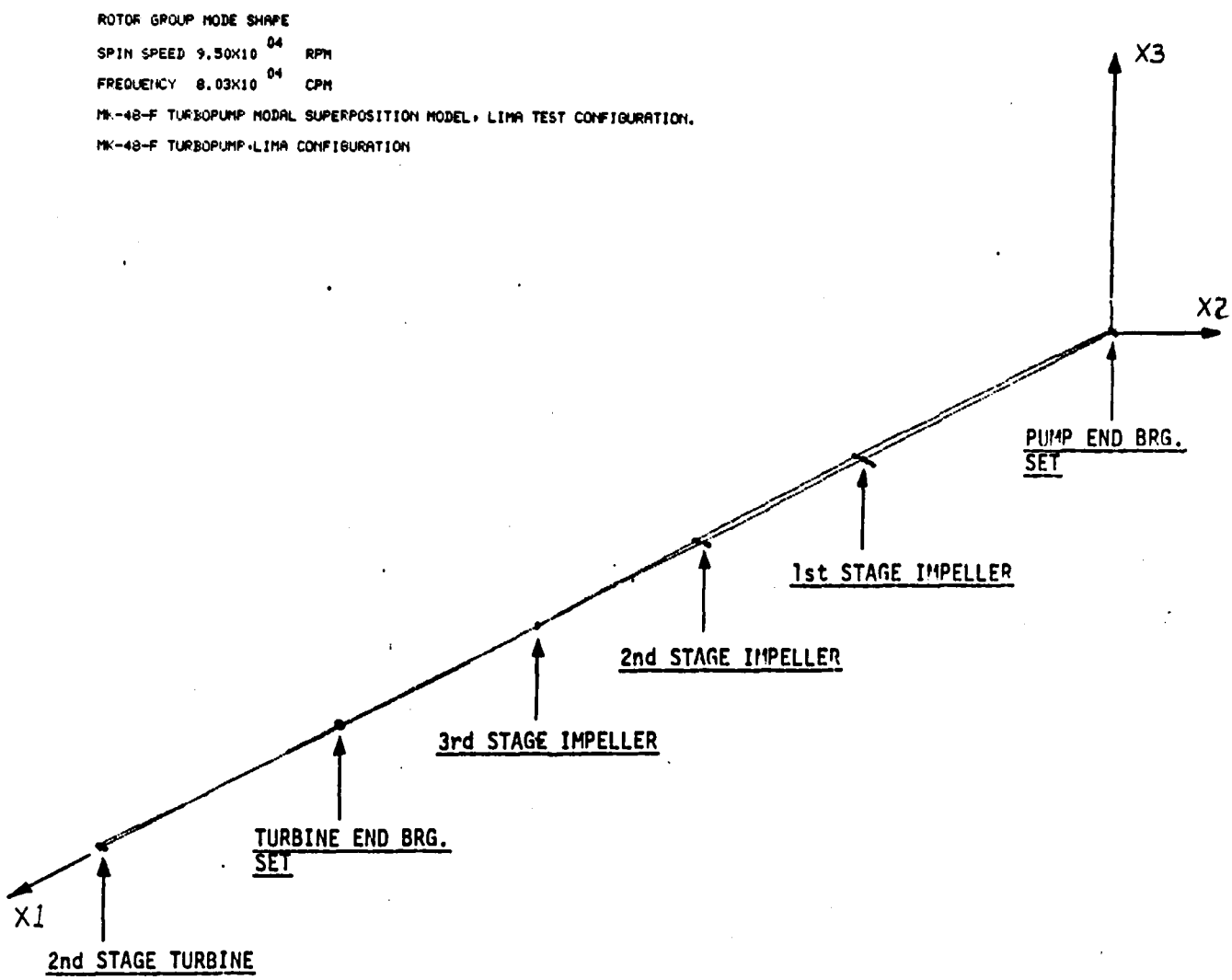

Figure 48. Mark-48F Turbopump Model, LIMA Configuration At 95,000 rpm: Predicted Rotor Mode Shape for Mode at 1338 Hz

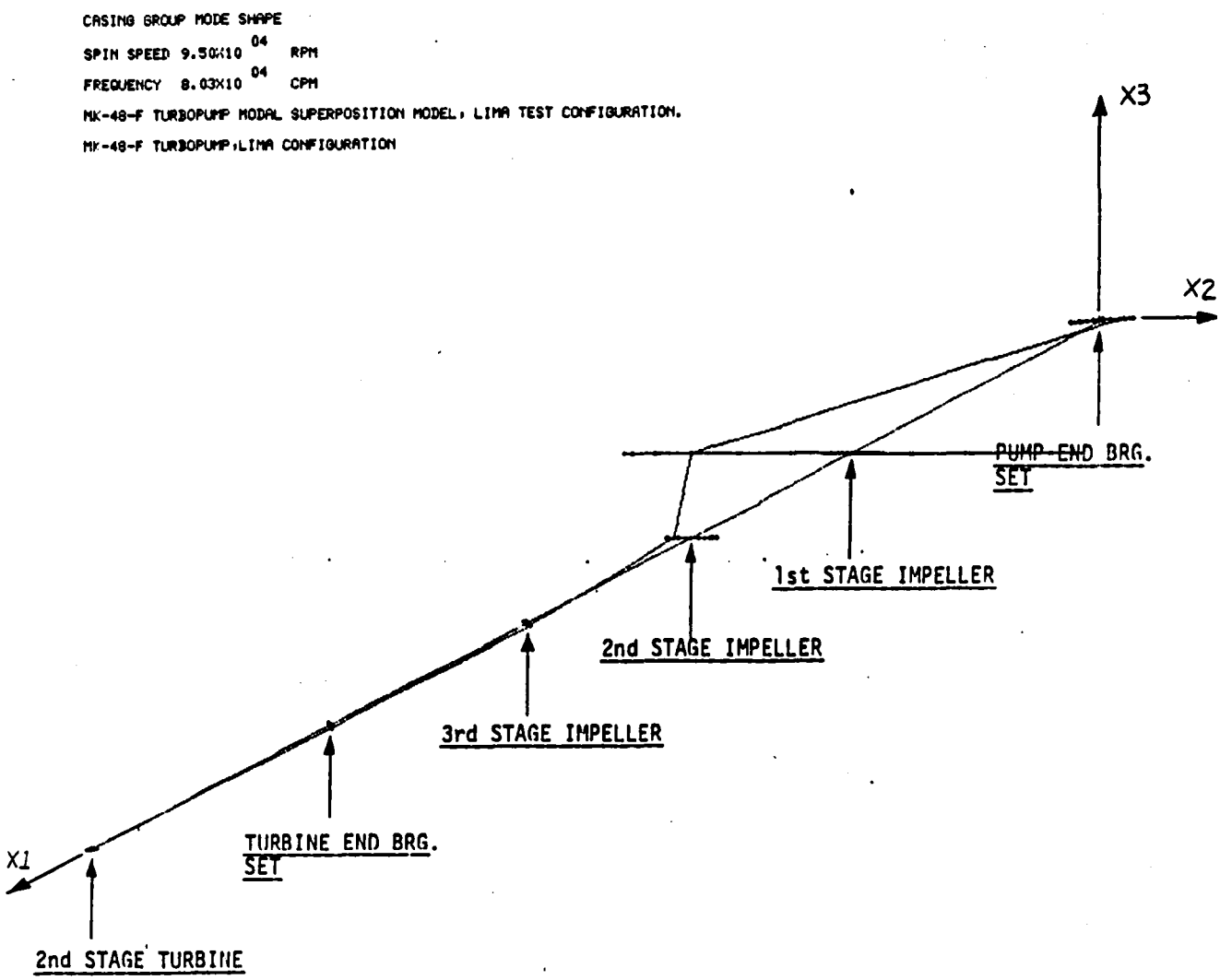

Figure 49. Mark-48F Turbopump Model, LIMA Configuration At 95,000 rpm: Predicted Case Mode Shape for Mode at 1338 Hz

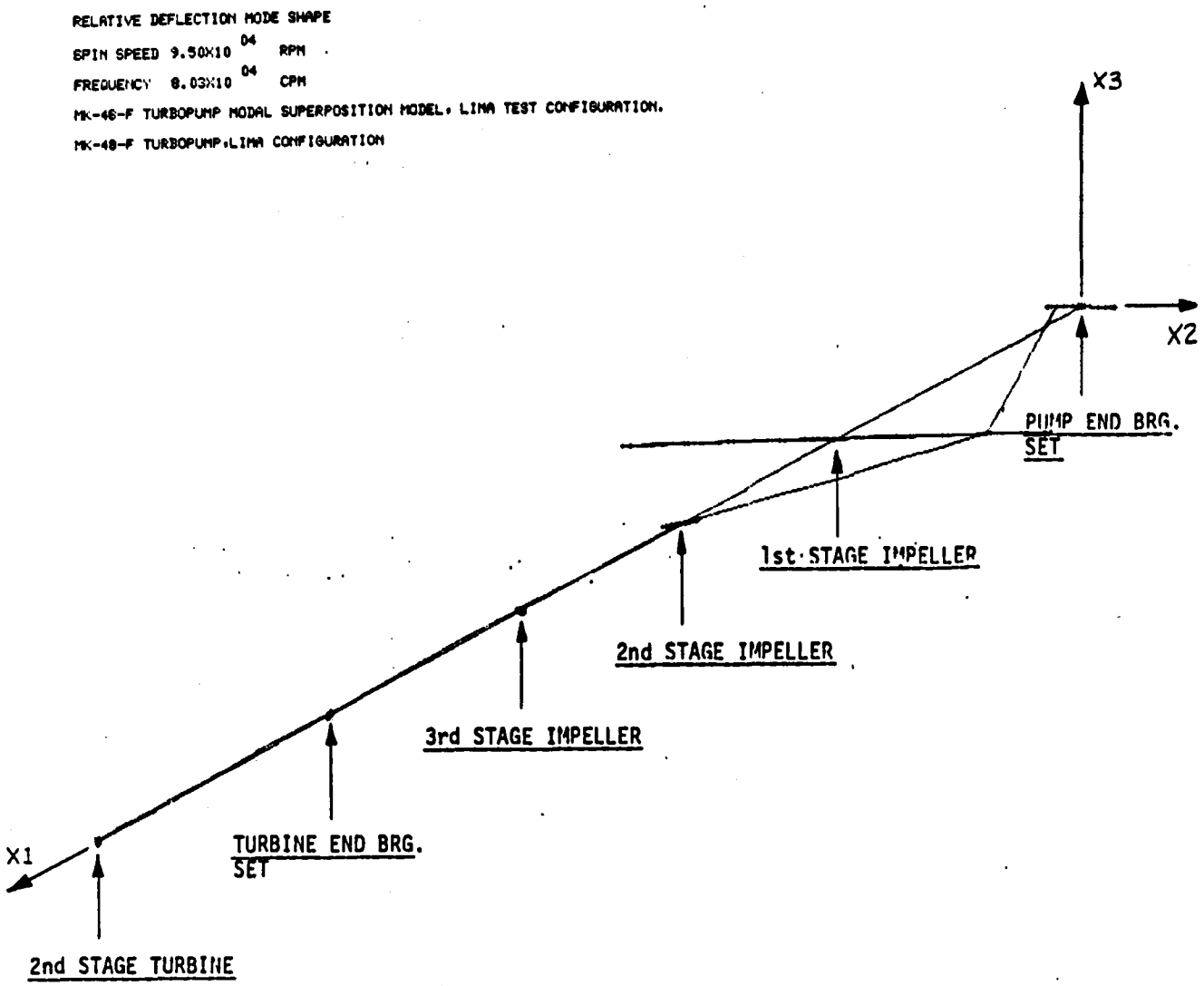

Figure 50. Mark-48F Turbopump Model, LIMA Configuration At 95,000 rpm: Predicted Relative Deflection Mode Shape for Mode at 1338 Hz

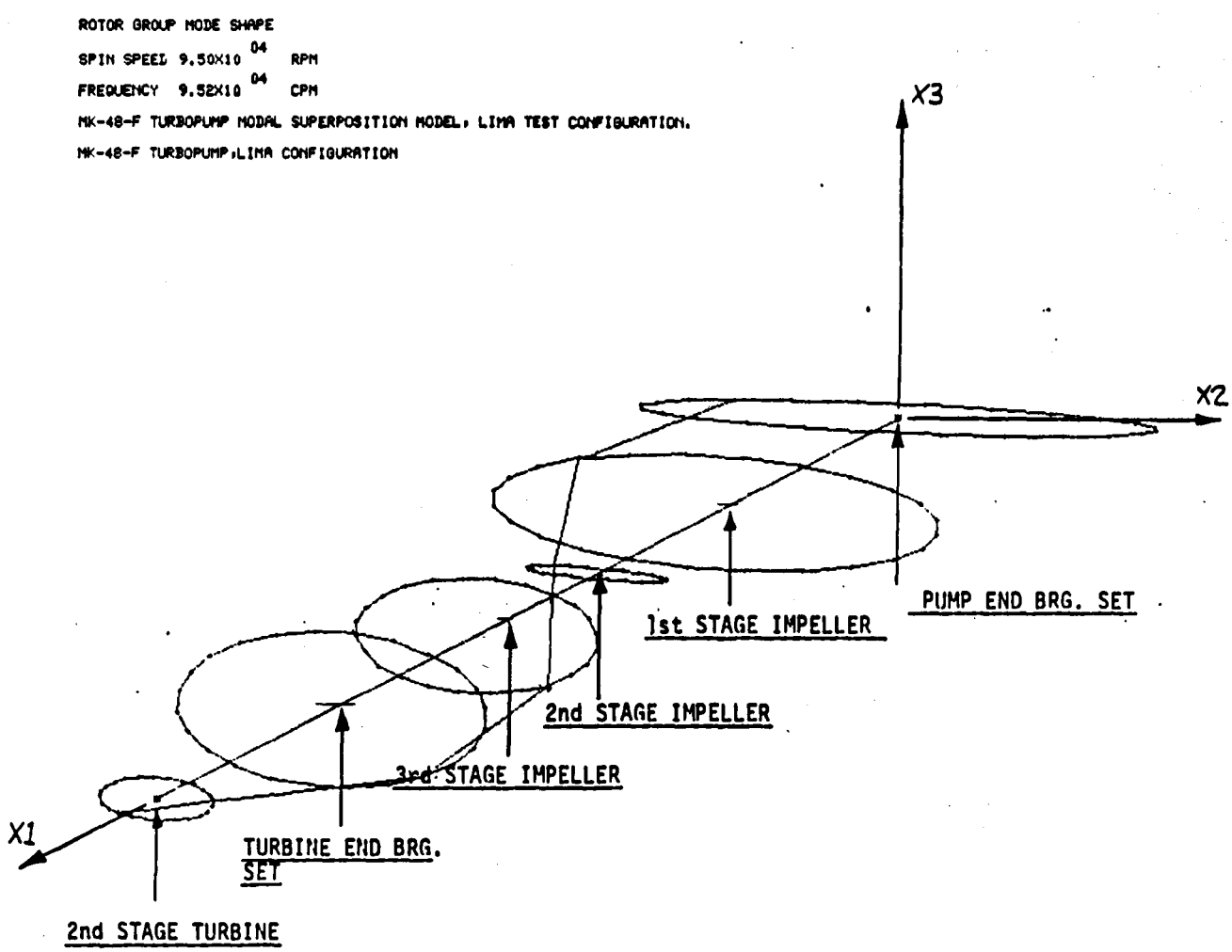

Figure 51. Mark-48F Turbopump Model, LIMA Configuration At 95,000 rpm: Predicted Rotor Mode Shape for Mode at 1587 Hz

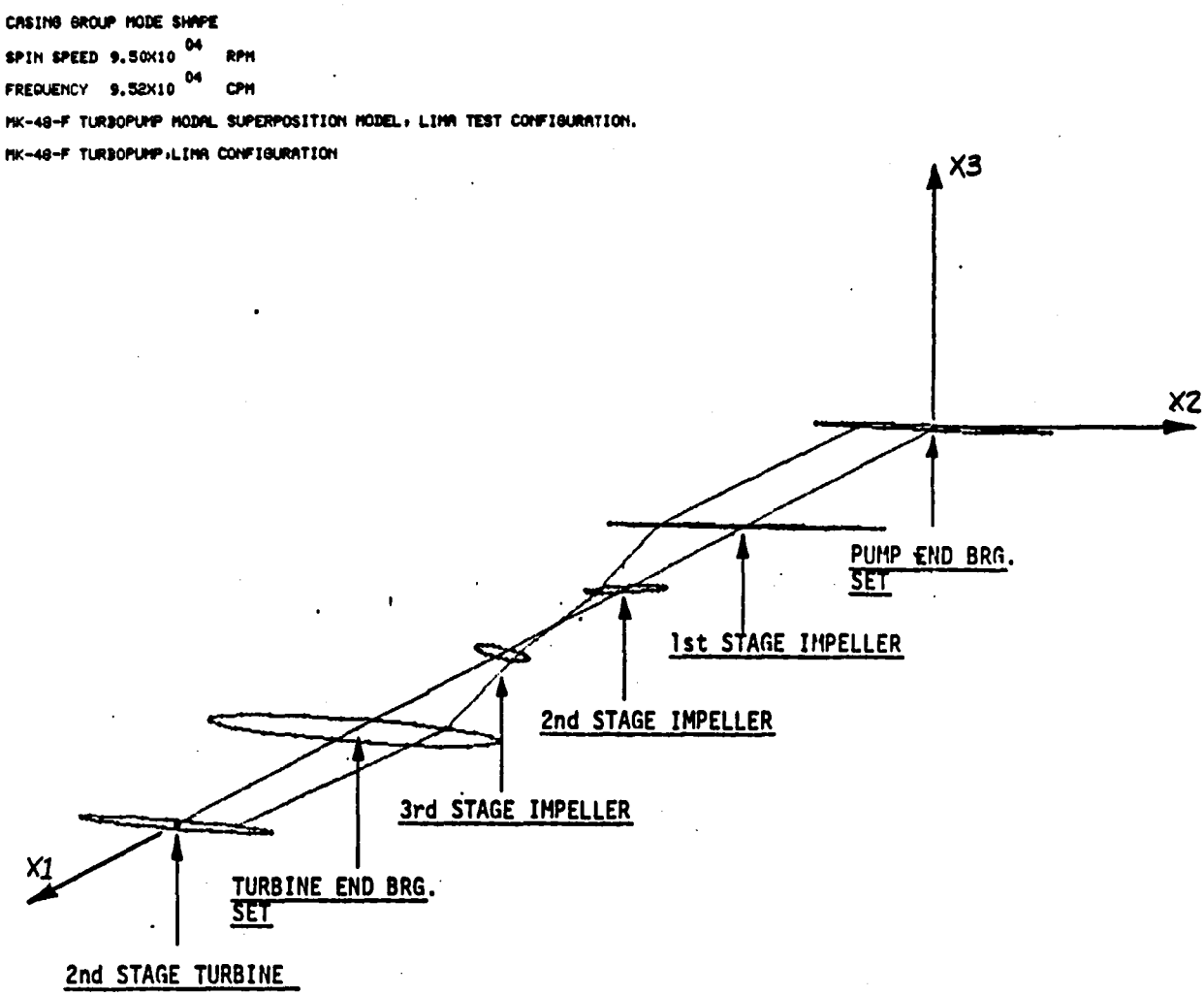

Figure 52. Mark-48F Turbopump Model, LIMA Configuration At 95,000 rpm: Predicted Case Mode Shape for Mode at 1587 Hz

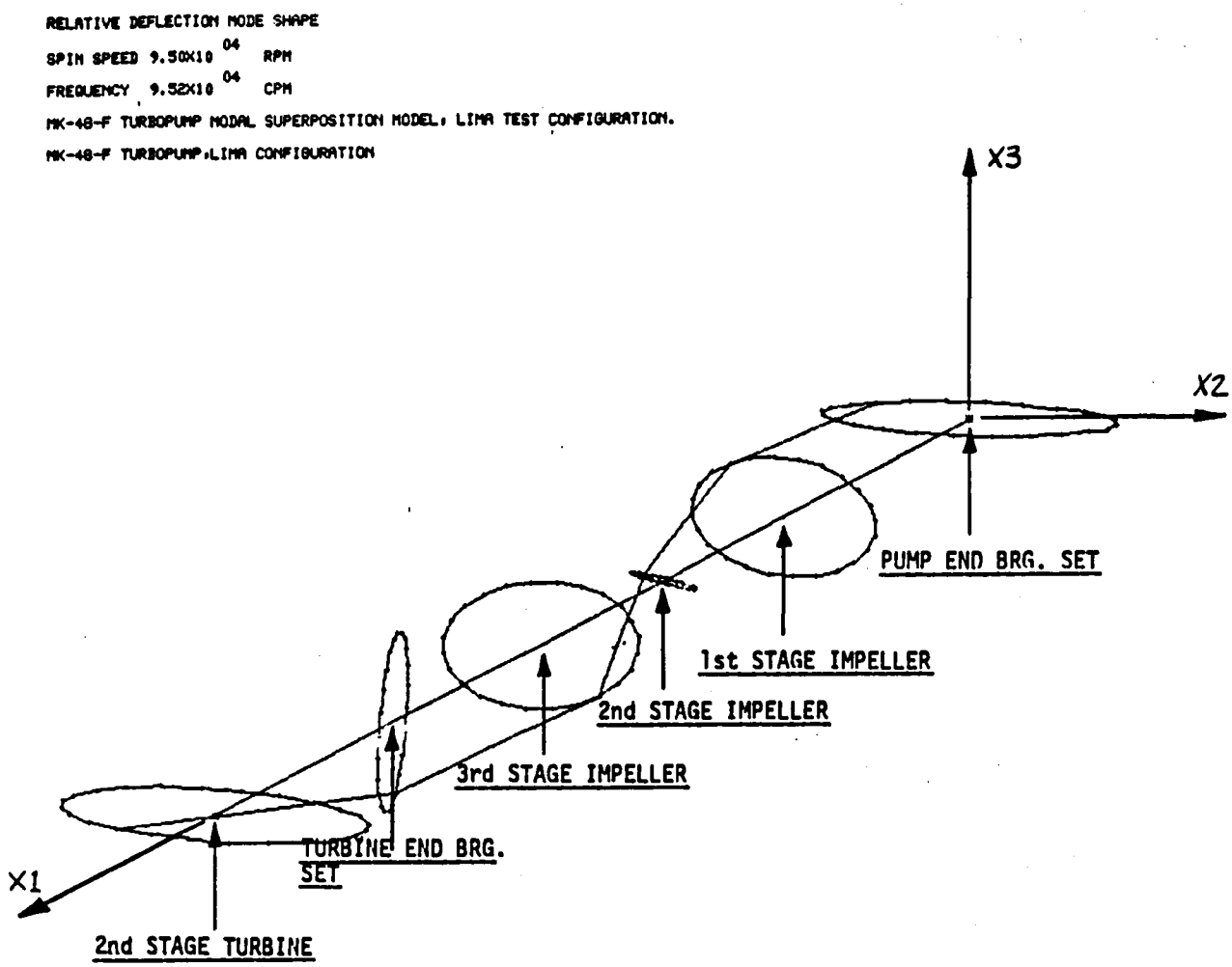

Figure 53. Mark-48F Turbopump Model, LIMA Configuration At 95,000 rpm: Predicted Relative Deflection Mode Shape for Mode at 1587 Hz

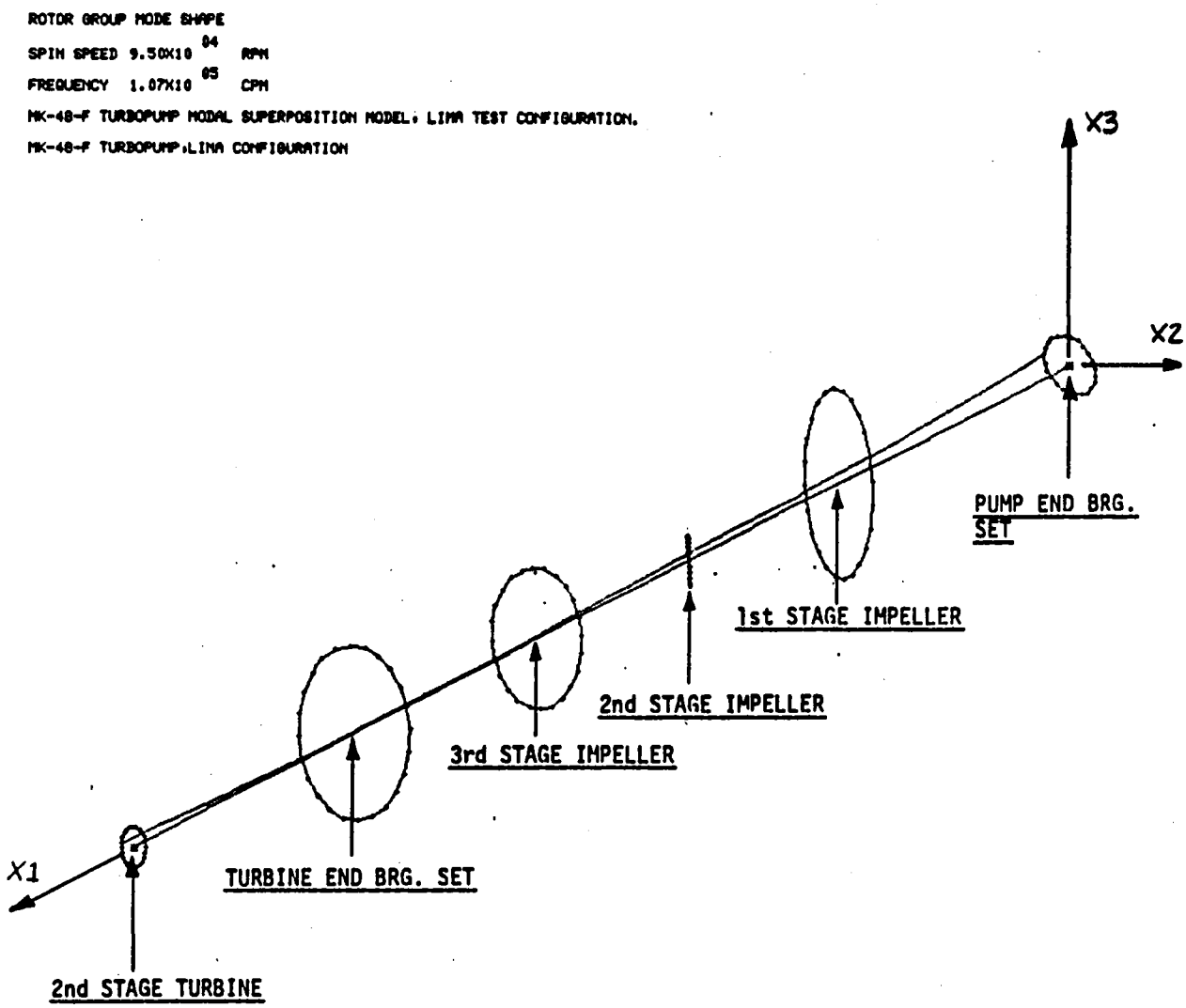

Figure 54. Mark-48F Turbopump Model, LIMA Configuration At 95,000 rpm: Predicted Rotor Mode Shape for Mode at 1783 Hz

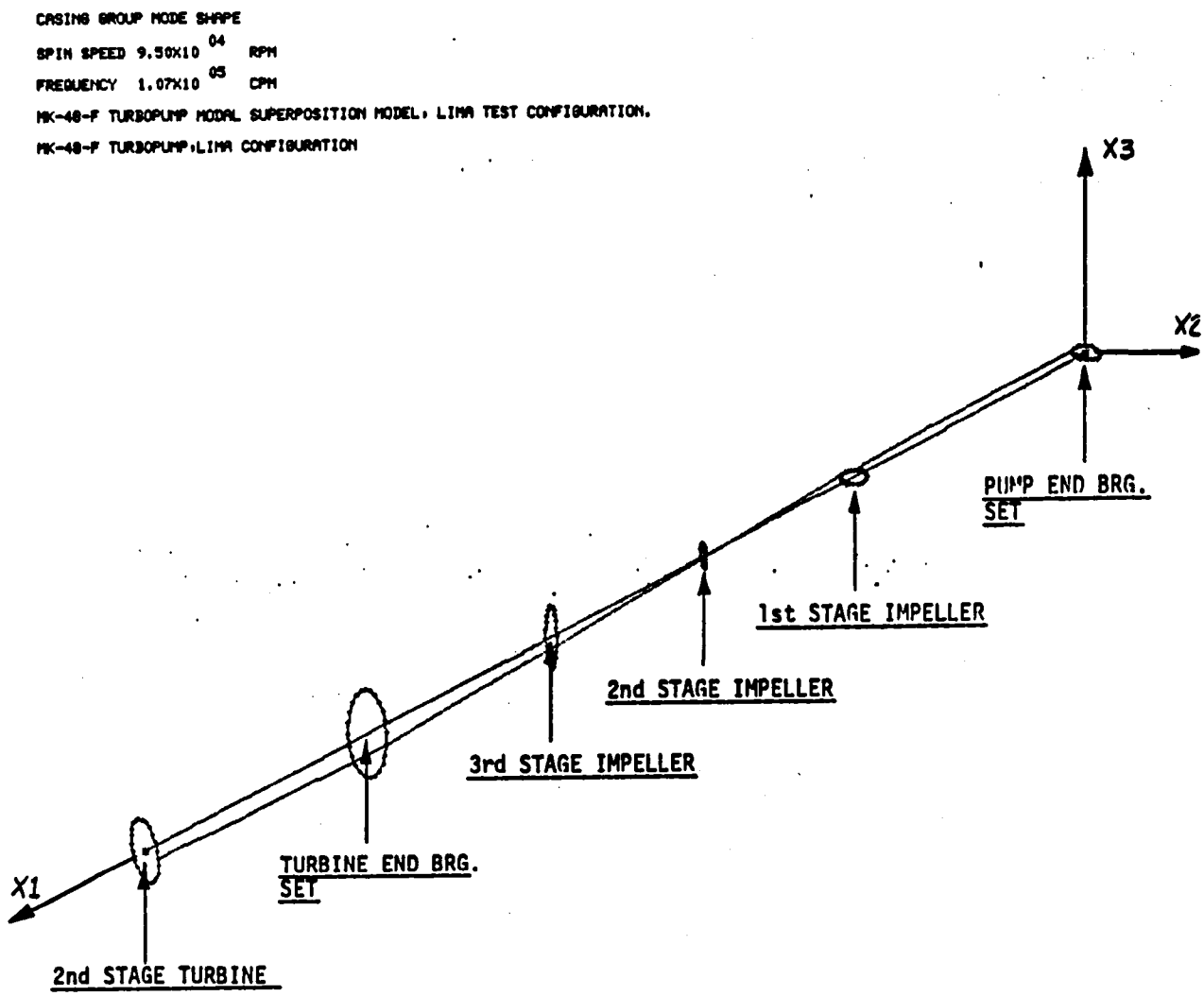

Figure 55. Mark-48F Turbopump Model, LIMA Configuration At 95,000 rpm: Predicted Case Mode Shape for Mode at 1783 Hz

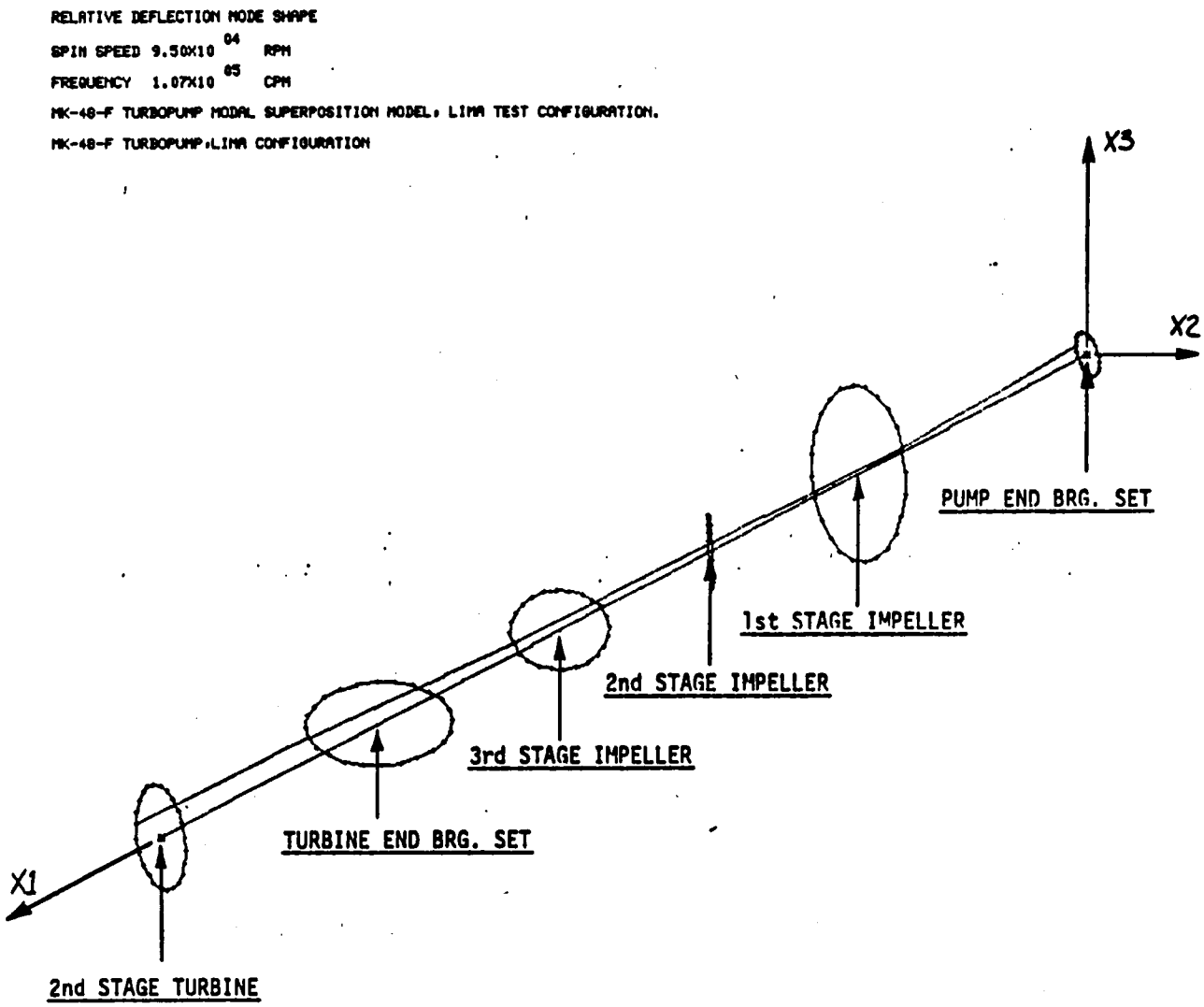

Figure 56. Mark-48F Turbopump Model, LIMA Configuration At 95,000 rpm: Predicted Relative Deflection Mode Shape for Mode at 1783 Hz

TABLE 1. MODAL TEST RESULTS FOR FREE-FREE ROTOR

MODE NO.	MODE NAME	FIG. NO.	NATURAL FREQUENCY (Hz)	MODAL PARAMETERS					
				MASS		STIFFNESS		DAMPING	
				(SLUGS)	(Kg)	(lb/in. X 10^6)	(N/m X 10^6)	(lb-sec/in.)	(N-sec/m)
1	FIRST BENDING	11	683	0.0963	1.41±	0.148	25.9	0.0594	10.4
2	FIRST TORSION	12	1251	4.20	61.3	21.9	3850.0	40.9	7150.0
3	SECOND BENDING	13	1721	0.0928	1.35	0.905	158.0	0.470	82.3

TABLE 2. ROTOR MODAL TEST/ANALYSIS FREQUENCY COMPARISON

MODE NO.	MODE NAME	TEST FREQUENCY (Hz)	ANALYSIS FREQUENCY (Hz)	PERCENTAGE DIFFERENCE BASED UPON TEST (±%)
1	FIRST BENDING	683	690	+1.02
2*	TORSIONAL	1251	—	—
3	SECOND BENDING	1721	1757	+2.09

*TORSIONAL MODE DETECTED IN TEST; TORSIONAL DEGREE OF FREEDOM NOT MODELLED ANALYTICALLY

TABLE 3. MODAL TEST RESULTS FOR FREE-FREE TURBOPUMP CASING

MODE NO.	MODE TYPE (NAME)	FIG. NO.	NATURAL FREQUENCY (Hz)	MODAL PARAMETERS					
				MASS		STIFFNESS		DAMPING	
				(SLUGS)	(Kg)	(lb/in. X 10^6)	(N/m X 10^6)	(lb-sec/in.)	(N-sec/m)
4	1ST BENDING PUMP INLET	37	828	2.39	34.9	5.39	944.	1.61	282.
5	CONTINUOUS 1ST BENDING	38	999	0.203	2.96	6.67	1170.	1.06	186
6A	CONTINUOUS 1ST BENDING TURB. END DOMINATED	39	1085	1.39	20.3	5.39	944.	1.28	224.
6B	CONTINUOUS 1ST BENDING TURB. END DOMINATED	40	1174	5.79	84.5	26.3	4610.	6.25	1090.
12	CLASSICAL 2ND BENDING COUPLED WITH TURB. INLT. DUCT.	41	1886	0.296	4.32	3.46	606.	7.11	1250.
13	TURBINE END HOOP BREATHING/BNDG.	42	2152	0.815	11.9	12.4	2170.	7.74	1360.
15	TURBINE EXIT HOOP BREATHING/BNDG.	43	2206	1.23	18.0	19.6	3430.	9.77	1710.
16	PUMP INLET & TURB. EXIT BREATH. BNDG.	44	2416	0.781	11.4	15.0	2630.	5.72	1000.
NOT CORRELATED	TURB. END BNDG./PUMP INLT. BRTHNG.	45	2454	2.11	30.8	41.7	7300.	4.25	744.

TABLE 4. CASING MODAL ANALYSIS/TEST FREQUENCY COMPARISON

MODE NO.	MODE TYPE (NAME)	NATURAL FREQUENCY (Hz)		PERCENT DIFFERENCE BASED UPON TEST(±%)
		ANALYSIS	TEST	
1	1st Bending; Turb. Inlet Torsion	247	250	-1.20
2	Turb. Inlet Bending; Body Bending	336	320	+5.00
3	2 Node Bending, Turb. End Torsion	537	565	-4.96
4	Focalized Bending of Turb. & Pump Ends	798	770/828	+3.63 to -3.62
5	"Classical" 1st Bending (Continuous)	906	999	-9.30
6	1st Bending Coupled w/turb. Inlet	1010	1085/1174	-6.91 to -14.0
7	Pump Inlet Breathing	1339	-	-
8	"Classical" 2nd Bending	1400	-	-
9	"Classical" 2nd Bending	1418	1543	-8.10
10	Turb. Brg. Support Axial	1621	-	-
11	Turb. End Hoop Breathing	1747	-	-
12	"Classical" 2nd Bend. w/Turb. Inlet	1769	1886	-6.15
13	Whipping of Turb. Inlet/Turb. Breathing	2313	2152	+7.48
14	Axial Fold-over of Implr. 1 Housing	2410	-	-
15	Whipping of Turb. Inlet/Turb. Exit Brthg.	2521	2206	+14.3
16	Turb. Inlet Bend./Turb. Brthg./Pump Brthg.	3071	2415	+27.2

TABLE 5. NATURAL FREQUENCIES OF MARK-48F TURBOPUMP, LIMA CONFIGURATION AT 95,000 rpm FROM MODAL SUPERPOSITION ANALYSIS

MODE NO.	NATURAL FREQUENCY (Hz)
1	159
2	178
3	210
4	299
5	330
6	372
7	456
8	506
9	570
10	647
11	702
12	883
13	892
14	954
15	1178
16	1198
17	1338
18	1587
19	1783
20	1956
21	1985

APPENDIX A

DISCUSSION OF THEORETICAL MODAL ANALYSIS OF DISCRETE SYSTEMS

Page Missing in Original Document

APPENDIX A

DISCUSSION OF THEORETICAL MODAL ANALYSIS OF DISCRETE SYSTEMS

Modal analysis is a method of obtaining the response of a system by using the modal matrix as the transformation matrix between the system's physical coordinates, used to drive the equations of motion, and a set of modal coordinates. The modal matrix is an array of the system's eigenvectors. Since the eigenvectors are uncoupled and independent, the modal matrix may be considered a set of n independent vectors in n - dimensional space. This condition is known as orthogonality; each eigenvector is orthogonal to every other eigenvector in the n - space. As such, any vector in the n - space (any system response, physically) may be represented by a linear combination or superposition of the orthogonal eigenvectors. The use of modal analysis to predict system response has great advantages since the superposition of linear, independent vectors is mathematically simpler than the analysis and reduction of any set of dependent, simultaneous equations. Its tenets may be used not only to predict response, but also to superpose complex structural systems and experimentally to describe a structure's dynamics.

These tenets will now be developed. Consider the multidegree of freedom system shown in Fig. A-1. This is a discrete or lumped-parameter system and may represent real system, finite-element model or an experimental representation. The system has n - degrees of freedom defined by the generalized coordinates, q_1 through q_n. An equation of motion may be written for each mass as follows:

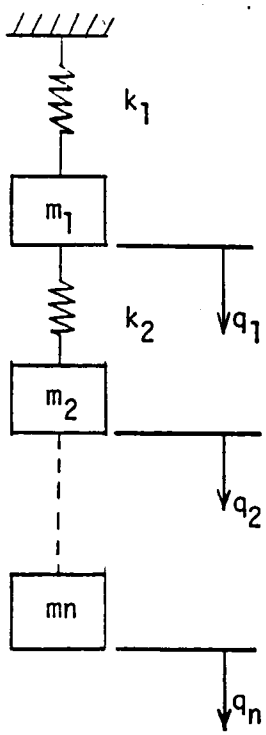

Figure A-1

$$m_1 q_1(t) + k_1 q_1(t) + k_2 [q_1(t) - q_2(t)] = f_1(t)$$

$$m_2 q_2(t) + k_2 q_2(t) + k_3 [q_2(t) - q_3(t)] = f_2(t)$$

$$\vdots$$

$$m_n f_n(t) + k_n q_n(t) = f_n(t)$$

Or, for a general system in matrix form:

$$[m][\ddot{q}] + [k][q] = [f] \qquad \text{(A-1)}$$

In order to determine the steady-state response due to sinusoidal motion, let $f(t) = Fe^{i\omega t}$ and seek a solution of the form $q = Qe^{i\omega t}$

$$q = Qe^{i\omega t}$$
$$\dot{q} = i\omega Qe^{i\omega t}$$
$$\ddot{q} = -\omega^2 Qe^{i\omega t}$$

Substituting these expressions into Eq. A-1:

$$-\omega^2 [m][Q] + [k][Q] = [F]$$

For free-vibration, $f = 0$, thus:

$$\omega^2 [m][Q] - [k][Q] = 0 \qquad \text{(A-2)}$$

Equation (A-2) is a statement of the eigenvalue problem. This set of equations has a solution when the determinant of coefficient matrix is zero:

$$\det \left\{\omega^2 [m] - [k]\right\} = 0$$

There is a set of n eigenvalues, $\omega_1, \omega_2, \ldots \omega n$ which yield a zero determinant. There is also an eigenvector corresponding to each eigenvalue which is a solution to Eq. A-2. The eigenvalues and eigenvectors are the natural frequencies and normal modes of the system, respectively. If an eigenvalue is designated ωr and an eigenvector ψr, Eq. A-2 may be rewritten as follows:

$$\omega_r^2 [m][\psi_r] - [k][\psi_r] = 0 \qquad \text{(A-3)}$$

It can be shown that for symmetric mass and stiffness matrices, the modal vectors possess the orthogonality property. Another solution to Eq. A-2 might be designated ω_s and ψ_s. Equation A-2 may then be written as:

$$\omega_s^2 [m][\psi_s] - [k][\psi_s] = 0 \qquad \text{(A-4)}$$

To demonstrate orthogonality exists between eigenvectors, premultiply both sides of Eq. A-3 by $[\psi_s]^T$ and both sides of Eq. A-4 by $[\psi_r]^T$ and rewrite as:

$$\omega_r^2 [\psi_s]^T [m] [\psi_r] = [\psi_s]^T [K] [\psi_r] \qquad \text{(A-5)}$$

$$\omega_s^2 \left[\psi_r\right]^T \left[m\right] \left[\psi_s\right] = \left[\psi_r\right]^T \left[K\right] \left[\psi_s\right] \tag{A-6}$$

Recalling the [m] and [k] are symmetric matrices, Eq. A-6 is transposed and subtracted from Eq. A-5 to obtain

$$\left(\omega_r^2 - \omega_s^2\right) \left[\psi_s\right]^T \left[m\right] \left[\psi_r\right] = 0$$

In general, two system frequencies ω_r and ω_s are not equal, therefore,

$$\left[\psi_s\right]^T \left[m\right] \left[\psi_r\right] = 0 \tag{A-7}$$

Equation A-7 is a statement of the orthogonality condition. The property of orthogonality implies the modal matrix is a set of independent vectors in n - space. Any vector may, therefore, be generated by a linear combination of the linearly independent eigenvectors. If such an arbitrary vector is designated by [x], this concept may be expressed as

$$\left[x\right] = \sum_{r=1}^{n} C_r \left[\psi_r\right] \tag{A-8}$$

where C_r, r = 1, 2, ... n are coefficients defined by

$$C_r = \left[\psi_r\right]^T \left[m\right] \left[x\right]$$

Equation A-8 is known as the expansion theorem and is the basis for determination of system response by modal analysis.

The expansion theorem is used to represent the response of the system as a superposition of the normal modes. Hence,

$$\left[q\right] = \left[\psi\right] \left[\eta\right] \tag{A-9}$$

where [η] are the modal coordinates. The modal matrix [ψ] is used as the transformation matrix between system's physical coordinates [q] and its modal coordinates [η]. It follows that

$$\left[\ddot{q}\right] = \left[\psi\right] \left[\ddot{\eta}\right] \tag{A-10}$$

Substituting Eq. A-9 and A-10 into Eq. A-1:

$$\left[m\right] \left[\psi\right] \left[\ddot{\eta}\right] + \left[k\right] \left[\psi\right] \left[\eta\right] = \left[f\right] \tag{A-11}$$

Premultiplying both sides of Eq. A-11 by $\left[\psi\right]^T$

$$\left[\psi^T\right]\left[m\right]\left[\psi\right]\left[\ddot{\eta}\right] + \left[\psi\right]^T\left[k\right]\left[\psi\right]\left[\eta\right] = \left[\psi\right]^T\left[f\right] \tag{A-12}$$

By definition, normal modes are such that

$$\left[\psi\right]^T\left[m\right]\left[\psi\right] = \left[I\right]$$

and

$$\left[\psi\right]^T\left[K\right]\left[\psi\right] = \left[\omega^2\right] \tag{A-13}$$

where [I] is the identity matrix

For a free-vibration, [f] = [0], hence

$$\left[\ddot{\eta}\right] + \left[\omega^2\right]\left[\eta\right] = \left[0\right] \tag{A-14}$$

Which is a set of uncoupled differential equations having the form of an undamped single degree of freedom system. Modal Analysis uncouples the equations of motion via a linear coordinate transformation. The transformation matrix is the modal matrix.

In this form, it is simpler to superpose complex structures or determine system response.

The results obtained using the modal coordinates may be translated back to the original physical coordinate system by use of Eq. A-9, A-10 and A-13.

In the process of the superposition of component structures (such as turbopump rotor and case) the uncoupled equations of motion for each component become coupled again by additions such as springs, damping and gyroscopics. For a turbopump the modal equations of motion become:

$$\left[\begin{array}{c|c} I & 0 \\ \hline 0 & I \end{array}\right]\left\{\begin{array}{c} \ddot{\eta}_R \\ \hline \ddot{\eta}_C \end{array}\right\} = -\left[\begin{array}{c|c} \omega_R^2 & 0 \\ \hline 0 & \omega_C^2 \end{array}\right]\left\{\begin{array}{c} \eta_R \\ \hline \eta_C \end{array}\right\} + \dot{\phi}\left[\begin{array}{c|c} \psi_R^T\, G\, \psi_R & 0 \\ \hline 0 & 0 \end{array}\right]\left\{\begin{array}{c} \dot{\eta}_R \\ \hline \dot{\eta}_C \end{array}\right\}$$

$$- \left[\begin{array}{c|c} \psi_R^T K_1 \psi_R & \psi_R K_2 \psi_C \\ \hline \psi_C^T K_3 \psi_R & \psi_C^T K_4 \psi_C \end{array}\right]\left\{\begin{array}{c} \eta_R \\ \hline \eta_C \end{array}\right\}$$

$$- \left[\begin{array}{c|c} \psi_R^T C_1 \psi_R & \psi_R^T C_2 \psi_C \\ \hline \psi_C^T C_3 \psi_R & \psi_C^T C_4 \psi_C \end{array}\right]\left\{\begin{array}{c} \dot{\eta}_R \\ \hline \dot{\eta}_C \end{array}\right\} \tag{A-15}$$

where subscripts

$R \equiv$ rotor

$C \equiv$ case

$K_{1,2,3,4} \equiv$ partitions of stiffness matrix defining coupling elements such as bearing stiffnesses

$C_{1,2,3,4} \equiv$ partitions of damping matrix defining coupling elements such as bearing damping

$G \equiv$ rotor gyroscopic matrix

Since these modal equations of motion are now coupled, solution of them for turbopump frequencies and mode shapes requires solution of an eigenvalue problem. Benefit is still gained from the modal superposition process because the degrees of freedom of the problem may be greatly reduced.

This superposition process was used in the analysis of the Mark 48F turbopump.

REFERENCES

A-1. Meirovitch, L., Analytical Methods in Vibrations; McMillan Co., New York, Pub., 1967.

A-2. Klosterman, A. L., "On the Experimental Determination and Use of Modal Representations of Dynamic Data;" Dissertation submitted to the Department of Mechanical Engineering, University of Cincinnati, 1971.

A-3. Rowan, B. F., "Rotordynamics Analysis of the Space Shuttle Main Engine High Pressure Oxidizer Pump;" Rockwell International/Rocketdyne Division Technical Paper, 1980.

Page Missing in Original Document

APPENDIX B

DISTRIBUTION LIST FOR FINAL REPORT

CONTRACT NAS3-22480

	No. of Copies
National Aeronautics & Space Administration Lewis Research Center 21000 Brookpark Road Cleveland, Ohio 44135	
Attn: Contracting Officer, MS 501-11	1
E. A. Bourke, MS 501-5	5
Technical Utilization Office, MS 3-16	1
Technical Report Control Office, MS 5-5	1
AFSC Liaison Office, MS 501-3	2
Library, MS 60-3	2
Office of Reliability & Quality Assurance, MS 500-211	1
R. E. Connelly, MS 501-6	12
Patent Counsel, MS 500-318	1
National Aeronautics & Space Administration Headquarters Washington, D. C. 20546	
Attn: Office of Aeronautics & Space Technology	1
Director, Study, Analysis & Planning/RX	1
Director, Space Propulsion & Power/RP	1
F. W. Stephenson/RTP-6	1
Office of Space Flight	1
Director, Advanced Programs/MT	1
Director, Advanced Studies/MTE	1
Office of Industry Affairs & Technology Utilization	1
Director, Technology Utilization/KT	1
National Aeronautics & Space Administration Ames Research Center Moffett Field, CA 94035	
Attn: Library	1
National Aeronautics & Space Administration Flight Research Center P. O. Box 273 Edwards, CA 93523	
Attn: Library	1

National Aeronautics & Space Administration
George C. Marshall Space Flight Center
Huntsville, Alabama 35812
Attn: Library 1
J. L. Sanders/PD13 1
R. Richmond/EP24 1
J. A. Lombardo/EP21 1
O. K. Goetz/EP21 1
F. J. Dolan/EH14 1

National Aeronautics & Space Administration
Goddard Space Flight Center
Greenbelt, Maryland 20771
Attn: Library 1

National Aeronautics & Space Administration
John F. Kennedy Space Center
Cape Canaveral, Florida 32931
Attn: Library 1

National Aeronautics & Space Administration
Lyndon B. Johnson Space Center
Houston, Texas 77001
Attn: Library 1
H. O. Pohl/EP 1

National Aeronautics & Space Administration
Langley Research Center
Langley Station
Hampton, Virginia 23365
Attn: Library 2

NASA Scientific & Technical Information Facility
P. O. Box 33
College Park, Maryland 20740
Attn: NASA Representative 10

Office of the Director of Defense
Research & Engineering
Washington, D. C. 20301
Attn: Office of Asst. Director (Chemical Technology) 1

Jet Propulsion Laboratory
4800 Oak Grove Drive
Pasadena, CA 91103
Attn: Library 1
D. Dipprey 1

Defense Documentation Center
Cameron Station
Building 5
5010 Duke Street
Alexandria, Virginia 22314
Attn: TISIA 1

Advanced Research Projects Agency
Washington, D. C. 20525
Attn: Library 1

Aeronautical System Division
Air Force Systems Command
Wright-Patterson Air Force Base
Dayton, Ohio
Attn: Library 1

Air Force Missile Test Center
Patrick Air Force Base, Florida
Attn: Library 1

Air Force Systems Command
Andrews Air Force Base
Washington, D. C. 20332
Attn: Library 1

Air Force Rocket Propulsion Laboratory
Edwards, CA 93523
Attn: Library 1

AFRPL/LK Col. B. A. Loving
Edwards AFB, CA 93523 1

Air Force Office of Scientific Research
Bldg. 410
Bolling Air Force Base
Washington, D. C. 20332
Attn: Library 1

U. S. Air Force
Washington, D. C.
Attn: Library 1

Air Force Aero Propulsion Laboratory
Research & Technology Division
Air Force Systems Command
U. S. Air Force
Wright-Patterson AFB, Ohio 45433
Attn: Library 1

Arnold Engineering Development Center
Air Force Systems Command
Tullahoma, Tennessee
Attn: Library 1

Space & Missile Systems Organization
Worldway Postal Center
P. O. Box 92960
Los Angeles, CA 90009
Attn: Library (Technical Data Center) 1
Lt. Cold J. Graetch 1

Office of Research Analyses (OAR)
Holloman Air Force Base
New Mexico 88330
Attn: Library (RRRD) 1

RTD (RTNP)
Bolling Air Force Base
Washington, D. C. 20332 1

Bureau of Naval Weapons
Department of the Navy
Washington, D. C.
Attn: Library 1

Naval Research Branch Office
1030 E. Green Street
Pasadena, CA 91101
Attn: Library 1

Picatinny Arsenal
Dover, New Jersey 07801
Attn: Library 1

U. S. Naval Research Laboratory
Washington, D. C. 20390
Attn: Library 1

U. S. Army Research Office (Durham)
Box CM, Duke Station
Durham, North Carolina 27706
Attn: Library 1

U. S. Army Missile Command
Redstone Scientific Information Center
Redstone Arsenal, Alabam 35808
Attn: Document Section 1

U. S. Naval Missile Center
Point Mugu, CA 93041
Attn: Technical Library 1

U. S. Naval Weapons Center
China Lake, CA 93557
Attn: Library 1

Aerospace Corporation
2350 E. El Segundo Blvd.
Los Angeles, CA 90045
Attn: Library 1
R. L. Doobler 1
I. Madison 1

Airesearch Mfg. Co. of California
A Division of the Garrett Corp.
2525 W. 190th St.
Torrence, CA 90509
Attn: Library 1

Airesearch Mfg. Co. of Arizona
A. Div. of the Garrett Corp.
402 South 36th St.
Phoenix, Arizona 85034
Attn: Library 1

Atlantic Research Corp.
5390 Cherokee Ave.
Alexandria, Virginia 22314
Attn: Library 1

Battelle Memorial Institute
505 King Avenue
Columbus, Ohio 43201
Attn: Library 1

Aerojet Liquid Rocket Co.
P. O. Box 13222
Sacramento, CA 95813
Attn: Library 1
A. Siebenhaar 1
J. Salmon 1

Bell Aerospace Company
Box 1
Buffalo, New York 14240
Attn: Library 1

Boeing Company
Space Division
P. O. Box 868
Seattle, Washington 98124
Attn: Library 1

John Hopkins University
John Hopkins Road
Laurel, Maryland 20810 1

Chrysler Corp.
Defense-Space Group
P. O. Box 757
Detroit, Michigan 48231
Attn: Library 1

Curtiss-Wright Corporation
One Rotary Drive
Woodridge, New Jersey 07075
Attn: Library 1

Deposits & Composites Incorporated
318 Victory Drive
Herndon Industrial Park
Herndon, Virginia 22070
Attn: J. C. Withers 1

Fairchild Republic Company
Fairchild Industries
Farmingdale, L. I., NY 11735
Attn: Library 1

General Dynamics/Convair
P. O. Box 1128
San Diego, CA 92112
Attn: Library 1

General Electric Company
Valley Forge Space Technology Center
P. O. Box 8555
Philadelphia, PA 19101
Attn: Library 1

Grumman Aerospace Corporation
Bethpage, L. I., NY 11714
Attn: Library 1

Hamilton Standard Corporation
Windsor Locks, Connecticut 06096
Attn: Library 1

Hughes Aircraft Company
Space & Communications Group
P. O. Box 92919
Los Angeles, CA 90009
Attn: Library 1

IIT Research Institute
Technology Center
Chicago, Illinois 60616
Attn: Library 1

Walter Kidde & Company
Belleville Division
675 Main St.
Belleville, New Jersey 07109
Attn: Library 1

Lockheed Missiles & Space Company
P. O. Box 504
Sunnyvale, CA 94087
Attn: Library 1

Marquardt Corporation
16555 Saticoy Street
Box 2013 South Annex
Van Nuys, CA 91409
Attn: Library 1

Martin-Marietta Corporation
P. O. Box 179
Denver, Colorado 80201
Attn: Library 1

McDonnell Douglas Astronautics
5301 Bosa Avenue
Huntington Beach, CA 92647
Attn: Library 1

Northrop Corporation
1800 Century Park East
Century City, CA 90067
Attn: Library 1

Pratt & Whitney Aircraft Group
United Technologies Corporation
400 Main Street
East Hartford, CN 06108
Attn: Library 1

Pratt & Whitney Aircraft Group
Government Products Division
P. O. Box 2691
West Palm Beach, FL 33402
Attn: Library 1
J. Brown 1

Space Division
A Division of Rockwell International
12214 Lakewood Blvd.
Downey, CA 90241
Attn: Library 1

Rocket Research Corporation
Willow Road at 116th Street
Redmond, Washington 98052
Attn: Library 1

Sundstrand Aviation Mechanical
2421 Eleventh Street
Rockford, Illinois 61101
Attn: Library 1

Thiokol Corporation
P. O. Box 1000
Newton, PA 18940
Attn: Library 1

TRW Systems Group
1 Space Park
Redondo Beach, CA 90278
Attn: Library 1

Sundstrand Corporation
Advanced Technology Group
1005A Courtney Drive
Dayton, OH 45431
Attn: W. K. Thorson 1

TRW
23555 Euclid Avenue
Cleveland, Ohio 44117
Attn: Library 1

Vought Corporation
P. O. Box 5907
Dallas, Texas 75222 1

J. P. Layton
60 Penn Lyle Road
Princeton Jct., New Jersey 08550 1

R. J. Salkeld
5921 Floris Heights Road
Malibu, CA 90265 1

Dr. Lloyd Barrett
University of Virginia
Department of Mechanical & Aerospace Engineering
Charlottesville, VA 22801 1

Dr. Dara W. Childs
Texas A&M University
Mechanical Engineering Dept.
College Station, TX 77843 1

Professor M. C. Ek
Californdia State University
Department of Mechanical Engineering
Northridge, CA 91324 1

End of Document